STUDIA UNIVERSITATIS
BABEŞ-BOLYAI

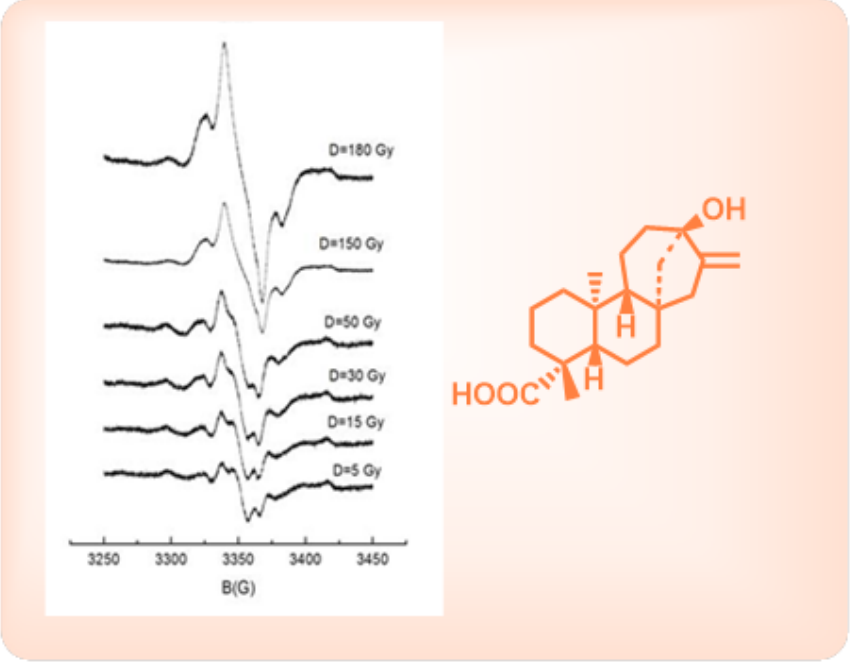

CHEMIA

3/2022

STUDIA UNIVERSITATIS BABEȘ-BOLYAI CHEMIA

3/2022

http://chem.ubbcluj.ro/~studiachemia/;
http://www.studia.ubbcluj.ro/serii/chemia/index_en.html

YEAR **Volume 67 (LXVII) 2022**
MONTH **SEPTEMBER**
ISSUE **3**

S T U D I A
UNIVERSITATIS BABEŞ–BOLYAI
CHEMIA

3

ISSUE DOI:10.24193/subbchem.2022.3

STUDIA UBB EDITORIAL OFFICE: B.P. Hasdeu no. 51, 400371 Cluj-Napoca, Romania, Phone + 40 264 405352

CUPRINS – CONTENT – SOMMAIRE – INHALT

Studia Universitatis Babes-Bolyai Chemia has been selected for coverage in Thomson Reuters products and custom information services. Beginning with V. 53 (1) 2008, this publication is indexed and abstracted in the following:

- Science Citation Index Expanded (also known as SciSearch®)
- Chemistry Citation Index®
- Journal Citation Reports/Science Edition

STUDIA UBB CHEMIA, LXVII, 3, 2022 (p. 7-16)
(RECOMMENDED CITATION)
DOI:10.24193/subbchem.2022.3.01

DETERMINATION OF THE ANTIOXIDANT ACTIVITY OF DIFFERENT TYPES OF COFFEE BY MEANS OF BRIGGS-RAUSCHER ANALYTICAL METHOD

GABRIELLA SZABÓ[a], EMESE CSIKI[a], ÁRPÁD-FERENC SZŐKE[a], NORBERT MUNTEAN[a,b*]

ABSTRACT. The antioxidant activity of coffee brews was determined in batch conditions by means of a Briggs-Rauscher oscillating system. This method consists of the measurement of the inhibition time caused by the addition of a diluted coffee sample to the oscillating system. The inhibition time vs. the relative concentration of the diluted coffee sample shows linear dependence. The slope of these lines was used to calculate a relative antioxidant activity for each sample. It was concluded that the method of preparation greatly influenced the resulting coffee brew, with the filtering method showing the best results with up to 50% higher antioxidant activity. As such, it was chosen as a standard to compare activity values. It can also be noted that decaffeinated coffee samples show significantly lower activity than caffeine-containing ones.

Keywords: *Briggs-Rauscher oscillating reaction, inhibitory effect, analytical method, coffee extract, antioxidant activity*

INTRODUCTION

One of the most consumed beverages worldwide is coffee due to its flavor and several health benefits. According to the International Coffee Organization, the annual consumption in the world is around 9.8 billion kg/year [1]. The two most popular species are *Coffea arabica* and *Coffea robusta*. The coffee beans have a complex composition containing lipids, proteins, soluble fibers, minerals, antioxidants and volatile compounds. This depends on

[a] *Babeş-Bolyai University, Faculty of Chemistry and Chemical Engineering, Department of Chemistry and Chemical Engineering, Hungarian Line of Study, 11 Arany Janos str., RO-400028, Cluj-Napoca, Romania*
[b] *Babeş-Bolyai University, Research Center for Advanced Analysis, Instrumentation and Chemometrics, ANALYTICA, 11 Arany Janos str., RO-400028, Cluj-Napoca, Romania*
** Corresponding author: norbert.muntean@ubbcluj.ro*

genetic aspects, degree of maturation, soil composition, cultivation practices, climate, etc. When comparing the two main species, it can be noted that, generally, Coffea robusta has a higher content of caffeine and antioxidants while Arabica provides a better aroma [2, 3]. It should be noted that the high level of antioxidants in Robusta has several benefits for the plant (e.g. increased resistance to plant diseases, UV-radiation). Nevertheless, this difference in antioxidant content disappears during the roasting process [3].

The health benefits of coffee are attributed to its high antioxidant content [4]. Several compounds with antioxidant properties are already present in raw coffee beans, such as chlorogenic acids (CGA), which are mainly responsible for scavenging free radicals and interactions with reactive species [5, 6, 7].

During the roasting process, due to several chemical reactions like hydrolysis, degradation, isomerization, and incorporation into melanoidins, *ca.* 99% of the CGA decomposes [8]. Nevertheless, the melanoidins and different metabolites formed during the process also show significant antioxidant properties [9, 10].

It is well known, that processing conditions (e.g. temperature, dry or wet conditions, organic solvents, water, or vapor) affect the chemical composition of the coffee beans and subsequently change their antioxidant activity too. Similarly, the quality of the coffee extract is also greatly affected by the brewing process [11]. There are several brewing techniques, such as infusion, decoction, and percolation. During infusion, the almost boiling water is passed through the roasted and ground beans under pressure and espresso coffee is obtained. In the case of decoction, to obtain the extract, the raw material is boiled, resulting in Turkish-style coffee. The beverage can be obtained by percolation too, which consists of filtering hot water through the coffee powder, dissolving the soluble compounds. The question that arises is how the preparation method influences the antioxidant activity of the coffee brew.

Several methods are used in order to determine antioxidant activity. Most of them are based on measuring the trolox equivalent antioxidant capacity (TEAC), the total radical-trapping antioxidant parameter (TRAP), the oxygen radical absorbance (ORAC) [12], and the 2,2-Diphenyl-1-picrylhydrazyl radical scavenging activity (DPPH) [13]. All these methods are based on the generation of free radicals that react with the antioxidant. Because of the different nature of the radicals, the varying pH of the environment, and the solvent used, the results obtained with different methods are not comparable [14]. A method based on the inhibition of the Briggs-Rauscher (BR) oscillating system was developed by R. Cervelatti & al., and

used for the first time to put in evidence soybean antioxidants [15]. The BR reaction consists of the oxidation of an organic substrate by iodate in an acidic medium and Mn catalyst in the presence of H_2O_2. During the reaction, free radicals are generated, among them hydroperoxyl (HOO·) and hydroxyl (HO·), which also occur naturally in the human body [16]. The BR method is based on the cessation of the oscillation due to the interaction of the radicals with the antioxidants. The total consumption of the antioxidants added to the BR active mixture cause the regeneration of the oscillatory regime. The elapsed time between the cessation and regeneration of the oscillation (*i.e.* the inhibition time) is proportional to the concentration of the antioxidant. The main advantage of the BR method, compared to other techniques, is the acidic pH of the testing system (pH≈2) appropriate to that of the human stomach fluid, which is a great opportunity to obtain information on the behavior of antioxidants in such conditions. It is well known, that the antioxidant activity of the species is dependent on the pH of the systems [16].

The aim of this work is to determine the antioxidant activity of different coffee samples with the Briggs-Rauscher method.

The novelty of the study consists in the types of commercial coffees chosen, as they are among the most widely consumed in Romania, which increases the regional significance of the findings. Additionally, as the sample preparation method (coffee brewing process) can greatly influence the antioxidant activity of the systems, a comparative study was realized to study this aspect. It should also be noted that even though the Briggs-Raucher method was previously used successfully to determine antioxidants that are present in raw and roasted coffee beans [17], information on its effective use for the coffee beverage is limited in the literature [18].

RESULTS AND DISCUSSION

Impact of the brewing method on the antioxidant activity of coffee

To determine the most effective brewing method (*i.e.* the one that results in the highest antioxidant activity), four types of coffee were studied: espresso, filtered, turkish and moka pot.

The inhibition time was determined for several dilutions and calibration curves were fitted on them [19]. Variation of the inhibition time in function of the relative antioxidant concentration was found to be linear, as can be seen in Figure 1.

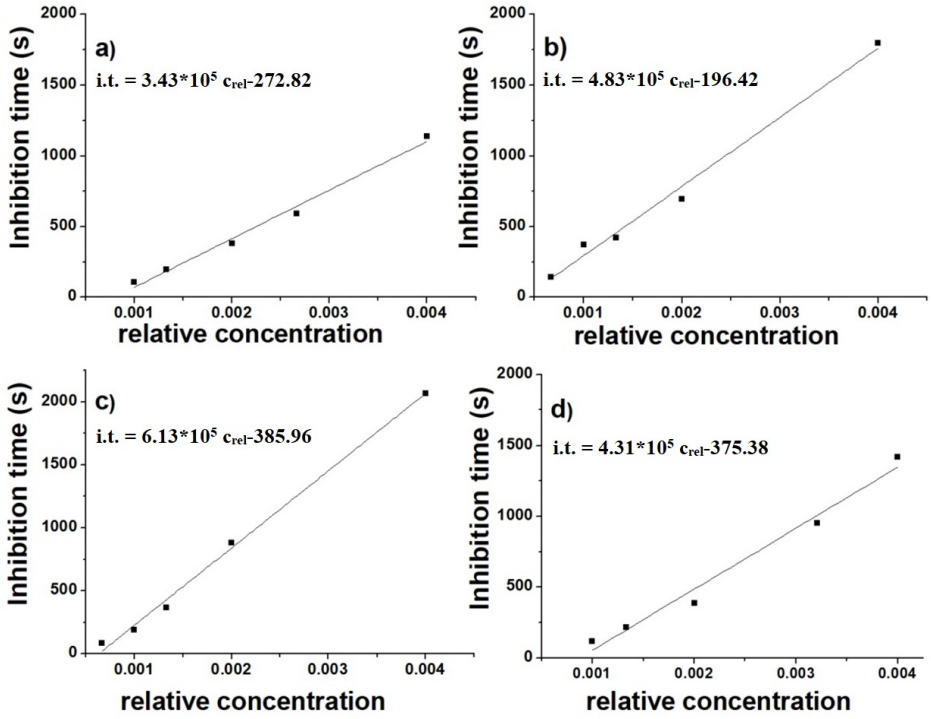

Figure 1. The calibration curves of the different types of coffee brew:
a) Espresso; b) Turkish; c) Filtered; d) Moka pot
*i.t. is the abbreviated form of inhibition time

The qualitative analytical information is the slope of the calibration curve, a higher slope gives a higher antioxidant activity.

As can be observed from Table 1., the filtering method yields a brew with the highest antioxidant activity. As such, it was chosen as the standard for further studies.

The relative antioxidant activity (R.A.S.) was also calculated as the ratio of the slope of each preparation method and that of the chosen standard (*i.e.* filtered coffee).

R.A.S. = slope(method)/slope(standard). Equation (1)

Table 1. Analytical parameters of the calibration curves obtained with different coffee brew preparation methods

Brewing method	Equations of the calibration curve	R^2
Espresso	$3.43*10^5$ c_{rel}-272.82	0.9879
Turkish	$4.83*10^5$ c_{rel}-196.42	0.9912
Filtered	$6.13*10^5$ c_{rel}-385.96	0.9965
Moka pot	$4.31*10^5$ c_{rel}-375.38	0.9951

The R.A.S. values obtained for the brewing methods are compared in Figure 2.

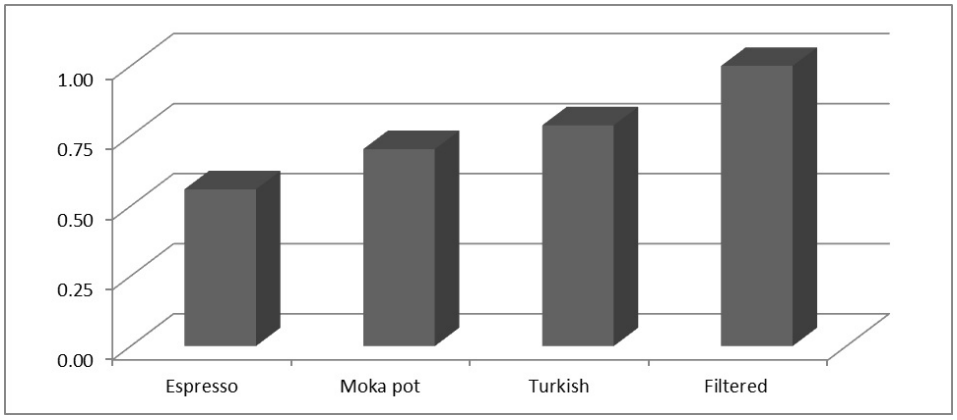

Figure 2. The R.A.S. values of the coffee brew

According to the R.A.S. values, the filtered coffee has 25-50% greater antioxidant activity than the samples prepared by other methods (Figure 2.). For example, the coffee made with an espresso machine had almost 50% less antioxidant activity. The higher antioxidant activity of the filtered coffee can be explained by the longer extraction time (approximately 10 minutes longer compared to other methods), as well as the lower extraction temperature. These results are in good accordance with literature data, which show a reduced antioxidant potential for a brew prepared with an Espresso machine compared to the Drip (Filtered) or Turkish methods [20, 21]. In the case of the filtering method, it should be noted that due to differences in the flow of hot water, results may vary significantly in the case of different brewing apparatuses [20, 21].

The antioxidant activity of different types of coffee, the effect of decaffeination

As filtering proved to be the method that yields the highest antioxidant activity, it was used for further studies regarding commercially available coffee samples.

Six types of popular commercially available coffee were studied: Lavazza, Lavazza (decaffeinated), Jacobs, Jacobs (decaffeinated), Fort, Tchibo.

The resulting calibration curves are presented in Figure 3.

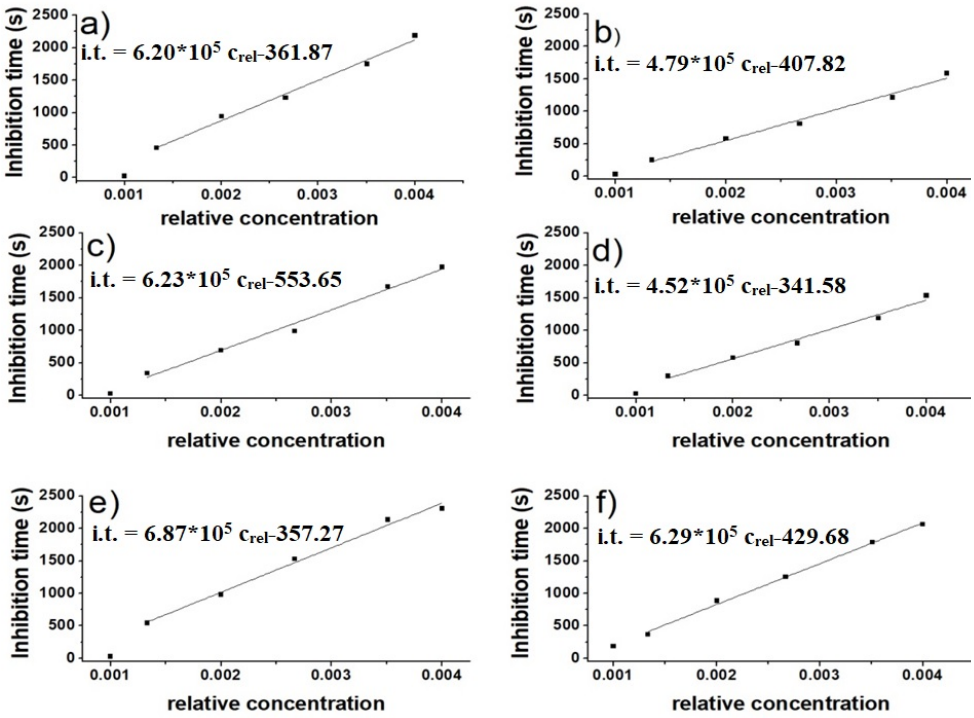

Figure 3. The calibration curves of coffee brews prepared by the filtering method from different commercially available coffees a) Lavazza; b) Lavazza (decaffeinated); c) Jacobs; d) Jacobs (decaffeinated); e) Fort; f) Tchibo
*i.t. is the abbreviated form of inhibition time

The obtained fitted calibration curves can be seen in Table 2.

Table 2. Analytical parameters of the calibration curves obtained for different commercially available coffees with the filtering method

Coffee type	Equations of the calibration curve	R^2
Lavazza	$6.20*10^5$ c_{rel}-361.87	0.9923
Lavazza (decaffeinated)	$4.79*10^5$ c_{rel}-407.82	0.9852
Jacobs	$6.23*10^5$ c_{rel}-553.65	0.9878
Jacobs (decaffeinated)	$4.52*10^5$ c_{rel}-341.58	0.9865
Fort	$6.87*10^5$ c_{rel}-357.27	0.9912
Tchibo	$6.29*10^5$ c_{rel}-429.68	0.9935

The relative antioxidant activity of each coffee brew was calculated using Equation (1), regarding the R.A.S. values. Results are compiled in Figure 4.

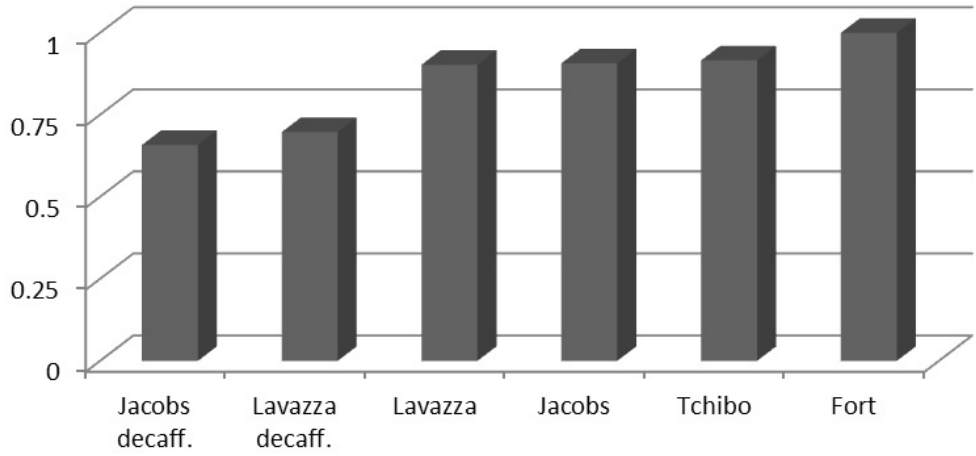

Figure 4. Comparative study of the R.A.S. values of coffee brews prepared by the filtering method from different commercially available coffees.

Results show that Fort brand coffee has the highest antioxidant activity, however, the difference between coffee brands is relatively small in the case of caffeine-containing samples (less than *ca.* 10%). This can be explained by the fact that all ground coffee was prepared in similar conditions. These results are in good accordance with literature data, which show similar antioxidant contents for coffees even if the place of origin is different, both when comparing green and roasted beans [3].

According to the two-sample t-test (95% confidence level), results show that decaffeinated coffee has a statistically significantly lower antioxidant activity (calculated t value of 6.91, with a critical t value of 2.78) compared to caffeine-containing samples. This effect of decaffeination meant that these samples had an antioxidant strength of up to *ca.* 35 % lower than the corresponding caffeine-containing coffees even though caffeine does not inhibit the active BR system. The results are probably due to the caffeine extraction process which decreases the concentration of antioxidants in the coffee beans [22]. This is in good accordance with data from the literature, showing that decaffeinated brews have *ca.* 30% lower antioxidant activity [3].

CONCLUSIONS

One purpose of this work was to study the influence of the coffee brewing method on the antioxidant activity. For this, we compared four types of brews: filtered, moka pot, turkish and espresso. It was determined that the brewing method significantly affects the antioxidant activity of the resulting coffee brew, and that the highest antioxidant activity can be obtained by the filtering method.

This was followed by a comparative study of several commercially available coffee samples. It can be concluded that in the case of caffeine-containing samples, the antioxidant activity is similar regardless of the brand. In comparison, the decaffeination process significantly reduced antioxidant activity compared to the corresponding caffeine-containing samples.

Results show similar trends to data in literature obtained by other methods, proving the effectiveness of the BR method to determine the antioxidant activity of coffee samples. The fact that the pH of the testing environment is similar to that of stomach acid constitutes an advantage when analyzing samples meant for human consumption.

EXPERIMENTAL SECTION

The proposed method was implemented by connecting a double-walled vessel with a volume of 10 mL to a FALC FA 90 thermostat. Water circulation through the temperature jacket provided a constant temperature of 20°C [19]. The oscillations were monitored electrochemically with a handmade Ag/AgI indicator electrode. The cell also contained a Pt-wire counter electrode. The system was connected to a computer through a PCI 6036 E data-acquisition interface.

The coffee brew was prepared in all cases from 10 g of ground, roasted coffee (used immediately after opening the commercial packaging) and 200 ml of distilled water. The resulting coffee brew was also used immediately after preparation. Several dilutions were prepared from this stock solution. The relative concentrations of these were calculated as the reciprocate of the dilution factor.

Chemicals and procedure

All chemicals were of analytical grade and were used without further purification. Stock solutions with the following concentration were made: $[H_2SO_4]_0$=220 mM, $[KIO_3]_0$=180 mM, $[MA]_0$=200 mM, $[MnSO_4]_0$=260 mM, $[H_2O_2]_0$=5.28 mM by using double distilled water.

The mixing order was: malonic acid, $MnSO_4$, H_2SO_4, KIO_3, and H_2O_2. Oscillations start after the addition of H_2O_2. At the third oscillation, 0.250 mL of diluted coffee brew was added to the reactor using an automatic pipette [19].

REFERENCES

1. International Coffee Organization, www.ico.org (accessed 04.05.2022)
2. R. Briandet; E.K. Kemsley; R.H. Wilson; *J. Agric. Food Chem.*, **1996**, *44(1)*, 170–174
3. A. Yashin; Y. Yashin; J.Y. Wang; B. Nemzer; *Antioxidants*, **2013**, *2(4)*, 230-245
4. A. Farah; M. Monteiro; V. Calado; L.C. Trugo; *Food Chem.,* **2006**, *98*, 373–380
5. Y.-F. Chu; *Coffee: Emerging Health Effects and Disease Prevention*, John Wiley & Sons, Inc., **2012**, pp.21-50
6. D.P. Moreira; M.C. Monteiro; M. Ribeiro-Alves, C.M. Donangelo, I.C. Trugo; *J. Agric. Food Chem.*, **2005**, *55(15)*, 6110-6117
7. F. Natella; M. Nardini; I. Giannetti; C. Dattilo; C. Scaccini; *J. Agric. Food Chem.*, **2002**, *50(21),* 6211-6216
8. D. Perrone, R. Donangelo, C.M. Donangelo, A. Farah; *J. Agric. Food Chem.*, **2010**, *58*, 12238-12243
9. C. Delgado-Andrade, F.J. Morales; *J. Agric. Food Chem.*, **2002**, *50(13),* 3698-3703
10. C. Lee; *Clin. Chim. Acta*, **2000**, *295,* 141-154
11. D. Komes; A. Belščak-Cvitanović, Effects of Preparation Techniques on the Antioxidant Capacity of Coffee Brews, in *Processing and Impact on Antioxidants in Beverages*, V. Preedy Eds.; Academic Press, **2014**, pp. 87-97
12. I. Baldim; C.R.F. Souza; A. Durazzo; M. Lucarini; A. Santini; E.B. Souto; W.P. Oliveira; *Foods*, **2020**, *9(8)*,1110

13. D. Huang; B. Ou; R.L. Prior; *J. Agric. Food Chem*., **2005**, *53(6)*, 1841–1856
14. K. Höner; R. Cervelatti; *Eur. Food Res. Technol*., **2002**, *215*, 437-442
15. R. Cervellati; N. Crespi-Perellino; S. Furrow; A. Minghetti; *Helv. Chim. Acta*, **2000**, *83*, 3179-3190
16. S. Biswas; R. Das; E.R. Banerjee; AIMS Biophys., **2017**, *4(4)*, 596-614
17. E. Džomba; S. Gojak-Salimović; *Glas. Hem. Tehnol. Bosne Herceg.,* **2017***, 48*, 9-14
18. K. Lightbourne; S. Salamah; J. Hankemeyer; K. Rivera; L.C. Fernandez-Torres; *MOL2NET'16 Conference book*, **2016**, 1-3
19. N. Muntean; G. Szabó; *Studia UBB Chemia*, **2013**, *LVII, 2,* 175 – 183
20. K. Janda; K. Jakubczyk; I. Baranowska-Bosiacka; P. Kapczuk; J. Kochman; E. Rębacz-Maron; I. Gutowska; *Foods*, **2020**, *9(2)*, 121
21. T. Niseteo; D. Komes; A. Belščak-Cvitanović; D. Horžić; M. Budeč; *Food Chem.*, **2012**, *134(4)*, 1870-1877
22. S.J.V. Vicente; Y.S. Queiroz; S.L.D. Gotlieb; E.A.F.S. Torres; *Braz. Arch. Biol. Technol.*, **2014**, *57*, 110-118.

STUDIA UBB CHEMIA, LXVII, 3, 2022 (p. 17-35)
(RECOMMENDED CITATION)
DOI:10.24193/subbchem.2022.3.02

THE PHYTOCHEMICAL ANALYSIS AND ANTIOXIDANT CAPACITY DETERMINATION OF FIVE *HYPERICUM* SPECIES

ADAEZE ADEJOKE ADEHUWA-OLABODE[a], ASMITA SAUTREAU[a], LAURIAN VLASE[b], ANA-MARIA VLASE[c,*], DANA MUNTEAN[b]

ABSTRACT. Medicinal plants are a valuable source of lead compounds and novel drugs. The *Hypericum* L. species traditionally treats skin wounds, sciatica, and depression. Presently, only a small percentage of the *Hypericum* species have been phytochemically characterised and 60% still requires analysis. Ethanolic and methanolic extracts were obtained by ultrasound assisted extraction and maceration extraction methods. Polyphenols, sterols, methoxyflavones, hyperforin and hypericin were detected through HPLC-MS analysis. ABTS assay was used to evaluate the total antioxidant capacity. *H. maculatum* and *H. moserianum* had the highest antioxidant capacity. The most abundant polyphenol in *H. humifusum, H. moserianum* and *H. miracle-pistache* was chlorogenic acid. For *H. maculatum* and *H. perforatum*, hyperoside and rutoside were the most abundant polyphenols. Sterols and methoxyflavones were quantified for the first time in all the species. β-sitosterol was the most abundant sterol across all species and ergosterol was absent in all species. Hispidulin was the only methoxyflavone (in small concentrations) found in all species except *H. miracle-pistache*. Hypericin was absent in *H. moserianum* and *H. miracle-pistache* and was most abundant in *H. maculatum.* Interestingly, *H. miracle-pistache* had higher concentrations of hyperforin than *H. perforatum.* The phytochemical profile of analysed *Hypericum* species prove to be a valuable bioactive's source.

Keywords: *Phytochemical analysis, antioxidant activity, Hypericum species, hyperforin, hypericin*

[a] *University of Portsmouth, Faculty of Pharmacy, St. Michael's Building, White Swan Road, PO1 2DT, Portsmouth, United Kingdom*

[b] *Iuliu Haţieganu University of Medicine and Pharmacy, Faculty of Pharmacy, Department of Pharmaceutical Technology and Biopharmacy, 8 Victor Babeş str., RO-400012, Cluj-Napoca, Romania*

[c] *Iuliu Haţieganu University of Medicine and Pharmacy, Faculty of Pharmacy, Department of Pharmaceutical Botany, 23 Marinescu str., RO-400337, Cluj-Napoca, Romania*

** Corresponding author: anamaria.gheldiu@yahoo.com*

INTRODUCTION

The *Hypericum* L. genus belongs to the *Hypericaceae* family containing 484 species [1]. According to medicinal folklore, the *Hypericum* species can be used both internally and externally with various therapeutic applications such as a diuretic, used to treat sciatica, skin wounds, burns, eczema, and depression [2]. Previous literature has identified flavonoids (e.g. quercetin and hyperoside), phloroglucinol derivates (e.g. hyperforin) and naphthodianthrones (e.g hypericin) as common constituents to the *Hypericum* species [3]. Presently, only a small percentage of the *Hypericum* species have been phytochemically characterized and 60% still require analysis [4]. This propels the need to screen more *Hypericum* species for novel bioactives with pharmacological properties.

H. perforatum (St. John's wort) is the most commercially recognized member of the species, with a range of pharmacological properties [5]. These include antiviral, anti-inflammatory, wound-healing, and apoptosis-inducing properties [6]. Many studies have demonstrated its high efficacy in treating mild to moderate depression with few adverse effects, making it safer compared to other antidepressants [7]. Hyperforin (responsible for the antidepressant activity) and hypericin (causes photosensitivity to the skin) are the two most studied phytochemicals in *H. perforatum.* However, research has concluded that the broad range of pharmacological activities of *H. perforatum* is not dependent on a single compound [8] but is a result of the synergistic efforts of several constituents, which cannot be separated into active compounds [10].

Hyperforin, a natural phloroglucinol [9], is the most neuroprotective bioactive in the plant [10], eminent for its treatment of mild to moderate depression with fewer side effects over other major antidepressants [11]. Hyperforin inhibits serotonin uptake by activating the transient receptor potential channel protein 6 (TRPC6) [12]. This increases the intracellular concentrations of sodium and calcium, resulting in a decreased sodium gradient between the neurons and synapse, which ultimately decreases monoamine neurotransmitter reuptake. This mechanism differs from the conventional antidepressants, possibly pointing to a new class of antidepressants [13]. Hyperforin also displays antitumor, antiangiogenic, and antibacterial activity [16].

Hypericin is a polycyclic quinone [14] with four hydroxyl groups adjacent to two carbonyl groups [15]. The hydroxyl hydrogen can transfer the hydroxyl oxygen and carbonyl oxygen in the presence of fluorescent light due to the resonance of the structure and relatively short distance between the oxygen atoms (~2.5 Å). As a result, when exposed to fluorescent light, the hydrogen is constantly in flux between the two oxygen atoms. This makes hypericin very photoreactive, as it can generate reactive oxygen species and

singlet oxygen ($^1O_2$), acting as a sensitizer in photodynamic reactions (type II mechanism) [16]. This can lead to lipid peroxidation, severe necrosis and sunburn to the skin when ingested excessively by humans [17]. However, the photo-reactivity of hypericin has demonstrated antiviral properties, including the inhibition of protein-kinase activity needed for replication of some viruses [18].

Considering the pharmacological and possible therapeutic uses of hypericin and hyperforin, quantifying their concentrations in each *Hypericum* species were of special interest. Identifying more natural sources of these compounds could be used for more clinical studies.

Lipid peroxidation and free radicals contribute pathogenically to some chronic diseases such as atherosclerosis, coronary heart disease and cancer [19]. The cardioprotective and anticarcinogenic effects of phenolic compounds are attributed to their antioxidant activity which alleviates lipid peroxidation and obviates free radicals [20]. Several epidemiological studies have agreed that exogenous antioxidant intake effectively prevents or suppress such diseases. Therapeutic use of natural antioxidants has gained global interest for preventing oxidative damage. Numerous phytochemicals in Hypericum reportedly act as antioxidants, such as flavonoids and tannins. These have displayed radical scavenging in a dose-dependent manner, showing potential for therapeutic drug use for conditions associated with free radical pathology [21].

Very few phytochemical and antioxidant reports exist for *H. humifusum, H. maculatum* and *H. moserianum* and no previous study exist for *H. miracle-pistache.* The present study aims to investigate the phytochemical profile and total antioxidant capacity of *H. moserianum, H. miracle-pistache, H. perforatum, H. humifusum* and *H. maculatum*, to assess whether they are good sources of bioactives, with special interest in their hyperforin and hypericin content.

Polar solvents such as methanol and ethanol are extensively used to extract various compounds from plants [22]. The diversified polarities and chemical properties of bioactives influences their solubility in a solvent, which then affects the extraction yield. As solvent type affects antioxidant capacity and extraction yield, methanol 25% (v/v), ethanol 50% (v/v), and ethanol 70% (v/v) were used as solvents to maximize the yield of phytochemical compounds in the extracts.

RESULTS AND DISCUSSION

A thorough analysis of the phytochemical profile of five *Hypericum* species was assessed. In addition, the antioxidant activity of the ethanolic and methanolic extracts was performed by using the ABTS assay. The tested vegetal extracts were obtained by two distinct methods: ultrasound assisted extraction (UAE) and maceration (ME).

UAE is known to increase the yield of extracts with shorter extraction time. The acoustic cavitation destroys the cell walls and increases contact between the phytochemicals and the solvent, by reducing particle size. However, longer extraction periods with ultrasound (>20 minutes) can induce degradation of some phytochemicals such as polyphenols, resulting in a lower yield. Therefore, samples were subject to UAE treatment for 10 minutes only. Compared to UAE, extraction by maceration (ME) carries no phytochemical degradation risk and was applied to a separate batch of each sample, to ensure all phytochemicals were in conditions favourable for their extraction.

Evaluation of polyphenols

A complex phenolic profile was displayed by all five *Hypericum* species, as they contained most polyphenols including chlorogenic acid, hyperoside, isoquercitrin, quercitrin, quercetol, epicatechin, and rutoside. The results of the phytochemical analysis are summarized in Table 1 and are expressed as mg/100 g of dry weight (d.w.) plant material.

Concentrations of chlorogenic acid ranged from 2.214 mg/100 g d.w. in *H. perforatum* (sample 20) to 1350.072 mg/100 g d.w. in *H. miracle-pistache* (sample 27). Chlorogenic acid was the most abundant polyphenol in *H. humifusum*, *H. moserianum* and *H. miracle-pistache* (983.023 mg/100 g d.w., 1160.206 mg/100 g d.w. and 1350.072 mg/100 g d.w. respectively). *H. perforatum* had the least amount across all the extraction and solvent conditions.

Hyperoside was the most abundant polyphenol in *H. maculatum* and concentrations ranged from 33.782 mg/100 g d.w. (sample 12) to 1689.227 mg/100 g d.w. (*H. maculatum*, sample 8) across the five species. Methanolic extracts of each species yielded the highest hyperoside concentrations, regardless of the extraction method.

Rutoside was the most abundant polyphenol in *H. perforatum* (1143.468 mg/100 g d.w., sample 6) and was not detected in *H. miracle-pistache* under other conditions, except for sample 13 (1.005 mg/100 g d.w.). *H. humifusum* had the lowest concentration of rutoside (0.857 mg/100 g d.w., sample 7) and was below levels of detection in other conditions. Methanolic extracts of all five *Hypericum* species yielded the highest amount of rutoside, particularly in the UAE batch.

The concentration of isoquercitrin ranged from 7.593 mg/100 g d.w. in *H. perforatum* (sample 25) to 1130.729 mg/100 g d.w. in *H. maculatum* (sample 8). Epicatechin was present in all five *Hypericum* species, ranging from 14.517 mg/100 g d.w. in *H. humifusum*, (sample 16) to 290.829 mg/100 g d.w. in *H. maculatum* (sample 8). Quercitrin concentration ranged from 1.861 mg/100 g d.w. in *H. miracle-pistache* (sample 13) to 702.580 mg/100 g d.w. in

Table 1. Concentration of polyphenols (mg/100 g d.w.) in five Hypericum species extracts assessed with LC-MS analytical method

Sample Code	Vegetal species	Extraction method	Solvent (v/v)	Gentisic acid	Chlorogenic acid	p-Coumaric acid	Ferulic acid	Hyperoside	Isoquercitrin	Rutoside	Quercitrin	Quercetin	Luteolin	Kaempferol	Apigenin	Epicatechin	Catechin	Syringic acid	Gallic acid	Proto-catechuic acid	Vanillic acid
1	H. per	UAE	EtOH70%	x	4.026	3.691	2.225	204.717	72.627	578.471	84.496	222.270	0.951	5.391	ND	62.634	39.298	ND	1.209	7.372	3.491
2	H. hum	UAE	EtOH70%	x	587.061	ND	ND	114.844	54.904	x	37.757	18.690	2.058	x	ND	21.192	1.422	1.821	2.269	15.294	1.726
3	H. mac	UAE	EtOH70%	x	231.940	3.450	4.501	723.119	345.243	11.249	36.635	675.484	2.334	8.177	0.775	215.578	61.124	ND	1.933	18.467	3.754
4	H. m-p	UAE	EtOH70%	ND	1311.570	1.464	ND	488.019	352.948	ND	7.282	35.189	ND	0.947	ND	126.219	35.407	ND	ND	0.932	ND
5	H. mos	UAE	EtOH70%	ND	1059.876	ND	ND	89.344	50.127	220.858	495.244	8.542	ND	ND	ND	108.149	76.981	ND	0.442	1.284	ND
6	H. per	UAE	MtOH25%	x	4.328	4.895	3.590	526.373	218.721	1143.468	133.866	48.586	1.435	2.870	0.775	92.997	83.243	1.650	2.048	17.925	5.948
7	H. hum	UAE	MtOH25%	x	983.023	x	ND	308.791	155.999	0.857	93.844	5.624	3.648	x	ND	36.685	4.195	3.545	3.702	37.306	1.810
8	H. mac	UAE	MtOH25%	x	244.472	5.858	7.028	1689.227	1130.729	26.984	88.235	229.758	3.302	4.328	ND	290.829	95.160	1.333	2.803	31.918	6.401
9	H. mos	UAE	MtOH25%	ND	1160.206	x	ND	130.807	75.093	298.052	702.550	1.550	ND	ND	ND	158.731	107.665	1.765	ND	0.670	ND
10	H. per	UAE	EtOH50%	x	4.479	3.149	2.478	72.551	10.059	253.962	66.548	47.026	ND	x	ND	73.669	55.317	ND	2.247	10.614	4.831
11	H. hum	UAE	EtOH50%	x	669.952	x	x	83.436	32.867	x	37.383	52.367	1.712	1.411	ND	26.958	2.951	2.264	3.614	19.918	3.393
12	H. mac	UAE	EtOH50%	x	144.821	3.811	6.068	33.762	8.826	x	50.657	103.734	0.329	1.212	ND	196.712	56.025	ND	2.981	24.189	6.337
13	H. m-p	UAE	EtOH50%	ND	1302.511	1.284	x	380.213	252.162	1.005	1.861	83.529	ND	2.670	ND	117.755	38.118	ND	ND	1.614	ND
14	H. mos	UAE	EtOH50%	ND	1136.048	ND	ND	88.826	45.196	223.976	513.940	15.039	ND	0.253	ND	133.539	93.156	ND	ND	1.450	ND
15	H. per	ME	EtOH70%	x	3.346	3.571	2.630	202.436	70.161	588.863	100.949	302.762	1.228	6.356	0.873	46.722	39.601	ND	2.141	14.403	3.646
16	H. hum	ME	EtOH70%	x	687.165	ND	ND	131.222	62.764	x	45.796	31.445	2.472	0.850	ND	14.517	1.657	2.014	2.793	23.464	2.029
17	H. mac	ME	EtOH70%	x	184.449	4.293	5.815	485.842	219.337	9.616	46.731	794.800	2.403	9.958	ND	202.947	63.522	ND	3.305	24.730	5.927
18	H. m-p	ME	EtOH70%	ND	1254.799	1.404	x	448.110	322.743	ND	6.722	41.190	ND	1.212	ND	89.105	30.185	ND	0.519	1.440	ND
19	H. mos	ME	EtOH70%	ND	1126.385	ND	ND	94.837	52.265	236.000	526.092	13.002	ND	x	ND	93.292	72.588	ND	ND	1.415	ND
20	H. per	ME	MtOH25%	x	2.214	2.848	1.872	308.998	125.496	645.125	69.186	27.151	0.951	1.875	ND	47.044	32.647	0.614	1.338	9.726	3.508
21	H. hum	ME	MtOH25%	x	475.029	ND	ND	160.869	79.716	x	48.787	2.166	2.127	x	ND	19.005	2.682	1.987	1.844	18.492	1.204
22	H. mac	ME	MtOH25%	x	117.115	3.510	3.287	846.785	565.309	13.178	62.622	118.930	1.435	2.937	ND	155.528	48.945	0.924	1.091	19.044	3.760
23	H. m-p	ME	MtOH25%	ND	807.501	1.344	ND	476.720	335.380	ND	7.843	3.312	ND	ND	ND	108.943	34.474	2.068	ND	0.517	ND
24	H. mos	ME	MtOH25%	ND	943.314	ND	ND	103.960	60.295	238.572	561.614	2.101	ND	ND	ND	120.563	102.071	1.710	ND	0.697	ND
25	H. per	ME	EtOH50%	x	5.762	3.510	3.894	60.006	7.593	218.038	51.592	48.513	ND	x	ND	70.155	50.863	ND	2.494	11.784	4.824
26	H. hum	ME	EtOH50%	x	856.817	1.645	x	70.996	25.316	x	39.439	63.158	2.265	1.676	ND	28.001	3.199	2.530	4.339	22.533	5.298
27	H. m-p	ME	EtOH50%	ND	1350.072	1.404	6.877	341.755	215.839	x	5.226	125.261	ND	3.799	ND	98.820	33.295	ND	0.413	1.842	ND
28	H. mos	ME	EtOH50%	ND	1105.398	ND	ND	83.124	38.723	217.295	515.435	18.617	ND	0.452	ND	115.877	87.561	ND	ND	1.587	ND

H. per - H. perforatum, H. hum - H. humifusum, H. mac - H. maculatum, H. m-p - H. miracle-pistache and H. mos - H. moserianum. EtOH 70% - Ethanol 70% (v/v), EtOH 50% - Ethanol 50% (v/v), MtOH 25% - Methanol 25% (v/v).aftaric acid, caffeic acid, sinapic acid, myricetol and patuletin were not detected in any of the five species and therefore not represented on the results table. ND – Not determined, X – found in traces, identified on MS.

H. moserianum, (sample 9). With regards to the experiment conditions, UAE and methanolic extracts of all five *Hypericum* species had higher yields of isoquercitrin, quercitrin and epicatechin than their counterparts.

Regarding *H. humifusum*, Toiu *et al*. [23] reported lower chlorogenic acid concentration (<0.02 mg/100 g d.w.), but Nogueira *et al*. [24] reported a significantly higher amount (4.18 mg/100 g d.w.) than the present study. Toiu *et al*. [25] found higher levels of rutoside (1.4±0.09 mg/100 g d.w.) but reported similar levels of hyperoside (229.83±5.42 mg/100 g d.w.) and lower levels of quercitrin (27.08±2.64 mg/100 g d.w.) in ethanolic extracts.

Oniga et al. [25] reported significantly lower levels of chlorogenic acid (27.15±0.19 mg/100 g d.w.) in methanolic extracts of *H. maculatum*, similar levels of rutoside (11.00±0.1 mg/100 g d.w.) and hyperoside (545.14±2.96 mg/100 g d.w.). However, UAE extracted significantly higher hyperoside levels in the present study (sample 8).

The polyphenolic profile of *H. perforatum* reported by *Silva et al*. [26] was congruent the present study. However, higher levels of *p*-coumaric acid (32.2±0.16 mg/100 g d.w.) was reported by Wojdyło *et al*. [27] for *H. perforatum*. For *H. miracle-pistache*, Crockett *et al*. [28] only qualitatively reported the presence of isoquercitrin and quercitrin. Differences between the present study and comparative studies can be accounted for by factors such as genetic variation within the plant species, soil composition or geographical origins, which can affect phytochemical composition [29].

Evaluation of methoxyflavones

Three distinct methoxyflavones (hispidulin, hypericin, and hyperforin) were identified in the evaluated *Hypericum* species. The results are given in Table 2 and are expressed as mg/100 g of dry weight (d.w.) plant material.

The concentration of hispidulin ranged from 0.010 mg/100 g d.w. (*H. moserianum*, sample 28) to 0.432 mg/100 g d.w. (*H. maculatum*, sample 3). Hispidulin was absent in *H. moserianum* (except in sample 28) and *H. miracle-pistache*.

Hyperforin was absent in *H. humifusum* but was present in low concentrations in the other species, ranging from 4.583 mg/100 g d.w. in *H. miracle-pistache* (sample 4) to 0.022 mg/100 g d.w. in *H. moserianum* (sample 28). Similar results for ethanolic extracts *H. perforatum* were reported by Maggi *et al.* [30] Hyperforin was absent in all methanolic extracts, except *H. miracle-pistache* (sample 23) and *H. moserianum* (sample 9 and 24), suggesting methanol as the least favourable solvent for hyperforin extraction. However, other studies have successfully extracted hyperforin in methanol [32]. Ethanol 70% (v/v) yielded the highest amounts of hyperforin for both extraction techniques, presenting as the most favourable solvent.

Table 2. Concentration of hypericin and hyperforin (mg/100 g d.w.) in five Hypericum species

Sampl. code	*Vegetal species*	*Extraction method*	*Solvent (v/v)*	*Hispidulin*	*Hypericin*	*Hyperforin*
1	*H. per*	UAE	EtOH 70%	0.111	5.892	0.155
2	*H. hum*	UAE	EtOH 70%	0.061	0.884	ND
3	*H. mac*	UAE	EtOH 70%	0.432	5.695	0.051
4	*H. m-p*	UAE	EtOH 70%	ND	ND	4.583
5	*H. mos*	UAE	EtOH 70%	ND	ND	0.049
6	*H. per*	UAE	MeOH 25%	0.160	0.110	ND
7	*H. hum*	UAE	MeOH 25%	0.097	1.567	ND
8	*H. mac*	UAE	MeOH 25%	0.379	1.855	ND
9	*H. mos*	UAE	MeOH 25%	ND	ND	0.032
10	*H. per*	UAE	EtOH 50%	0.021	0.857	0.536
11	*H. hum*	UAE	EtOH 50%	0.053	0.181	ND
12	*H. mac*	UAE	EtOH 50%	0.063	2.829	0.082
13	*H. m-p*	UAE	EtOH 50%	ND	ND	0.091
14	*H. mos*	UAE	EtOH 50%	ND	ND	ND
15	*H. per*	ME	EtOH 70%	0.087	5.092	0.352
16	*H. hum*	ME	EtOH 70%	0.062	0.023	ND
17	*H. mac*	ME	EtOH 70%	0.255	6.419	0.134
18	*H. m-p*	ME	EtOH 70%	ND	ND	2.056
19	*H. mos*	ME	EtOH 70%	ND	ND	0.069
20	*H. per*	ME	MeOH 25%	0.064	ND	ND
21	*H. hum*	ME	MeOH 25%	0.056	1.631	ND
22	*H. mac*	ME	MeOH 25%	0.147	0.099	ND
23	*H. m-p*	ME	MeOH 25%	ND	ND	0.800
24	*H. mos*	ME	MeOH 25%	ND	ND	0.054
25	*H. per*	ME	EtOH 50%	0.019	1.482	0.357
26	*H. hum*	ME	EtOH 50%	0.064	0.260	ND
27	*H. m-p*	ME	EtOH 50%	ND	ND	0.062
28	*H. mos*	ME	EtOH 50%	0.010	ND	0.022

H. per - H. perforatum, H. hum - H. humifusum, H. mac - H. maculatum, H. m-p - H. miracle-pistache and H. mos - H. moserianum. ND – Not determined. UAE-ultrasound assisted extraction; ME-maceration. EtOH 70% - ethanol 70% (v/v), EtOH 50% - ethanol 50% (v/v), MtOH 25% - methanol 25% (v/v).

Hypericin was absent in *H. moserianum* and *H. miracle-pistache*. *H. maculatum* (6.419 mg/100 g d.w., sample 17) had the highest amount of hypericin, and *H. humifusum* (0.023 mg/100 g d.w., sample 16) had the lowest. Similar results for methanolic extracts of *H. maculatum* were reported by Mártonfi *et al*. [31] in the stamen (0.058 mg/g d.w.), but higher concentrations were found in the petals (0.096 mg/g d.w.). Ethanolic extracts (EtOH 70%) obtained by UAE of *H. perforatum* had a significantly higher amount of hypericin than *H. humifusum* (5.892 mg/100 g d.w., 0.884 mg/100 g d.w. respectively) in the present study. However, *Nogueira et al*. [26] reported the opposite and found higher concentrations of hypericin (0.24 mg/100 g d.w.) in *H. humifusum* than in *H. perforatum* (0.07 mg/100 g d.w.). Ethanol 70% (v/v) yielded the highest concentrations of hypericin (samples 1,3,15 and 17).

Considering the pharmacological and possible therapeutic use of hypericin and hyperforin, quantifying their concentrations in each *Hypericum* species were of special interest. Identifying more natural sources of these compounds could be used for more clinical studies. Interestingly, *H. miracle-pistache* had higher concentrations of hyperforin than *H. perforatum* (sample 4 and 18 compared to sample 1 and 15 respectively). This suggests that *H. miracle-pistache* could be more efficacious in treating mild to moderate depression with fewer chances of causing photosensitivity to the skin as no hypericin was detected in the species (samples 4 and 18). However, additional clinical research is required to verify this hypothesis.

Evaluation of sterols

The results for the identification and quantification of sterols in *Hypericum* species are summarized in Table 3. All sterols (except ergosterol) were identified in all five species in varying amounts. The concentration of stigmasterol ranged from 0.338 mg/100 g d.w. (sample 3) to 16.008 mg/100 g d.w. (sample 23). β-Sitosterol was the most abundant sterol found in all five *Hypericum* species, ranging from 0.582 mg/100 g d.w. (*H. moserianum*, sample 19) to 386.767 mg/100 g d.w. (*H. miracle-pistache*, sample 23). Campesterol concentrations ranged from 0.062 mg/100 g d.w. (*H. humifusum*, sample 7) to 1.778 mg/100 g d.w. (*H. maculatum*, sample 22).

Hernández *et al*. was the only previous study that identified campesterol, β-sitosterol and stigmasterol in *H. perforatum* and confirmed the absence of ergosterol [32]. However, the study did not quantify the sterols. This is the first report to identify and quantify sterols in the aerial parts of the assessed *Hypericum* species (except *H. perforatum*).

Table 3. The concentration of sterols (mg/100 g d.w.) in five Hypericum species extracts

Sample code	*Vegetal species*	*Extraction method*	*Solvent (v/v)*	*Stigmasterol*	*Beta-Sitosterol*	*Campesterol*
1	*H. per*	UAE	EtOH70%	2.658	75.335	0.582
2	*H. hum*	UAE	EtOH70%	1.349	13.345	0.202
3	*H. mac*	UAE	EtOH70%	0.338	9.306	0.068
4	*H. m-p*	UAE	EtOH70%	0.401	9.994	ND
5	*H. mos*	UAE	EtOH70%	ND	ND	ND
6	*H. per*	UAE	MtOH25%	0.755	13.309	0.140
7	*H. hum*	UAE	MtOH25%	0.378	2.956	0.062
8	*H. mac*	UAE	MtOH25%	ND	1.979	ND
9	*H. mos*	UAE	MtOH25%	15.808	365.674	0.767
10	*H. per*	UAE	EtOH50%	ND	ND	ND
11	*H. hum*	UAE	EtOH50%	ND	ND	ND
12	*H. mac*	UAE	EtOH50%	ND	1.637	ND
13	*H. m-p*	UAE	EtOH50%	ND	ND	ND
14	*H. mos*	UAE	EtOH50%	ND	ND	ND
15	*H. per*	ME	EtOH70%	0.872	14.695	0.160
16	*H. hum*	ME	EtOH70%	0.987	10.304	0.174
17	*H. mac*	ME	EtOH70%	0.619	16.592	0.112
18	*H. m-p*	ME	EtOH70%	6.811	170.129	0.625
19	*H. mos*	ME	EtOH70%	ND	0.582	ND
20	*H. per*	ME	MtOH25%	5.489	99.799	0.941
21	*H. hum*	ME	MtOH25%	3.338	35.187	0.547
22	*H. mac*	ME	MtOH25%	9.096	334.936	1.778
23	*H. m-p*	ME	MtOH25%	16.008	386.767	0.966
24	*H. mos*	ME	MtOH25%	9.643	214.720	0.507
25	*H. per*	ME	EtOH50%	ND	ND	ND
26	*H. hum*	ME	EtOH50%	ND	ND	ND
27	*H. m-p*	ME	EtOH50%	ND	ND	ND
28	*H. mos*	ME	EtOH50%	ND	ND	ND

H. per - H. perforatum, H. hum - H. humifusum, H. mac - H. maculatum, H. m-p - H. miracle-pistache and H. mos - H. moserianum. ND – Not determined. UAE-ultrasound assisted extraction; ME-maceration. EtOH 70% - ethanol 70% (v/v), EtOH 50% - ethanol 50% (v/v), MtOH 25% - methanol 25% (v/v).

A pattern was evident for all sterols with regards to extraction techniques and solvents used. Ethanol 50% (v/v) extracted no sterols in all five *Hypericum* species, except in *H. maculatum* where β-sitosterol (sample 12) was extracted. This suggested that ethanol 50% (v/v) was the least favourable solvent for sterol extraction. The richest extracts of each sterol were obtained using methanol 25% (v/v) with ME, followed by ethanol 70% (v/v) with UAE. For *H. moserianum*, methanol was the only solvent to successfully extract stigmasterol (sample 9 and 24, UAE and ME respectively). This suggested that the optimum conditions for β-sitosterol, campesterol and stigmasterol extraction was methanol and ME.

The evaluation of antioxidant activity

The ABTS assay is widely used to assess antioxidant capacity. Total antioxidant capacity (TAC) indicates the additive and synergistic action of all antioxidants present in a complex sample [33]. The results of this assay are expressed as Trolox equivalents (TE) per L of plant extract and are given in Table 4.

As the TAC for each *Hypericum* species were tested under a combination of six different conditions, the highest antioxidant level for each species were compared. The total antioxidant capacity ranged from 83.788 mM TE/L for *H. moserianum* (sample 14) and *H. maculatum* (sample 3 and 8) to 46.288 mM TE/L in *H. humifusum* (sample 7). Sample 9 for *H. moserianum* (15.227 mM TE/L) presents as an outlier as it was much lower than other results for *H. moserianum* in their respective conditions (samples 5,14, 19 and 28). Most of the extracts displayed the greatest antioxidant capacity in ethanol 50% (v/v). All *Hypericum* species (except *H. miracle-pistache*), displayed their highest antioxidant activity under UAE, however the ME counterparts also displayed similar antioxidant levels (see Table 4).

The strong TAC of *H. maculatum* (101.8 ± 1 μM TE/g) was supported by Zheleva-Dimitrova *et al*. [34] The same study reported significant scavenging ability for *H. perforatum* (81.2% ± 0.4 for ABTS), however the present study found moderate scavenging ability (58.788 mM TE/L, sample 10) for *H. perforatum*.

Flavonoids and polyphenols are major contributors to antioxidant activity, due to their ability to limit the oxidative degradation of lipids [35]. Phenolic compounds act as hydrogen donors, reducing agents and free radical scavengers [36]. The number of hydroxyl groups in the aromatic ring of a phenolic compound contributes to the difference in antioxidant activity between phenolic compounds. According to Zhang *et al.* [37], phenolic compounds with five hydroxyl groups (such as catechin and epicatechin),

present as the most active free radical scavengers. For flavonoids, the 4-carbonyl (ring Z), 3',4'-orthodihydroxy structure (ring Y), and 3,5-OH groups (creating a catechol-like structure in ring Z) ensures effective radical scavenging. The C2=C3 double bond in configuration with the 4-keto arrangement is responsible for electron delocalization from ring Y, resulting in increased radical-scavenging activity. The catechol structure in ring X compensates for antioxidant capacity in absence of the *o*-dihydroxy structure (ring Y) (see Figure 1) [27].

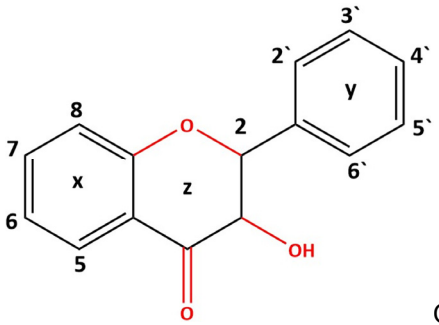

Quercetin (OH -3', 4', 5, 7)

Figure 1. General structure of flavonoids with annotations for quercetin. For quercetin, the catechol structure (ring Y), 2,3-double bond joined to the 4-carbonyl group (ring Z) allows delocalization of the phenoxyl radical electron to the flavonoid nucleus. Increase in resonance stabilization for electron delocalization is attributed to the 3-hydroxy group with the 2,3-doube bond, resulting in higher antioxidant value [27]

Glycosides formed from quercetin (a flavonoid) such as isoquercitrin, hyperoside and quercitrin, also display antioxidant activity. However, compared to quercetin, the glycosides are more water soluble due to the sugar portion of the molecules and a higher degree of absorption, leading to greater bioavailability in the body [38].

The highest concentration of quercitrin (794.800 mg/100 g d.w., sample 17) was found in *H. maculatum*, which also had a high concentration of hyperoside (1689.227 mg/100 g d.w., sample 8) and isoquercitrin (1130.729 mg/100 g d.w., sample 8) (Table 1). *H. moserianum* had high levels of chlorogenic acid (1160.206 mg/100 g d.w., sample 9) with high quercitrin levels (702.580 mg/100 g d.w., sample 9). The present study supports the correlation of antioxidant capacity to phenolic compounds as species that contained the highest concentrations of polyphenols and flavonoids corresponded with species that displayed high antioxidant activity.

Table 4. Trolox equivalent antioxidant capacity (TEAC) of five Hypericum species (expressed as mM TE/L - Trolox equivalent/L plant extract)

Sample code	***Vegetal species***	***Extraction method***	***Solvent (v/v)***	**TEAC *(mM TE/L)***
1	*H. per*	UAE	EtOH70%	35.682
2	*H. hum*	UAE	EtOH70%	44.015
3	*H. mac*	UAE	EtOH70%	83.788
4	*H. m-p*	UAE	EtOH70%	59.167
5	*H. mos*	UAE	EtOH70%	77.727
6	*H. per*	UAE	MtOH25%	56.894
7	*H. hum*	UAE	MtOH25%	46.288
8	*H. mac*	UAE	MtOH25%	83.788
9	*H. mos*	UAE	MtOH25%	15.227
10	*H. per*	UAE	EtOH50%	58.788
11	*H. hum*	UAE	EtOH50%	41.742
12	*H. mac*	UAE	EtOH50%	72.424
13	*H. m-p*	UAE	EtOH50%	70.909
14	*H. mos*	UAE	EtOH50%	83.788
15	*H. per*	ME	EtOH70%	47.424
16	*H. hum*	ME	EtOH70%	40.606
17	*H. mac*	ME	EtOH70%	74.318
18	*H. m-p*	ME	EtOH70%	60.303
19	*H. mos*	ME	EtOH70%	75.076
20	*H. per*	ME	MtOH25%	27.727
21	*H. hum*	ME	MtOH25%	36.818
22	*H. mac*	ME	MtOH25%	48.561
23	*H. m-p*	ME	MtOH25%	58.030
24	*H. mos*	ME	MtOH25%	78.485
25	*H. per*	ME	EtOH50%	53.106
26	*H. hum*	ME	EtOH50%	39.467
27	*H. m-p*	ME	EtOH50%	72.803
28	*H. mos*	ME	EtOH50%	78.485

H. per - H. perforatum, H. hum - H. humifusum, H. mac - H. maculatum, H. m-p - H. miracle-pistache and H. mos - H. moserianum. UAE-ultrasound assisted extraction; ME-maceration. EtOH 70% - ethanol 70% (v/v), EtOH 50% - ethanol 50% (v/v), MtOH 25% - methanol 25% (v/v).

CONCLUSIONS

In this study, *H. perforatum, H. humifusum, H. maculatum, H. miracle-pistache and H. moserianum* were investigated for their phytochemical profile and antioxidant activity. To the best of the authors knowledge, stigmasterol, campesterol, β-sitosterol and hispidulin were quantified for the first time in all assessed species. Among the polyphenols determined, chlorogenic acid, hyperoside, rutoside, isoquercitrin, quercitrin and quercetol were abundant across all five species. *H. maculatum* had the highest hypericin concentration and can be further investigated for photo-induced cytotoxic activity. *H. miracle-pistache* contained the highest hyperforin concentration which was of interest as *H. perforatum* is commercially marketed due to its antidepressant activity. However, with considerably higher amounts of hyperforin found in *H. miracle-pistache*, it may prove more effective than *H. perforatum* with even slimmer chances of photosensitivity as no hypericin was detected. However, more clinical research regarding its efficacy, therapeutic dose and safety for consumption is suggested before it can also be considered for commercial use. *H. maculatum* and *H. moserianum* exhibited the highest antioxidant activity, while *H. humifusum* presented with the lowest. Therefore, the *Hypericum* species serve as a useful source of bioactives, to the nutraceutical and pharmaceutical industry.

A key finding of this study was that *H. miracle-pistache* contained higher amounts of hyperforin than *H. perforatum* and hypericin was absent in the species. Several factors such as genetic variation within the plant species, soil composition or geographical origins can affect the phytochemical composition and consequently *in vitro* and *in vivo* activity. More specific to this study, the use of different extraction methods (UAE and ME) and different solvents influence the yield. Little comparative studies exist for *H. miracle-pistache*, so further phytochemical research should be conducted on the species to account for these factors and further certify the chemical composition of the species.

Further research into the clinical safety of ingesting *H. miracle-pistache* could also be conducted. This should highlight any adverse effects and a safe maximum amount which can be consumed daily. Finally, the clinical efficacy for mild to moderate depression could be assessed and compared to *H. perforatum*, with a safe and effective therapeutic dose identified. As *H. miracle-pistache* contained high amounts of chlorogenic acid and hyperoside, other clinical applications to conditions such as diabetes or Alzheimer's disease could be assessed.

EXPERIMENTAL SECTION

2.1 – Collection and identification of plant materials

Hypericum perforatum, Hypericum humifusum and *Hypericum maculatum* were gifted by Prof. Laurian Vlase. Fresh *Hypericum moserianum* and *Hypericum miracle-pistache* plants were store bought from a local supplier in Cluj-Napoca, Romania. Dr. Vlase Ana-Maria confirmed the authenticity of the plants, and a voucher specimen was deposited for each species at the Department of Pharmaceutical Botany, Faculty of Pharmacy. Aerial parts of each *Hypericum* species were prepared for lyophilisation by freezing for three hours at -20°C. The samples were lyophilised (SP Scientific Advantage 2.0, USA) at -55°C, 200 mTorr for one day and at -25°C, 200 mTorr for another four days. The samples were then milled into a powder and stored in amber glass bottles.

2.2 - Preparation of methanolic and ethanolic extracts

200 mg of each *Hypericum* species were mixed with the extraction solvents (2 ml of methanol 25% (v/v), ethanol 70% (v/v) and ethanol 50% (v/v)) in separate test-tubes for each solvent. An aliquot of each sample was filtered by centrifuge (Sigma 3-30 KHS, Sigma Laborzentrifugen GmbH, Germany) at the following settings: 25°C for 10 minutes at 10000 min^{-1}, 9168 g^{-1}, 12154 rotor. Ultrasound-assisted extraction (UAE) was performed (Transsonic 700, Elma D-788224, Singen, Germany) at 35 kHz, for 10 minutes every hour, for five hours daily, for nine days. For maceration (ME) the mixtures were shaken hourly, for five hours daily, for nine days.

2.3 - Determination of total antioxidant capacity

Total radical scavenging capacity was measured by ABTS assay previously described [39]. The Trolox equivalent antioxidant capacity (TEAC) assay reflects the ability of antioxidants to decolourise the blue-green 2,2-azinobis(3-ethylbenzothiazoline-6-sulphonate)) ($ABTS^{\cdot+}$) radical, to a degree proportional to their concentration [40]. The ABTS reaction mixture consisted in 0.4 M acetate buffer (pH=5.8) and 10 mM $ABTS^{\cdot+}$ solution in 30 mM acetate buffer (pH=3.6). 12.5 µL of each extract was assessed spectrophotometrically (Analytik Jena Specord® 200 plus, Germany) at 660 nm, after 5 minutes reaction time with ABTS radical solution. Trolox, dissolved in a phosphate buffer (20 mmol/L, pH 7.4) with five-fold serial dilutions (0.05 mM – 1 mM), was used to make the calibration curve with a good regression coefficient (R^2>0.9972). The results of the assay were expressed in mM Trolox equivalents (TE)/L of plant extract.

2.4.1 – General HPLC and mass spectrometer equipment

The experiment was conducted on an Agilent 1100 HPLC series system (Agilent Technologies, Santa Clara, CA, USA) equipped with a G13311A gradient pump, column thermostat, G1322A binary degasser, G1313A auto sampler and a G1316AUV detector coupled with an Agilent 1100 mass spectrometer (MS) (LC/MSD Ion Trap VL).

2.4.2 - Qualitative and quantitative determinations of polyphenols

The HPLC-MS/MS method described by Vlase *et al.* [41,42] was adopted, with modifications of acetic acid replacing potassium phosphate in the mobile phase. 18 polyphenols were analysed: apigenin, caffeic acid, chlorogenic acid, caftaric acid, fisetin, ferulic acid, gentisic acid, hyperoside, isoquercitrin, kaempferol, luteolin, myricetol, patuletin, *p*-coumaric acid, quercitrin, quercetin, rutoside and sinapic acid. For chromatographic separation a reverse-phase analytical column was employed (Zorbax SB-C18, 100 x 3.0 mm i.d., 3.5 µm), with a mixture of methanol:acetic acid 0.1% (v/v) as the mobile phase and binary gradient [43]. The elution began with a linear gradient, starting with 5% methanol then 42% methanol, for 35 minutes. For the next 3 minutes isocratic elution followed with 42% methanol, rebalancing with 5% methanol in the next 7 minutes. The flow rate was 1 mL min^{-1}, the injection volume was 5 µL, with a column temperature of 48°C [44].

Compound detection was performed in UV and MS mode. Each compound was detected at wavelengths corresponding to the maximum absorption of their respective UV spectrum. Therefore, the UV detector was set at 330 nm for 17 minutes for polyphenolic acid detection, then 370 nm until 38 minutes to detect flavonoids and their aglycones. For quantitative determination, a calibration curve with a 0.5 µg-5 µg/ml range was made for each compound [45].

For six other polyphenols (catechin, epicatechin, vanillic acid, gallic acid, protocatechic acid and syringic acid) a Zorbax SB-C18 column, 100 x 3.0 mm i.d., 3.5 µm, with a mixture of methanol:acetic acid 0.1% (v/v) as the mobile phase and binary gradient was used to carry out chromatographic separation (starting with 3% methanol at 3 minutes, 8% methanol at 8.5 minutes, 20% methanol until 10 minutes then rebalance column with 3% methanol). The flow rate was 1 ml/min with a 5 µL injection volume [46].

The mass-spectrometer operated with an electrospray-ion source in negative mode (nebulizer 60 psi (nitrogen), drying gas nitrogen at 12 L/min flow rate, 360°C temperature, +3000 V capillary potential). The analysis mode was specific ion monitoring for polyphenolcarboxylic acids and AUTO MS for flavonoids and their aglycones. ChemStation and DataAnalysis software from Agilent USA processed the chromatographic data [47].

2.4.3 – Qualitative and quantitative determinations of methoxyflavones

The separation of methoxyflavones (acacetin, casticin, eupatilin, eupatorine, hispidulin and jaceosidin), was performed on a Zorbax SB-C18 analytic column (100 x 3.0mm i.d., 3.5 µm) at 48°C, in MS/MS, MRM mode [48]. Acetic acid 0.1% (v/v) and methanol made up the mobile phase beginning with 45% methanol and ending at 50% methanol for 8 minutes. The injection volume was 5 µL with a 0.9 ml/min flow rate and a gradient. The mass-spectrometer operated using an electrospray ion source in negative mode, under the following optimized conditions: nitrogen gas at 325°C, 12 L/min flow rate, 60 psi (nebulizer pressure), +2500 V capillary voltage and MS/MS specific ion monitoring analysis mode. To quantify each flavone in the extracts, the intensity of the selected ions from the mass spectra was considered. To construct the five point plot calibration curves, the standard solutions of each flavones were dissolved in methanol and successive dilutions were made in methanol:water (75:25 v/v).

2.4.4 - Qualitative and quantitative determinations of sterols

A previously described method was used to identify and quantify the phytosterols in *Hypericum sp.* extracts [49]. The following analytical standards were used: β-Sitosterol, campesterol, ergosterol and stigmasterol. Zorbax SB-C18 (100 x 3.0mm i.d, 3.5 µm) reverse-phase analytical column fitted with a Zorbax SB-C18 guard column was used for sterol separation, at 40°C under isocratic conditions in MS/MS, MRM mode. Acetonitrile:methanol (30:70 v/v) mixture made up the mobile phase, with a 1 ml/min flow rate and a 4 µL injection volume. The mass-spectrometer operated using an atmospheric pressure chemical ionization (APCI) interface, in positive mode, under these conditions: nebulizer 50 psi, gas (nitrogen) at 7 L/min flow rate, 250°C temperature, -4000 V capillary potential. Multiple analysis mode was used instead of single ion monitoring to limit background interference (MS/MS instead of just MS).

2.4.5 - Qualitative and quantitative determinations of hyperforin and hypericin

HPLC/ESI-MS (ion trap) analysis of hyperforin and hypericin was performed on a Zorbax SB-C18 (100 x 3.0 mm i.d, 3.5 µm) analytical column with a 0.2-micron filter (Agilent) at 45°C with a 1 ml/min flow rate [50,51].

Hypericin: The mobile phase was acetonitrile:ammonium acetate (1 mM) (50:50 v/v) solution with a 5 µL injection volume. The mass-spectrometer functioned using an electrospray ion source in negative mode, under the following optimized conditions: nitrogen gas at 325°C with a 12 L/min flow rate, nebulizer pressure of 60 psi and a 3000 V capillary voltage. The analysis mode was set to ion monitoring m/z 503 [52].

Hyperforin: For the mobile phase, 1 mM ammonium acetate solution was mixed with acetonitrile 35:65 (v/v). For detection, the mass-spectrometer operated using an electrospray ion source in negative MS/MS mode under the following optimized conditions: nitrogen gas at 350°C with a 12 L/min flow rate, nebulizer pressure of 60 psi and a 2500 V capillary voltage. The analysis mode used was transition monitoring m/z 535.4.

REFERENCES

1. K. Doukani, A.S.M. Selles, H. Bouhenni. *Naturally Occurring Chemicals Against Alzheimer's Disease*, 1st ed.; Academic Press - Elsevier Inc., Amsterdam, Netherlands, **2021,** Chapter 3.1.11, pp. 155-165.
2. A. Smelcerovic, V. Verma, M. Spiteller, S. Ahmad, S. Puri, G. Qazi. *Phytochemistry*, **2006**, *67(2)*, 171-177.
3. A. Nahrstedt, V. Butterweck. *Pharmacopsychiatry*, **1997**, *30(2)*, 129-34.
4. S.L. Crockett, N.K.B Robson. *Med Aromat Plant Sci Biotechnol*, **2011**, *5(Special Issue 1)*, 1–13.
5. F. Pellati, S. Benvenuti, M. Melegari. *J Chromatogr A*, **2005**, *1088(1)*, 205–17.
6. G. Roscetti, O. Franzese, A. Comandini, E. Bonmassar. *Phytother Res*, **2004**, *18(1)*, 66-72.
7. A.R. Bilia, S. Gallori, F.F. Vincieri. *Life Sci*, **2002**, *70(26)*, 3077–3096.
8. M. Brolis, B. Gabetta, N. Fuzzati, R. Pace, F. Panzeri, F. Peterlongo. *J Chromatogr A,* **1998**, *825(1)*, 9-16.
9. B.I.P. Schiavone, A. Rosato, M. Marilena, C. Franchini, F. Corbo, L. Verotta L *et al. Anti-Cancer Agents Med Chem*, **2014**, *14(10)*, 1397–401.
10. R.H. Poppenga. *Clin Tech Small Anim Pract*, **2002,** *17(1)*, 6-18.
11. M.A. Medina, B. Martínez-Poveda, M.I. Amores-Sánchez, A.R. Quesada. *Life Sci*, **2006**, *79(2)*, 105-111.
12. K. Leuner, V. Kazanski, M. Muller, K. Essin, B. Henke, M. Gollasch et al. *FASEB J*, **2007**, *21(14)*, 4101-4111.
13. D. Gâtea, L. Vlase, M. Tămaș, I. Oniga. *Contrib Bot*, **2010**, *45*, 35-40.
14. D. Gâtea, M. Șipoș, M. Tămaș, B. Pașca. *Analele Univ din Oradea, Fasc Biol*, **2010**, *Tom XVII*, 111-115.
15. J.W. Petrich. *Int Rev Phys Chem*, **2000**, *1(3)*, 479-500.
16. L.P. Christensen. *Polyphenols in Human Health and Disease*, 1st ed.; Elsevier Inc., Amsterdam, Netherlands, **2014**, Chapter 62, pp. 793–818.
17. K.M. Klemow, A. Bartlow, J. Crawford, N. Kocher, J. Shah, M. Ritsick. *Herbal medicine: Biomolecular Clinical Aspects*, 2nd ed.; CRC Press/Taylor & Francis, London, UK, **2011**, Chapter 11.
18. P. Agostinis, A. Vandenbogaerde, A. Donella-Deana, L.A. Pinna, K.T. Lee, J. Goris J et al. *Biochem Pharmacol*, **1995**, *49(11)*, 1615–22.

19. D. Zheleva-Dimitrova, P. Nedialkov, G. Kitanov. *Pharmacogn Mag*, **2010**, *6(22)*, 74–78.
20. J.D. Potter. *Lancet*, **2005**, *366(9485)*, 527–530.
21. E. Czinner, K. Hagymási, A. Blázovics, Á Kéry, É Szőke, É Lemberkovics. *J Ethnopharmacol*, **2001**, *77(1)*, 31-35.
22. A. Pop, I. Fizeșan, L. Vlase, M.E. Rusu, J. Cherfan, M. Babotă, A-M. Gheldiu, I. Tomuță, D-S. Popa. *Antioxidants*, **2021**, *10(4)*, 607.
23. A. Toiu, L. Vlase, C.M. Drăgoi, D. Vodnar, I. Oniga. *Farmacia*, **2016**, *64(5)*, 663-667.
24. T. Nogueira, M.A. Medeiros, M.J. Marcelo-Curto, B.E. García-Pérez, J. Luna-Herrera, M.C. Costa. *Ind Crops Prod*, **2013**, *47(1)*, 126–131.
25. I. Oniga, A. Toiu, D. Benedec, I. Tomuţă, L. Vlase. *Farmacia*, **2016**, *64(2)*, 171–174.
26. B.A. Silva, F. Ferreres, J.O. Malva, A.C.P. Dias. *Food Chem*, **2005**, *90(1–2)*, 157–167.
27. A. Wojdyło, J. Oszmiański, R. Czemerys. *Food Chem*, **2007**, *105(3)*, 940–949.
28. S.L. Crockett, N.K.B. Robson. *Med Aromat Plant Sci Biotechnol*, **2011**, *5(Special Issue 1)*, 1–13.
29. B. Božin, N. Kladar, N. Grujić, G. Anačkov, I. Samojlik, N. Gavarić et al. *Molecules*, **2013**, *18(10)*, 11733–11750.
30. F. Maggi, G. Ferretti, M. Ricciutelli, N. Pocceschi, L. Menghini. *Fitoterapia*, **2004**, *75(7–8)*, 702–711.
31. P. Mártonfi, M. Repčák, L. Mártonfiová. *Biologia*, **2006**, *61(4)*, 473-478.
32. D. Hernández-Saavedra, I.F. Pérez-Ramírez, M. Ramos-Gómez, S. Mendoza-Díaz, G. Loarca-Piña, R. Reynoso-Camacho. *Med Chem Res*, **2015**, *25(1)*, 163-172.
33. M.E. Rusu, I. Fizeșan, A. Pop, A Mocan, A-M. Gheldiu, M. Babotă et al. *Molecules*, **2020**, *25(9)*, 2187.
34. D. Zheleva-Dimitrova, P. Nedialkov, G. Kitanov. *Pharmacogn Mag*, **2010**, *6(22)*, 74–78.
35. A. Toiu, A. Mocan, L. Vlase, A.E. Pârvu, D.C. Vodnar, A-M. Gheldiu et al. *Molecules*, **2019**, *24*, 1597.
36. A. Toiu, L. Vlase, D.C. Vodnar, A-M. Gheldiu, I. Oniga. *Molecules*, **2019**, *24*, 2666.
37. Z. Zhang, L. Liao, J. Moore, T. Wu, Z. Wang. *Food Chem*, **2009**, *113(1)*, 160–165.
38. J. Pei, A. Chen, L. Zhao, F. Cao, G. Ding, W. Xiao. *J Agric Food Chem*, **2017**, *65(29)*, 6042-6048.
39. A. Toiu, L. Vlase, A-M. Gheldiu, D. Vodnar, I. Oniga. *Farmacia*, **2017**, *65(3)*, 351-355.
40. M.E. Rusu, C. Georgiu, A. Pop, A. Mocan, B. Kiss, O.Voștinaru et al. *Antioxidants*, **2020**, *9*, 424.

41. D. Hanganu, D. Benedec, L. Vlase, I. Popica, C. Bele, O. Raita et al. *Farmacia*, **2016**, *64(4)*, 498-201.
42. D. Benedec, D. Hanganu, L. Filip, I. Oniga, B. Tiperciuc, N-K. Olah et al. *Farmacia*, **2017**, *65(2)*, 252-256.
43. A.D. Farcaș, C. Zăgrean-Tuza, L. Vlase, A-M. Gheldiu, M. Pârvu, A.C. Moț. *Studia UBB Chemia*, **2020**, *LXV (2)*, 209-220.
44. M. Pârvu, L. Vlase, A.E. Pârvu, O. Roșca-Casian, A-M. Gheldiu, O. Pârvu. *Not Bot Horti Agrobo*, **2015**, *43(1)*, 53-58.
45. A. Mocan, L. Vlase, D.C. Vodnar, A-M. Gheldiu, R. Oprean, G. Crișan. *Molecules*, **2015**, *20*, 15060-15071.
46. M.E. Rusu, I. Fizeșan, A. Pop, A-M. Gheldiu, A. Mocan, G. Crișan et al. *Antioxidants*, **2019**, *8(10)*, 460.
47. C.N. Tiboc Schnell, G.A. Filip, N. Decea, R. Moldovan, R. Opris, S.C. Man et al. *Inflammopharmacology*, **2021**, *29*, 753-769.
48. A. Mocan, D. Vodnar, L. Vlase, O. Crișan, A-M. Gheldiu, G. Crișan. *Int J Mol Sci*, **2015**, *16*, 21109-21127.
49. A. Toiu, A. Mocan, L. Vlase, A.E. Pârvu, D.C. Vodnar, A-M. Gheldiu et al. *Front Pharmacol*, **2018**, *9*, 7.
50. A. Coste, L. Vlase, A. Halmagyi, C. Deliu, G. Coldea. *Plant Cell Tiss Organ Cult*, **2011**, *106*, 279–288.
51. A.C. Răclariu, R. Păltinean, L. Vlase, A. Labarre, V. Manzanilla, M.C. Ichim et al. *Sci Rep*, **2017**, *7*, 1291.
52. A.C. Sevastre-Berghian, V.A. Toma, B. Sevastre, D. Hanganu, L. Vlase, D. Benedec et al. *J Physiol Pharmacol*, **2018**, *69(5)*, 789-800.

STUDIA UBB CHEMIA, LXVII, 3, 2022 (p. 37-44)
(RECOMMENDED CITATION)
DOI:10.24193/subbchem.2022.3.03

OPTIMIZATION OF THE ECO-FRIENDLY SYNTHESIS OF SILVER NANOPARTICLES USING GOJI BERRIES' BIOACTIVE COMPOUNDS

LUMINIŢA DAVID[a], BIANCA MOLDOVAN[a]*

ABSTRACT. The numerous applications of metallic nanoparticles in different fields such as materials science, medicine, biology, led to the rapid development of various synthesis methods of these nanomaterials, among which the biogenic approach in obtaining nanoparticles has been proved to be an efficient alternative compared to other methods. The present study aims to investigate the potential of goji berries extract as source of bioactive compounds able to reduce the silver ions and to stabilize the resulting nanoparticles. Reaction parameters such as pH and $AgNO_3$ concentration were analyzed and optimized in order to obtain spherical, well dispersed and high yield silver nanoparticles. Five different pH values (6; 7; 8; 9; 10) and five ratios fruit extract: silver nitrate solution (1:1; 1:3; 1:7; 1:10; 1:15) were investigated and it was found that the silver nanoparticles obtained at pH=9 and 1:10 ratio demonstrated the highest monodispersity and were obtained in the highest yield. The obtained nanoparticles were characterized in terms of their size and shape using transmission electron microscopy (TEM) and UV-vis spectroscopy.

***Keywords*:** *silver nanoparticles, goji berries*

INTRODUCTION

The wide range of applications of nanosized materials led in the last decades to an explosion of nanotechnology research. Metallic nanoparticles are of a great interest due to their important uses in medicine, materials science, environment remediation, catalysis, biology, pharmacy [1-3]. There is a strong relationship between the size and shape of the nanoparticles and their properties and, consequently, their applications. These parameters are

[a] *Babeş-Bolyai University, Faculty of Chemistry and Chemical Engineering, 11 Arany Janos Str., RO-400028, Cluj-Napoca, Romania*
** Corresponding author: bianca.moldovan@ubbcluj.ro*

strongly influenced by the synthesis methods used to obtain the nanoparticles. Physical and chemical approaches such as thermal decomposition, chemical/ electrochemical reduction, laser ablation, attrition, mechanical milling, sol-gel techniques, have been developed but usually these methods involve either the use of hazardous reagents or expensive instruments, high temperature or pressure and can lead to low fabrication rate, significant energy consumption, poor size control and low stability of the obtained nanoparticles. Compared to these methods, the green synthetic approaches offer solutions to all these disadvantages, being fast, simple, non-toxic, low cost, and environmentally friendly [4-6]. Various biological resources can be used in the green synthesis methods of metallic nanoparticles, such as microorganisms, enzymes and plants. There are numerous studies which report the biosynthesis of metal nanoparticles by exploiting the reductive properties of phenolics, proteins, flavonoids and carbohydrates from various plant extracts, such as: *Camellia sinensis* [7], *Cornus sanguinea* [8], *Cornus mas* [9], *Citrus limon* [10], *Solanum licopersicum* [11].

Among metallic nanoparticles, silver nanoparticles are essential materials, especially because of their medical uses, possessing strong antibacterial, antifungal and antiviral properties [12] and also because of their high catalytic activity.

The plant extracts, especially those with pharmacological properties, have been widely used for the green synthesis of the AgNPs. Goji berries have been intensively used for medicinal purposes, especially in Asia as they contain a wide range of compounds with health promoting properties being a good source of phenolic compounds, proteins, carotenoids, fibres and minerals. Goji berries are the fruits of *Licium barbarum* L., a perennial shrub from Solanaceae family originating from South-West Asia and nowadays naturalized in America and Europe [13].

Goji berries extract has been reported to possess various biological properties, such as antioxidant, antimicrobial, antidiabetic, anti-inflammatory and anti-obesity effects. Their potent antioxidant activity originates in the presence of polyphenols in the goji berries, among which caffeic acid is the main compound [14]. Kaempferol, myricetin, catechin, apigenin, rutin, chlorogenic, coumaric, ferulic, ellagic and gallic acids are also identified in these fruits [15].

The presence of these compounds and their high reductive properties enabled us to choose goji berries as source of reducing and capping agents for the green synthesis of AgNPs. The aim of the present study was to exploit goji phytocompounds in the reduction reaction of the silver ions and to optimize the reaction conditions (pH and reactants' ratio) to obtain low dimensions, monodispersed, spherical in shape silver nanoparticles.

RESULTS AND DISCUSSION

The goji berries are well known for their remarkable antioxidant capacity, due to the presence of inherent metabolites, of which flavonoids and phenolic acids confer them this property. The presence of high amounts of chlorogenic acid, scopoletin, coumaric acid, rutin, caffeic acid, N-feruloyl tyramine [16] recommend them as suitable fruits for the plant assisted mediated green synthesis of metallic nanoparticles, as all these compounds can successfully act as reducing agents of metallic ions as well as capping and stabilizing agents of the obtained metallic nanoparticles.

The total phenolic content of the goji extract used in this study, assessed by the widely applied Folin-Ciocalteu method, was 7125±216.42 mg GAE/L.

The antioxidant activity of the extract was evaluated using the ABTS free radical scavenging assay and was found to be 1038.46±32.48 μM Trolox.

The optimal synthesis conditions of the silver nanoparticles using goji berries extract were determined by evaluating two synthesis parameters: pH value and fruit extract: $AgNO_3$ mixing ratio (v/v). These factors are known as key parameters in obtaining AgNPs using natural compounds. The impact of the pH value on the size, morphology and yield of the obtained AgNPs was investigated at 6; 7; 8; 9 and 10. The formation of silver nanoparticles was first visually observed by a colour change of the reaction mixture from faint orange to yellowish brown or deep brown, depending on pH of the reaction medium. The synthesis of AgNPs was validated using UV-vis spectroscopy. Silver nanoparticles possess unique optical properties due to their surface plasmon resonance (SPR). The surface plasmon vibration excitation of colloidal silver results in absorption peaks between 400-500 nm [17]. The UV-Vis spectra of the obtained silver nanoparticles are depicted in Figure 1.

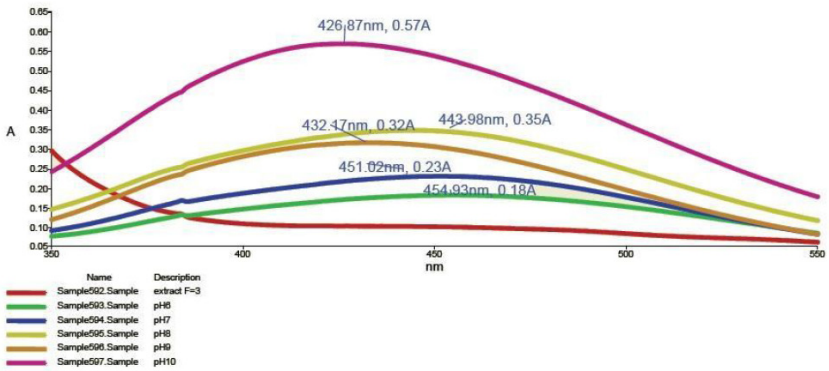

Figure 1. UV-Vis spectra of AgNPs obtained at different pH values

The synthesized AgNPs at all the investigated pH values presented the characteristic SPR peaks of silver nanoparticles between 426 and 454 nm. It can be observed that the intensity of the absorption bands decreases with the value of pH. As higher intensity of these bands can be attributed to higher concentration of nanoparticles, one can conclude that pH=10 conducted to the highest reaction yield. As predicted, acidic pH values could not stabilize the silver nuclei for subsequent growth of silver nanoparticle. By increasing the reaction medium pH, a gradually red shifted absorption band, until 426 nm for pH=10 was observed, indicating the obtain of smaller sized AgNPs [18]. At alkaline pH, the bioactive metabolites from the goji extract act as capping agents of the obtained nanoparticles, stabilizing these by preventing agglomeration.

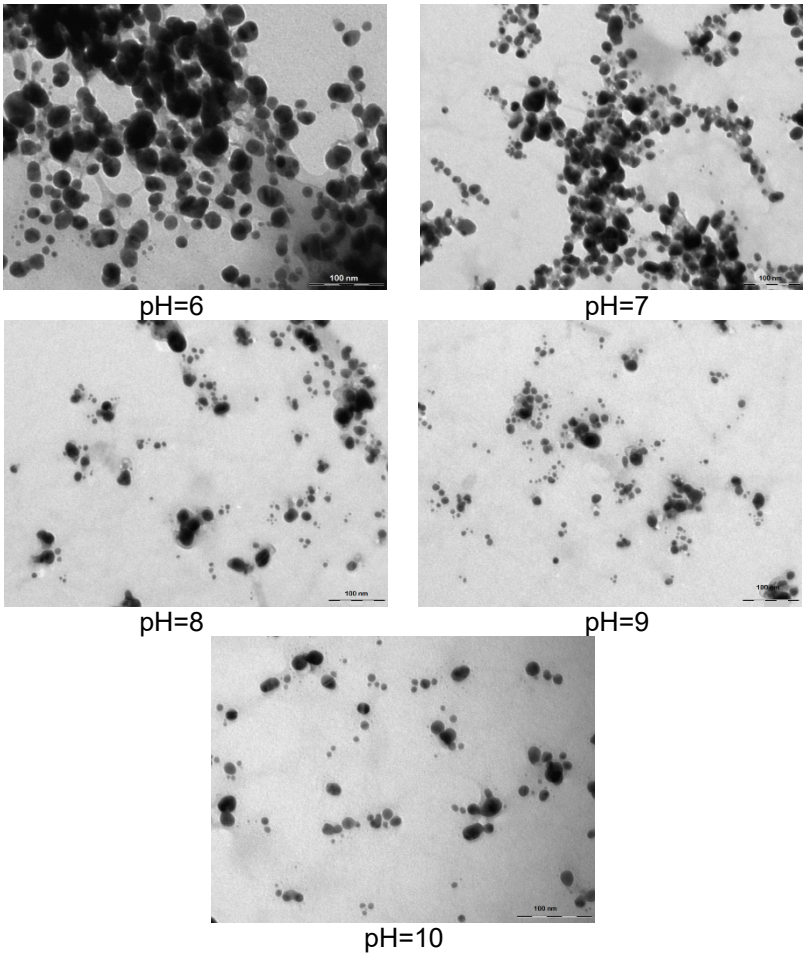

Figure 2. TEM images of AgNPs obtained at different pH values

The size and morphology of the goji berries mediated synthesized silver nanoparticles was analysed using the Transmission electron Microscopy (TEM) (Figure 2).

At pH = 6 and 7 the TEM images show the formation of mostly spherical nanoparticles with two broad size distributions, some presenting a diameter in the range of 20-30 nm and others being larger and of irregular shapes. There was also noticed an agglomeration tendency of the obtained nanoparticles, especially at pH=6. For the pH values in the range 8-10, smaller sized, dispersed nanoparticles, with more regular shapes were obtained. The alkaline conditions proved to be more appropriate for the synthesis of the AgNPs using goji extract, resulting uniform size and shape and small diameter nanoparticles, the influence of the pH on their properties being less important in this pH range, result in accordance with other studies reporting the phytomediated synthesis of silver nanoparticles [19]. The size of the nanoparticles obtained in alkaline conditions was in the range of 10-20 nm, with an average size of 17 nm at pH=10. All the obtained results indicated that the synthesis of AgNPs with the goji berry phytocompounds occurred with the highest yield at pH=10, resulting regular in shape, monodispersed and small sized nanoparticles.

The concentration of the reducing phytocompounds from the fruit extract has a strong influence on the size, shape and stability of the metallic nanoparticles [20]. Thus, establishing the optimal ratio between the fruit extract and silver nitrate solution could be of a great importance for obtaining small, uniform and stable AgNPs.

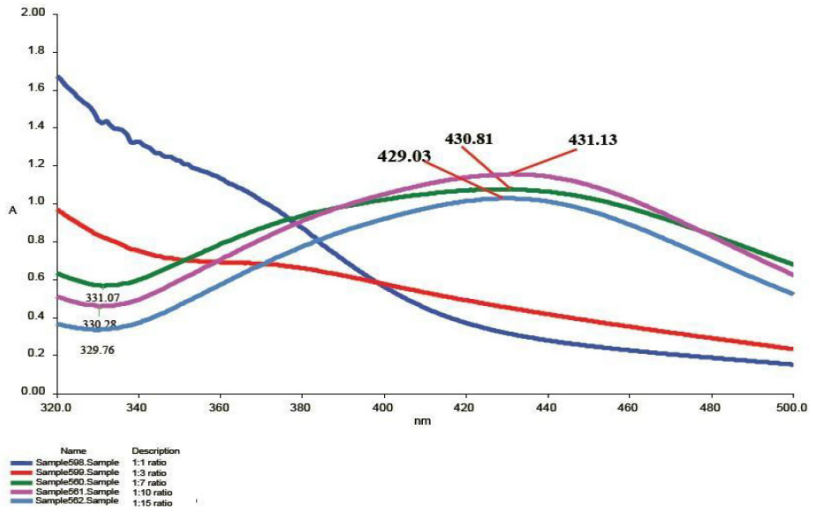

Figure 3. UV-Vis spectra of AgNPs obtained at different fruit extract: $AgNO_3$ ratios

Five different ratios: 1:1; 1:3; 1:7; 1:10 and 1:15 were analysed, the reaction being conducted at the optimum determined pH value, pH=10. The UV-Vis spectra of the silver nanoparticles obtained at these ratios (Figure 3) indicate that no reaction occurred at 1:1 and 1:3 ratio as no characteristic absorption band of the silver nanoparticles was noticed. The AgNPs obtained at 1:7; 1:10 and 1:15 displayed similar position of the SPR absorption band with a maximum in a very narrow range of wavelengths between 429 and 431 nm. This fact indicates that for ratios between 1:7 to 1:15, the size of the obtained nanoparticles was not influenced by this parameter. The highest yield was obtained for the 1:10 ratio.

CONCLUSIONS

The present study reports the green synthesis of silver nanoparticles using goji berries as source of phytocompounds which act as reducing and stabilizing agents. By optimizing the reaction conditions, among which pH and reactants ratio is very important, our protocol confers an easy way to obtain in high yield small sized uniform nanoparticles, spherical in shape, using a green method which involves non-toxic chemicals. The optimum determined pH value was 10, while the optimum fruit extract: metal precursor ratio was 1:10.

EXPERIMENTAL SECTION

Chemicals and reagents

All chemicals and reagents were purchased from Merck (Darmstadt, Germany), were of analytical grade and were used without further purification. A TYPDP1500 Water distiller (Techosklo LTD, Držkov, Czech Republic) was used to obtain the distilled water.

Fruit extract preparation

Commercially available dried goji berries were used to obtain the fruit extract, by mixing 5 grams of milled fruits with 100 mL distilled water. After 1 hour of stirring at room temperature, the mixture was vacuum filtered and the filtrate was further used to obtain the desired silver nanoparticles.

Determination of total phenolic content

The method developed by Singleton [21] using the Folin-Ciocalteu reagent was applied to determine the total phenolic content (TPC).

A 0.2 N Folin-Ciocalteu solution (1.5 mL) was mixed with goji berries extract (0.3 mL) and incubated in the dark for 5 min. After that, 1.2 mL of 0.7N Na_2CO_3 solution were added. After 2 hours incubation at room temperature, the absorbance of the resulting solution was measured at 765 nm, using an UV-VIS Perkin Elmer Lambda 25 double beam spectrophotometer. A calibration curve of gallic acid was used for quantitative determinations. The results were expressed as mg gallic acid equivalents (GAE)/L fruit extract.

Determination of antioxidant capacity

The antioxidant activity of the extract was evaluated using the $ABTS^{\cdot+}$ assay of Re et al. [22]. 360 mg of 2,2-azinobis-(3-ethylbenzothiazoline-6-sulfonate) (ABTS) were dissolved in 100 mL distilled water. To this solution, 100 mL potassium persulfate solution (2.45 mM) were added, in order to generate the stable ABTS radical cation. The mixture was allowed to react for 24 hours in the dark at room temperature. The resulting radical solution was diluted to an absorbance of 0.8 with distilled water. To 6 mL diluted ABTS solution, 0.1 mL goji extract were added and the absorbance was measured at 734 nm after 15 min. Trolox (6-hydroxy-2,5,7,8-tetramethylchroman-2-carboxylic acid) was used as standard to determine the antioxidant capacity of the investigated fruit extract, which was expressed in μM Trolox equivalents.

Synthesis and characterization of silver nanoparticles

Silver nitrate solution (1mM) was used as silver ions source for the phytomediated synthesis of the silver nanoparticles. 2 mL goji fruit extract was mixed with 20 mL $AgNO_3$ solution at room temperature. The pH values of the resulting reaction mixtures were adjusted in the range 6 to 10 by dropping 0.1 M NaOH solution. After 2 hours of stirring, the obtained nanoparticles were purified by centrifugation at 10.000 rpm for 20 min and washing with double distilled water. In order to investigate the influence of reactants' ratio on the reaction yield and on the size and shape of the obtained AgNPs, different volumes of silver nitrate solution were mixed with 2 mL fruit extract in order to achieve the desired ratios.

The obtained silver nanoparticles were characterized using consecrated methods, such as UV-Vis spectroscopy (using a Perkin Elmer Lambda 25 double beam spectrophotometer) and transmission electron microscopy (using a H-7650 120 kV Automatic transmission electron microscope, Hitachi, Tokyo, Japan).

ACKNOWLEDGMENTS

This work was supported by a grant of CNCS-UEFISCDI, project number PN-III-P1-1.1-TE-2021-0511, within PNCDI III.

REFERENCES

1. W.T. Liu, *J. Biosci Bioeng.*, **2006**, *102*, 1-7.
2. P. Mohampuria, N.K. Rana, S.K. Yadav, *J. Nanopart. Res.*, **2008**, *10*, 507-517.
3. R. Opris, V. Toma, D. Olteanu, I. Baldea, A. Baciu, F. Imre-Lucaci, A. Berghian Sevastre, C. Tatomir, B. Moldovan, S. Clichici, L. David, A. Florea, G.A. Filip, *Nanomedicine*, **2019**, 14, 275-299.
4. T.A.J. de Souza, L.R.R. Souza, L.P. Frankie, *Ecotoxicol. Environm. Safety*, **2019**, *171*, 691-700.
5. J.S. Choi, H.C. Jung, Y.J. Baek, B.Y. Kim, M.W. Lee, H.D. Kim, S.W. Kim, *Nanomaterials*, **2021**, *11*, 205.
6. S. Iravani, *Green Chemistry*, **2011**, *13*, 2638-2650.
7. W.R. Rolim, M.T. Pelegrino, B. de Araujo Lima, L.S. Ferraz, F.N. Costa, J.S. Bernardes, T. Rodigues, M. Brocchi, A.B. Seabra, *Appl. Surface Sci.*, **2019**, *463*, 66-74.
8. L. David, B. Moldovan, I. Baldea, D. Olteanu, P. Bolfa, S. Clichici, G.A. Filip, *Mat. Sci. Eng. C*, **2020**, *110*, 110709.
9. I. Baldea, A. Florea, D. Olteanu, S. Clichici, L. David, B. Moldovan, M. Cenariu, M. Achim, R. Suharoschi, S. Danescu, A. Vulcu, G.A. Filip, *Nanomedicine*, **2020**, 15, 55-75.
10. F. Ortega, V.B. Arce, M.A. Garcia, *Carbohydrate Polym.*, **2021**, *252*, 117208.
11. V.P. Giri, S. Pandey, M. Kumari, A. Tripathi, R. Katiyar, J.C. White, A. Mishra, *ACS Agric. Sci. Technol.*, **2022**, DOI:10.1021/acsagscitech.1c00252
12. J.R. Koduru, S.K. Kailasa, J.R. Bhamore, K.H. Kim, T. Dutta, K. Vellingiri, *Adv. Colloid Interface Sci.*, **2018**, *256*, 326-339.
13. B.B. Bidovic, D.D. Milincic, M.D. Marcetic, J.D. Djuris, T.D. Ilic, A.Z. Kostic, M.B. Pesic, *Antioxidants*, **2022**, *11*, 248.
14. P. Skenderidis, S. Leontopoulos, D. Lampakis, *Nutraceuticals*, **2022**, *2*, 32-48.
15. B. Cui, S. Liu, X. Lin, J. Wang, S. Li, Q. Wang, S. Li, *Molecules*, **2011**, *16*, 9116-9128.
16. M. Forino, L. Tartaglione, C. Dell'Aversano, P. Ciminiello, *Food Chem.*, **2016**, *194*, 1254-1259.
17. S. Ashokkumar, S. Ravi, V. Kathiravan, S. Velmurugan, *Environ. Sci. Pollution Res.*, **2014**, *21*, 11439–11446.
18. G.R. Sanchez, C.L. Castilla, N.B. Gomez, A. Garcia, R. Marcos, E.R. Carmona, *Mat. Letters* **2016**, *183*, 255–260.
19. S. Agnigotri, D. Sillu, G. Sharma, R.K. Rya, *Applied Nanosci.*, **2018**, *8*, 2077-2092.
20. A. Amittal, Y. Kisti, U.C. Banerjee, *Biotechnol. Adv.*, **2013**, *31*, 346-356.
21. V.L. Singleton, R. Orthofer, R.M. Lamuela-Raventos, *Meth. Enzymol.*, **1999**, 299, 152-178.
22. R. Re, N. Pellegrini, A. Proteggente, A. Pannala, M. Yango, C. Rice-Evans, *Free Rad. Biol. Med.*, **1999**, *26*, 1231-1237.

STUDIA UBB CHEMIA, LXVII, 3, 2022 (p. 45-60)
(RECOMMENDED CITATION)
DOI:10.24193/subbchem.2022.3.04

POSSIBLE ZINC DIETARY SUPPLEMENT ONTO RED GRAPE POMACE (*VITIS VINIFERA* L.) SUPPORT

SILVIA BURCĂ[a], CERASELLA INDOLEAN[a]*

ABSTRACT. This paper presents a report about the extraction of resveratrol with ethanol (EtOH) from red grape pomace (RGP) *Vitis vinifera* L. (Cluj, Transylvania region, Romania) and obtaining a dietary supplement with zinc on grape pomace support. The concentration of resveratrol (Rv) from the extract was spectrophotometrically determined at 305 nm wavelength, and was found to be 145 mg Rv/L. The material resulting after the extraction of resveratrol was processed to obtain a zinc dietary supplement support. The thermodynamic parameters, including Gibbs free energy (ΔG°), enthalpy (ΔH°) and entropy (ΔS°) of Zn^{2+} biosorption were calculated and the results indicate that the process is endothermic and spontaneous. The Zn^{2+} biosorption kinetics was analysed using pseudo-first- and pseudo-second-order models. The results indicate that biosorption of Zn^{2+} aqueous solution onto grape pomace support is best described by the pseudo-second-order model.

Keywords: *zinc, resveratrol, red grape pomace, food supplement, biosorption, kinetics*

INTRODUCTION

Zinc is an essential trace element for all forms of life. This metal plays important roles in growth and development, has an immune function, and is essential for neurotransmission, vision, reproduction, or intestinal ion transport. Many proteins in humans have functional zinc-binding sites, over 50 enzymes depend on the vital chemical reactions catalysed by zinc. Zinc may have a regulatory function, modulating the activity of cell-signalling enzymes and transcription factors [1-5].

[a] *Babeş-Bolyai University, Faculty of Chemistry and Chemical Engineering, Department of Chemical Engineering, 11 Arany Janos str., RO-400028, Cluj-Napoca, Romania*
** Corresponding author liliana.indolean@ ubbcluj.ro*

Clinical zinc deficiency in humans was first described in 1961, when the consumption of diets with low zinc bioavailability due to high phytate content was associated with adolescent nutritional dwarfism in the Middle East. Zinc insufficiency has been recognized by experts as an important public health issue, especially in low-resource countries [6-14].

The elderly population above the age of 60–65 years shows a higher risk of developing nutritional disorders caused by the ageing process, and zinc deficiency is an important factor in the origin of certain common diseases that affect and cause morbidity among this age group [15].

Zinc deficiency in humans is quite prevalent, affecting over two billion people [16]. Nutritional zinc deficiency is widespread throughout developing countries.

Therefore, the production of food supplements based on zinc is a field of interest in recent years.

Zinc supplements including zinc acetate, zinc gluconate, zinc picolinate, and zinc sulphate are commercially available. The recommended dietary allowance for adult men and women is 11 mg/day and 8 mg/day of zinc, respectively. Long-term consumption of zinc in excess of the tolerable upper intake level (UL, 40 mg/day for adults). Zinc bioavailability is relatively high in meat, eggs, and seafood; zinc is less bioavailable from whole grains and legumes, due to their high content in phytate that inhibits zinc absorption [17-23].

Grape pomace is a waste which, due to the significant quantities of wine produced throughout the world, pollutes the environment.

Discharging grape pomaces were shown to have a negative impact on flora and fauna due to their high pollution load [24]. Using grape pomace as fertilizer inhibits seeds germination, and the presence of lignin prevents the waste to be used as animal feed, reducing digestibility [25].

The red grape pomace (RGP) is a form of biomass that together with other organic residues from wine production can be used to obtain food supplements or to obtain bioethanol. It is composed of: bark, stems, seeds and moisture, but also of other components, among the main constituents would be organic acids and polyphenols, unsaturated lipids and sterols, vitamins and antioxidants, mineral elements (potassium, calcium, magnesium, iron, etc.), which gives it the quality of a functional ingredient.

Resveratrol (3,5,4'-trihydroxystilbene) and piceid (3,5,4'-trihydroxystilbene-3-β-D-glucoside) are two of the major stilbene phytoalexins which remain in significant quantities in grape pomace, after wine production. Therefore, their extraction from the RGP is an essential step for obtaining products with high antioxidant properties, before using the biomass as a support for zinc biosorption.

Consulting the literature it was found that grape pomace contains significant amounts of substances that can be considered beneficial to health [26, 27]. The most abundant in grape pomace are dietary fibres that are present in high levels (up to 85% depending upon the grape variety) and polyphenolic compounds that mainly (about 70%) remain in pomace after the winemaking process [27].

The proximate composition of RGP based on dry weight (quantity g/100 g) is: pH 3.6, ash, 6.8 wt %, humidity 74.3 w/w, residual sugars 1.6 % w/w, cellulose 19.6% w/w, hemicellulose 12.0 % w/w, protein 10.4 % w/w [28].

The aims of this study are to perform the extraction of resveratrol from red grape pomace (RGP) originating from the organic residues resulting from *Vitis vinifera* L. wine production (Cluj, Transylvania region) and, also, to study the Zn^{2+} biosorption onto RGP support in order to obtain a possible dietary supplement.

RESULTS AND DISCUSSION

Characterization of red grape pomace (RGP) biosorbent

The graphs from figure 1 showed different sample appearances before (a) and after (b, c) wine production.

a **(b)** **(c)**

Figure 1. Different grape types - (a). Residual grape pomace biomass, resulting from the wine processing of white grapes - (b) and red grapes (RGP) - (c).

The results of elemental analysis showed the presence of C (59.62%), N (3.1%), O (29.4%), Na (0.7%), Mg (0.1%), P (0.07%), K (0.31), Zn (0.21%) from RGP. The high carbon content of biomass makes RGP a good precursor material for biosorbents. Our results are in good agreement with the literature data [29].

The real density of RGP reflects the ratio of the mass material to its volume, without taking into account pore volume. The real density of RGP was also determined, resulting in an average particle diameter of 1.0-1.6 mm. Particle size was gravimetrically determined [30].

The apparent density of a biosorbent expresses the ratio of the mass of the material to its volume, including the volume of the pores. The apparent density of RGP obtained, with 1.0-1.6 mm, is gravimetrically determined. The porosity of RGP reflects the ratio between the pores volume and the total volume of material. The establishing of RGP specific surface area, with 1.0-1.6 mm, is achieved by using the gravimetric method for the desorption isotherm determination.

The BET equation will be used to calculate the specific surface area of the RGP biomass [13, 14, 17]. The results for physico-chemical characterization of RGP are: S_{BET} 324.3 m^2/g, apparent density 1.234 g/cm^3, real density 0.892 g/cm^3, porosity 38.34%.

A defining feature of the adsorption process is the porosity of the RGP. The higher its value is, the higher the adsorption capacity of material is.

Extraction of resveratrol from red grape pomace

Resveratrol (3,5,4'-trihydroxystilbene), (Rv), is a stilbenol, a polyphenol and a member of resorcinols, in which the phenyl groups are substituted at the positions 3, 5, and 4' by hydroxyl groups. It has a role as a phytoalexin, an antioxidant and a glioma-associated oncogene inhibitor, figure 2.

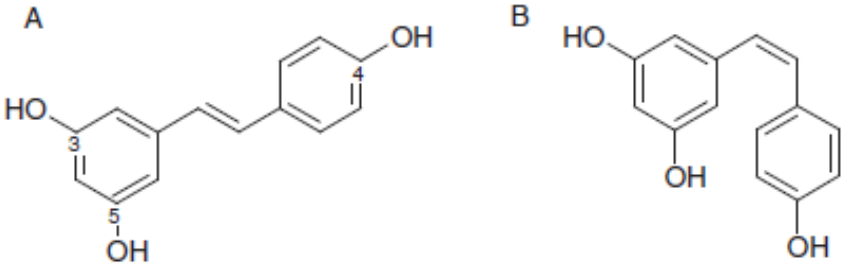

Figure 2. The chemical structure *trans*- (A) and *cis*- (B) of Rv.

The RGP *Vitis vinifera* (Cluj, Transylvania region) was treated with 96% EtOH, for 24 hours to extract Rv. To determine the extracted polyphenolic components, the Janway 6305 spectrophotometer was used, the UV-VIS spectrum was obtained for the wavelength range between 190- and 800 nm, figure 3.

To determine the Rv content from the RGP extract, it was worked at 305 nm, with a dilution of 1:100.

The spectrophotometer was calibrated, using standard solutions in the concentration range 0.1 – 1 × 10^{-4} M. With the absorbance values measured at 305 nm, the concentration of Rv in the alcoholic solution was calculated, this being 145 mg / L, for a ratio of mass of RGP / solvent of 1:20.

The effect of zinc ions concentration on the biosorption process

The experiments were conducted using 100 mL Zn^{2+} aqueous solutions with the Zn^{2+} concentrations between 181–341 mg Zn^{2+}/L, in batch conditions, with magnetic stirring at 200 rpm, at room temperature (T=293K, 20°C) and 2 g RGP biosorbent, with grain size of 0.6-1.0 mm. The variation of the Zn^{2+} concentration over time, until the equilibrium is established (constant residual concentration of Zn^{2+}) is presented in figure 4.

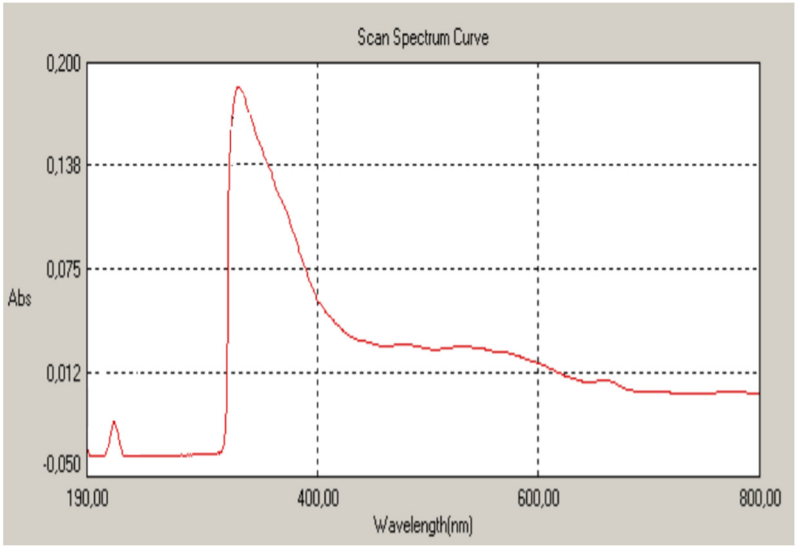

Figure 3. UV-VIS spectrum of the red grape extract (extraction in EtOH, 20°C (293K), dilution 1:100).

From the recorded experimental results, it was possible to reach equilibrium after about 90 minutes, the maximum adsorption capacity of Zn^{2+} on the obtained biomass being 11.92 mg Zn^{2+}/g (for initial concentration 341 mg Zn^{2+}/L), the efficiency calculated based on values obtained from experimental data being 88%

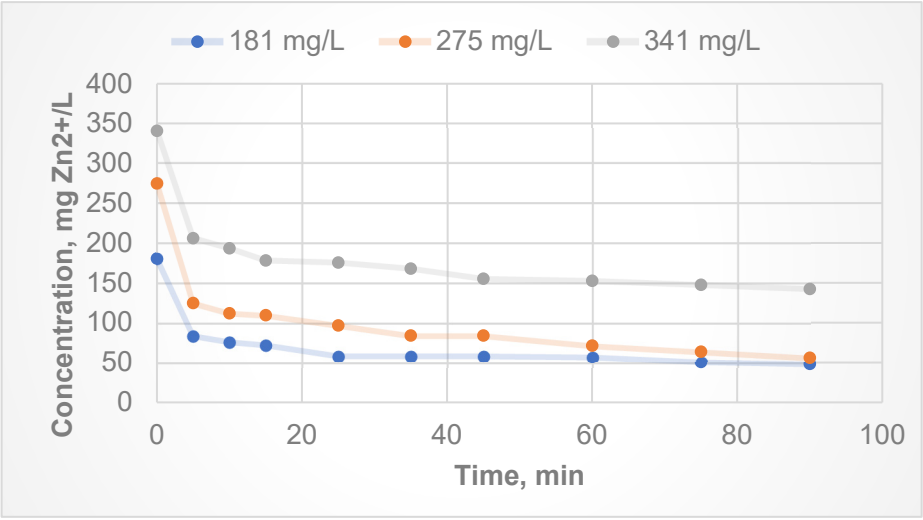

Figure 4. The influence of the initial Zn^{2+} concentration over the time evolution for biosorption onto RGP (181–341 mg Zn^{2+}/L, 2 g RGP, 0.6-1.0 mm, 293 K, pH= 6.3, 200 rpm).

The effect of the stirring rate

The study was conducted under the following conditions: room temperature (293K, 20°C), concentration of zinc solution 275 mg Zn^{2+}/L, grain size of RGP 0.6 - 1 mm, the ratio of addition of biomass/volume of zinc solution is 2 g RGP/100 mL; the stirring rates were 200, 300 and 400 rpm.

From the data collected after the experiment it can be seen that, after about 90 minutes, equilibrium is reached (until constant residual concentration), the adsorption capacity of the prepared biomaterial RGP being 10.94 mg Zn^{2+}/g for experiments conducted at 300 rpm. As the stirring rate increases from 200 to 300 rpm, the liquid layer around the adsorbent particles decreases and the amount of Zn^{2+} retained on the surface of the adsorbent material increases. If the experiment is carried out at 400 rpm, a decrease of adsorption capacity (q_e, mg/g) is observed, as a result of the increase of mechanical disorder, which probably leads to a slower establishment of the biosorption conditions, and, consequently, to a decrease of the biosorption efficiency (E, %), figure 5.

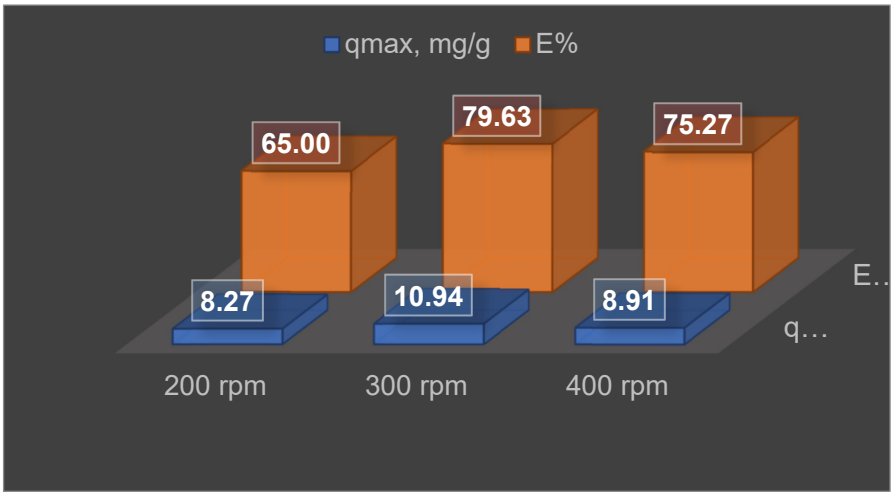

Figure 5. The maximum efficiency and adsorption capacity for Zn^{2+} biosorption process onto RGP biomass; the influence of stirring rate.

The effect of the grain size of RGP biosorbent

This study was performed under the following conditions: the room temperature (293K, 20°C), the concentration of zinc solution was 224 mg Zn^{2+}/L, magnetic stirring rate 300 rpm, grain size biomass granulation 0.4-0.6, 0.6 - 1 mm and >1mm, the ratio of RGP biomass/volume of zinc solution was 2 g RGP/100 mL Zn^{2+} solution.

The study of the particle granulation influence on the biosorption process revealed that, for the RGP material with granulation between 0.6–1 mm, the maximum adsorption capacity was 6.89 mg Zn^{2+}/g.

The increase of the RGP granulation leads to a decrease of the specific surface of the adsorbent material, which determines the decrease of the adsorption capacity (6.49 mg Zn^{2+}/g for grain size >1 mm), figure 6.

The influence of temperature on the biosorption process. Thermodynamic

The Zn^{2+} biosorption onto RGP was conducted using three different temperatures (20°C, 30°C and 40°C). It was observed that an increase in temperature leads to an increase in the biosorption efficiency, suggesting that the adsorption process is endothermic. Higher temperatures conduct to a decrease in biosorption efficiency, due to the fact that, after 40°C (313 K) desorption process begin, figure 7.

Similar results were reported in literature for the biosorption of Zn^{2+} onto different vegetal fibres wastes, [31].

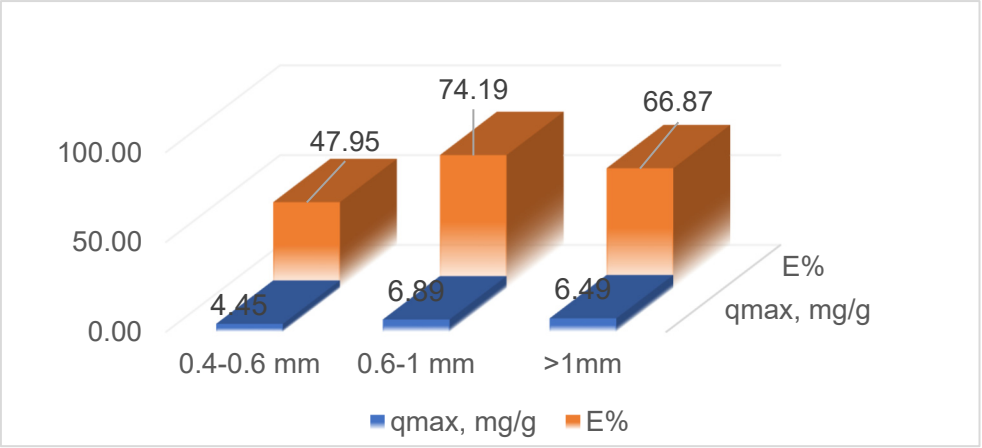

Figure 6. The effect of grain size biosorbent over the amount of Zn^{2+} uptake onto RGP biosorption (224 mg Zn^{2+}/L, 300 rpm, grain size biomass granulation 0.4-0.6, 0.6-1 mm, >1 mm, 2 g RGP/ 100 mL).

For each experiment, performed at a certain temperature, values of biosorption capacity (q_e) and Zn^{2+} concentration in solution, at equilibrium (C_e) were determined.

The equilibrium constant Kd, of the biosorption process, calculated as q_e/C_e, can be used to estimate the thermodynamic parameters, due to its dependence on temperature.

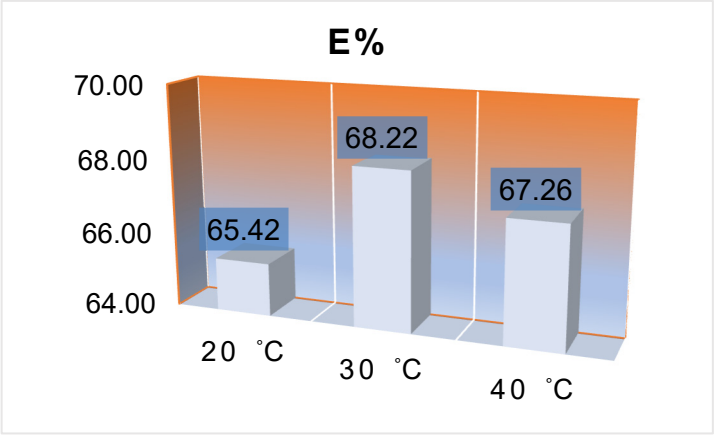

Figure 7. The influence of temperature over the adsorption efficiency of Zn^{2+} onto RGP (272 mg Zn^{2+}/L, 300 rpm, grain size biomass 0.6 - 1 mm, 2 g RGP/ 100 mL).

In order to describe the thermodynamic behaviour of the biosorption of Zn^{2+} onto RGP biomass, standard thermodynamic parameters, including the changes in standard free energy (ΔG°), enthalpy (ΔH°) and entropy (ΔS°) were calculated using the following equations:

$$\Delta G^o = -RTlnK_d \quad (1)$$

$$\Delta \mathrm{G^o} = \Delta \mathrm{H^o} - \mathrm{T}\Delta \mathrm{S^o} \quad (2)$$

where, R is the universal gas constant (8.314×10-3 kJ/K·mol), T is absolute temperature (K), and Kd is the distribution coefficient (L/g) calculated as q_e/C_e, where q_e is biosorption capacity (mg/g) and C_e is Zn^{2+} concentration in solution at equilibrium.

The ΔH° and ΔS° parameters were estimated from the following equation:

$$\mathrm{Kd} = \mathrm{qe/Ce} \quad (3)$$

from the slope and intercept of the lnKd versus 1/T plot [13, 32].

The plot of ln(Kd) as a function of 1/T (Figure 8) yields a straight line (R^2 =0.999) from which ΔH° and ΔS° were calculated, Table 1. The values of ΔG° for Zn^{2+} biosorption onto RGP were found to be negative for the experimental range of temperatures (Table 1) corresponding to a favourable process.

Table 1. The thermodynamic parameters for Zn^{2+} biosorption onto RGP biomass, at various temperatures.

Biomas	**∆H° (kJ/mol)**	**∆S° (kJ/K*mol)**	**∆G° (kJ/mol)**		
RGP	9.150	0.31	293K	303K	313K
			-1.996	-5.187	-8.378

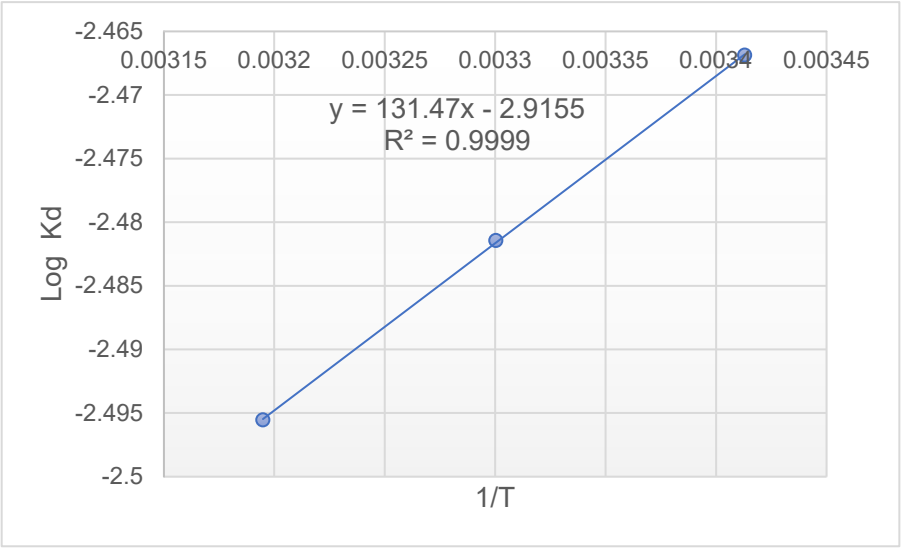

Figure 8. Plot of lnKd versus 1/T for Zn^{2+} biosorption onto RGP (Ci = 272 mg Zn^{2+}/L, 2 g RGP, 0.6 < d < 1.0 mm, 300 rpm).

Furthermore, the decrease in the values of ΔG° with temperature increasing indicates that the biosorption is more favoured at higher temperatures.

The positive value of ΔH° (Table 1) confirms the endothermic nature of the overall biosorption process. This means that, as the temperature increases, more energy is available to enhance the biosorption, but, until 40°C, desorption process begin. Our results are in good agreement with other literature data [30-32].

The endothermic process shows that the diffusion from bulk solution to RGP biosorbent surface may require energy to overcome interaction of dissolved ions with solvation molecules.

Moreover, the positive value of ΔS° (Table 1) points out the increased randomness at the solid/liquid interface during the biosorption of Zn^{2+} onto RGP [17-19].

Biosorption kinetics

Pseudo-first-order (Lagergren, [33]) and pseudo-second-order (Ho, [34]) models were used to study the biosorption kinetic.

Linear regression was used to determine the best fitting kinetic rate equation (coefficient of determination, R^2).

Lagergren suggested a first-order equation for the adsorption of liquid/solid system based on solid capacity, which can be expressed as follows:

$$\frac{dq_t}{dt} = k_1(q_e - q_t) \quad (4)$$

Integrating equation (4) from the boundary conditions t = 0 to t = t and $q_t = 0$ to $q_t = q_t$, gives:

$$ln(q_e - q_t) = lnq_e - k_1 t \quad (5)$$

where: q_e and q_t are the amounts of Zn^{2+} biosorbed (mg Zn^{2+}/g) at equilibrium and time t, respectively, k_1 is the rate constant of first order adsorption (1/min).

The pseudo-second-order kinetic model is derived based on the adsorption capacity of the solid phase, expresses as[19]:

$$\frac{dq_t}{dt} = k_2(q_e - q_t)^2 \quad (6)$$

Integrating eq. (6) from the boundary conditions t = 0 to t = t and $q_t = 0$ to $q_t = q_t$, gives:

$$\frac{1}{(q_e - q_t)} = \frac{1}{q_e} + k_2 t \quad (7)$$

where: q_e and q_t are the amounts of Zn^{2+} biosorbed (mg Zn^{2+}/g) at equilibrium and time t, respectively, k_2 is the rate constant of first order adsorption (g/mg·min).

Equation (7) can be rearranged in linear form, as follows:

$$\frac{t}{q_t} = \frac{1}{k_2 q_e{}^2} + \frac{t}{q_e} \quad (8)$$

Because the correlation coefficients are modest (between 0.92 and 0.95), and calculated adsorption capacities values show great differences by comparison to experimental values (values are not shown) it can be concluded that the Zn^{2+} biosorption onto RGP biomass cannot be classified as pseudo-first-order.

The linear plots of t/q_t versus t representation (Figure 9) allows the calculation of k_2, q_e values and the coefficient of determination, R^2 (Table 2), when pseudo-second-order kinetic model was applied for the considered adsorption process.

Table 2. Pseudo-first and pseudo-second order rate constants, calculated and experimental q_e values for Zn^{2+} biosorption onto RGP.

C (mg Zn^{2+}/L)	Pseudo-first order				Pseudo-second order		
	$q_{e\ exp}$ (mg/g)	$q_{e\ calc}$ (mg/g)	k_1 (min^{-1})	R^2	$q_{e\ calc}$ (mg/g)	k_2 (g/mg·min)	R^2
181	6.61	4.034	0.034	0.923	6.72	0.046	0.998
275	7.94	6.19	0.033	0.946	9.09	0.026	0.996
341	9.92	7.22	0.029	0.951	10.23	0.022	0.998

Values of 0.996-0.998 for R^2 were obtained for all concentrations considered (181–341 mg Zn^{2+}/L).

In addition, the calculated q_e values are very close to the experimental ones (Table 2).

Therefore, it was concluded that Zn^{2+} biosorption on RGP obey the pseudo-second-order kinetic model.

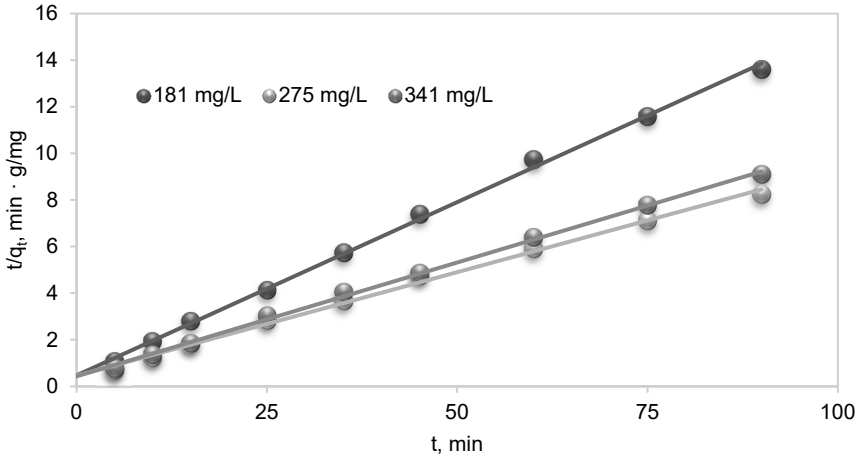

Figure 9. Plots of the pseudo-second-order kinetic model of Zn^{2+} biosorption, onto RGP biomass.

CONCLUSIONS

The study have shown that resveratrol (Rv) can be separated from grape pomace *Vitis vinifera* L. (Cluj, Transylvania region, Romania) with good efficiency, the extraction of Rv with EtOH from RGP biomass being 145 mg/L. The biosorption of Zn^{2+} aqueous solutions using red grape pomace (RGP) *Vitis vinifera* L. has been investigated under different experimental conditions, in batch mode. Biosorption process followed pseudo-second-order kinetic model. The positive enthalpy ($\Delta H° = 9$, 15 kJ mol-1) change for the adsorption process confirms the endothermic nature of the adsorption. The negative values of $\Delta G°$ suggest the spontaneous nature of the adsorption process.

EXPERIMENTAL SECTION

Preparation and characterization of the biosorbent

The biomass used in this work was red grape pomace, RGP (*Vitis vinifera L.,* Cluj, Transylvania region) from the winemaking process. After fermenting for ten days, the by-product was pressed and collected. The sample was dehydrated in a forced-air-drying oven at 50 °C/24 h.

The RGP was treated with 96% EtOH, for 24 hours to extract Rv [28], washed with water to remove traces of alcohol, dried and then treated with a 5% sodium hydroxide solution for 24 hours, to remove organic matter from carbon matrix (with the role of cleaning the internal channels and holes and obtaining a specific surface as large as possible).

The obtained biomass was washed with distilled water, then dried at 105 °C, for 24 hours. The biomass was ground and sieved. The granulation biosorbent material was obtained: 1.0-1.6 mm, 0.6 - 1.0 mm and 0.2 - 0.6 mm which was stored in plastic containers and used in the determinations of the experiments.

Representative RGP samples were investigated using gravimetric method (humidity, apparent density, real density, porosity humidity) [12] and elemental analysis using a Thermo Finnigan Flash EA 1 Series equipment.

The adsorption capacity of a porous material is correlated with properties, such as surface area, pore volume and porosity, these properties are specific to each material [35-38].

Preparation of Zn^{2+} solutions

The Zn^{2+} stock solution (1000 mg/L) was obtained by dissolving the necessary quantity of solid substance, $ZnSO_4 \times 7H_20$ (analytical purity reagent) in distilled water. From this solution, the solutions with known concentration in 181-341 mg/L range were further prepared.

The study of the biosorption process of the Zn^{2+} onto RGP

To determine the optimal parameters of the zinc ion biosorption process on the RGP (working temperature, biosorbent granulation), the pomace samples was contacted with the zinc solution of different concentrations, under magnetic stirring, using a Heidolph MR Hei device, standard equipped with a probe for recording temperature Heidolph EKT Hei-Con.

To determine the residual zinc concentration, samples were taken at different time intervals: 5, 10, 15, 25, 35, 45, 60, 75 and 90 minutes. Samples were appropriately diluted for spectrophotometric determination of zinc concentration using 100 ml graduated flasks. Zinc reagents were added to the collected samples. 10 minutes after the addition of the reagents, the absorbance readings were taken using the Jenway 6305 molecular absorption spectrophotometer, at a wavelength of 420 nm.

The experiments were repeated three times and concentration values were calculated using averaged concentration values.

The experimental data were used to determine the equilibrium time, the equilibrium concentrations, the amounts adsorbed at equilibrium and the efficiency.

The biosorption process capacity and efficiency was calculated with the equation *(9)* and *(10)*:

$$q = \frac{(C_0 - C_t)}{m} \times \frac{V}{1000} \ (mg/g) \tag{9}$$

$$E\ (\%) = \frac{C_0 - C_t}{C_0} \times 100 \tag{10}$$

where: q – biosorption capacity (mg Zn^{2+}/g);
C_0 – Zn^{2+} initial concentration (mg/L);
C_t – Zn^{2+} time *t* concentration (mg/L);
V – aqueous solution volume (mL);
m – biosorbent quantity (g);
E – efficiency (%)

REFERENCES

1. C. Hübner, H. Haase, *Redox Biol*., **2021**, *41*, 1-13.
2. B.L. Vallee; K.H. Falchuk; *Physiol Rev*., **1993**, 73*(1)*, 79-118.
3. M. Ruz; F. Carrasco; P. Rojas; K. Basfi-Fer; M.C. Hernandez; A. Perez; *Biol Trace Elem Res*., **2019**, 188*(1)*, 177-188.

4. A. Takeda; H. Tamano; *Int J Mol Sci*., **2017**, 18*(11)*, 18-29.
5. B. Sandstrom; *Br J Nutr*., **2001**, 85 Suppl 2:S, 181-185.
6. B. Boron; J. Hupert; DH. Barch; *J Nutr.*, **1988**, 118*(8)*, 995-1001.
7. P. Christian; K.P. West Jr., *Am J Clin Nutr*., **1998**. 68(2 Suppl), 435-441.
8. A.S. Prasad; J.A. Halsted; M. Nadimi; *Am J Med*., **1961**,31, 532-546.
9. M.E. Penny; *Ann Nutr Metab*., **2013**, *62 Suppl 1*, 31-42.
10. R. Devesa-Rey, X. Vecino, J.L. Varela-Alende, M.T. Barral, J.M. Cruz, A.B Moldes, *Waste Manage.*, **2011**, *31*, 2327-2335.
11. G. O. El-Sayed, *Desalination,* **2011**, *272*, 225**-**232.
12. M. Stanca; A. Măicăneanu; C. Indolean, Caracterizarea, valorificarea şi regenerarea principalelor materii prime din industria chimică şi petrochimică: îndrumar de lucrări practice“, Presa Universitară Clujeană, **2007**, pp.38-67.
13. L. Semerjian, *J. Hazard. Mater*. **2010**, *173*, 236-242.
14. Y. Bulut, Z. Tez, *J. Environ. Sci.* **2007**, *19,* 160-166.
15. E. Mocchegiani, J. Romeo, M. Malavolta, L. Costarelli, R. Giacconi, L.-E. Diaz, A. Marcos, *Age*, **2013**, *35*, 839–860.
16. A. S. Prasad, *Mol. Med*., **2008**, *14*, 353–357.
17. F. Ge, M.-M. Li, H. Ye, B.-X. Zhao, J. Hazard. Mat. **2012**, *211–212,* 366-372.
18. Y.S. Ho, G. McKay, *Water Res.* **2000**, *34*, 735-742.
19. A.Khaled, A. El-Nemr, A. El-Sikaily, O. Abdelwahab, *Desalination*, **2009**, *238*, 210-232.
20. K.V. Kumar, V. Ramamurthi, S. Sivanesan, *J. Colloid Interface Sci.*, **2005** *284*, 14-21.
21. T. Akar, Z. Kaynak, S. Ulusoy, D. Yuvaci, G. Ozsari, S.T. Akar, *J. Hazard. Mat*. **2009**, *163*, 1134-1141.
22. B. Nagy, C. Manzatu, A. Maicaneanu, C. Indolean,L. Silaghi-Dumitrescu, C. Majdik, *J. Wood Chem. Technol.* **2014**, *34*, 301-311.
23. C. Indolean, S. Burcă, A. Măicăneanu, M. Stanca, D. Rădulescu, *Studia UBB Chemia.*, **2013**, *LVIII2*, 23-34.
24. T.I. Lafka, V. Sinanoglou, E.S. Lazos, *Food Chem*., **2007**, *104(3)*,1206-1214.
25. M. L. Muncaciu, F. Zamora Marin, N. Pop, A.C. Babes, *Not. Bot. Horti. Agrobo*., **2017**, *45(2)*, 532-539.
26. A.B.B. Bender, C.S. Speroni, K.I.B. Moro, F.D.P. Morisso, D.R. dos Santos, L.P. da Silva, N.G. Penna, *LWT*, **2020**, *117*, 108652-108661.
27. F. Bennato, A. Di Luca, C. Martino, A. Ianni, E. Marone, L. Grotta, S Ramazzotti, A. Cichelli, G. Martino, *Foods*, **2020**, *9*, 508-
28. B. Antonić, S. Jančíková, D. Dordević, B. Tremlová, *Foods*, **2020**, *9*, 1627-1647.
29. I.E. Raschip, N. Fifere, M.V. Dinu, *Gels*, **2021**, *7*, 76-94.
30. R. Devesa-Rey; X. Vecino; J.L. Varela-Alende; M.T. Barral; J.M. Cruz; A.B Moldes; *Waste Manage.,* **2011**, *31,* 2327–2335.
31. S.J. Allen; G. McKay and J.F. Porter; *J. Colloid. Interface Sci*., **2004**, *280*, 322-333.
32. A.S. Prasad, *J. Trace Elem. Med. Biol*., **2014**, *28*, 357-420.
33. S. Lagergren, B.K. Svenska, *Kungliga Svenska Vetenskapsakademiens. Handlingar*, **1898**, *24(4)*, 1-39.

34. Y.S. Ho, G. Mckay, *Process Biochemistry*, **1999**, *34*, 451-465.
35. R. Han; W. Zou; W. Yu; S. Cheng; Y. Wang and J. Shi; *J. Hazard. Mater*., **2006**, *141*, 156-163.
36. O. Gercel; H.F. Gercel; A. Savas; C. Koparal; U.B. Ogutverenc; *J. Hazard. Mater*., **2008**, *160*, 668- 674.
37. B. Volensky; "New biosorbers for non-waste technology", CRC Press Inc., Boca Raton, Florida, **1990**, pp. 3-25.
38. F.A. Pavan; E.C. Lima; E.C. Dias; A.C. Mazzocato; *J. Hazard. Mater*., **2008**, *150*, 703-712.

STUDIA UBB CHEMIA, LXVII, 3, 2022 (p. 61-74)
(RECOMMENDED CITATION)
DOI:10.24193/subbchem.2022.3.05

CURCUMIN AND WHEY PROTEIN BINDING AND STRUCTURAL CHARACTERISTICS OF THEIR COMPLEX EVIDENCED BY ATOMIC FORCE MICROSCOPY

LEVENTE ZSOLT RACZ[a], GERTRUD-ALEXANDRA PALTINEAN[a], IOAN PETEAN[a], GHEORGHE TOMOAIA[b,c] , LUCIAN CRISTIAN POP[a], GEORGE ARGHIR[d], ERIKA LEVEI[e], AURORA MOCANU[a], CSABA-PAL RACZ[a], MARIA TOMOAIA-COTISEL[a,c] *

ABSTRACT. Curcumin (CCM) has beneficial effects on human health due to its pharmacological activities, which have a protective role against many diseases. Whey protein concentrate (WPC) is a product from the milk industry that is often used to improve and stabilize different foods. It helps curcumin improve its water solubility, poor bioavailability, low stability, and efficacy. Atomic force microscopy (AFM) was employed to highlight the surface topography of adsorbed films of pure curcumin, pure whey protein concentrate, and their CCM-WPC complex. The obtained results show that individual nanoparticles, NPs, were mobilized into the aqueous dispersion and successfully adsorbed onto the glass slides as thin films. Their NPs shape is rounded, and their diameter differs on each sample, namely about 30 nm for CCM, around 55 nm for WPC, and about 40 nm for the CCM-WPC complex. It proves that both CCM and WPC molecules generate a complex that embeds them in a compact structure. The surface roughness was also monitored, and pure CCM produces the smoothest and uniform film, meanwhile, the presence of WPC makes several pores in the film surface which increases the roughness value. The obtained results provide useful evidence for the application of whey protein as an effective carrier of curcumin, a bioactive polyphenol compound. In addition, this work supports the application of the CCM-WPC complex as health supplements.

Keywords: *Curcumin, whey protein concentrate, curcumin-whey protein complex, AFM, nanostructure, roughness*

[a] *Babeş-Bolyai University, Research Center of Physical Chemistry, Faculty of Chemistry and Chemical Engineering, 11 Arany Janos str., RO-400028, Cluj-Napoca, Romania*
[b] *Iuliu Hatieganu University of Medicine and Pharmacy, Department of Orthopedics and Traumatology, 47 Gen. Traian Mosoiu str., RO-400132, Cluj-Napoca, Romania*
[c] *Academy of Romanian Scientists, 3 Ilfov str., RO-050044, Bucharest, Romania*
[d] *Technical University, Faculty of Materials and Environment Engineering, 103-105 Muncii Boulevard, RO-400641, Cluj-Napoca, Romania*
[e] *INCDO-INOE2000, Research Institute for Analytical Instrumentation, 67 Donath str., RO-400293 Cluj-Napoca, Romania*
** Corresponding author: mcotisel@gmail.com*

INTRODUCTION

Curcumin (CCM) is a nutraceutical substance with many pharmacological activities such as antioxidant, anticancer and analgesic, anti-inflammatory, antiseptic, antiviral, antidiabetic, and antiparasitic, for which researchers' attention was directed to its study in the biomedical field [1]. This aspect is well documented in the literature: CCM prevents inflammatory diseases, inhibits carcinogenesis, controls neurological, respiratory, cardiovascular, metabolic, autoimmune diseases, and some cancers [2, 3]. It is a small molecular weight compound extracted from the rhizomes of the *Curcuma longa* plant and is used as a yellow spice in the food industry. Specialized literature and the Food and Drug Administration declared that curcumin utilization is safe and without toxic effect [4]. It is known as diferuloylmethane or (1E,6E)-1,7-bis(4-hydroxy-3-methoxyphenyl)-hepta1,6-diene-3,5-dione). Its structure contains two aromatic rings having phenolic o-methoxy groups, connected by a β-diketone fragment.

Curcumin has low water solubility that contributed to its poor bioavailability, stability, adsorption, and efficacy, limiting its therapeutic potential [5-9]. Approaches to improving this limitation of curcumin properties were highlighted in some research studies by the preparation of complex systems between curcumin and phospholipids, curcumin and proteins (whey protein, pea proteins, soy proteins or rice bran proteins), curcumin and β-cyclodextrins (βCD), and other colloidal systems for encapsulation or drug delivery based on liposomes, micelles and polymers [10-12]. CCM binds to proteins molecules through hydrogen bonds forming a complex that can improve the dispersibility, bioavailability and biological activity of curcumin [13]. β-Lactoglobulin is the main component of the whey protein which has the capacity to bind to CCM due to its hydrophobic core and its resistance to pepsin digestion. Therefore, the complex made by β-lactoglobulin and CCM can be an effective carrier of CCM in the intestinal tract to treat inflammatory bowel disease [14, 15]. In the case of cyclodextrins, the dedicated literature reveals that cyclodextrins are the best carriers for enhancing the solubility of CCM. The conical cavities of cyclodextrins are able of including various organic guests and form inclusion complexes. Regarding the CCM-βCD inclusion complexes, the literature emphasizes the release of drug and drug stability [16-20].

Whey protein concentrated (WPC) is a product resulting from cheese manufacturing in the milk industry. Whey protein is used as an ingredient in foods such as dairy, bakery products, beverages, and meat products [21]. It is a low-cost chemical product that is non-toxic and presents good biocompatibility. WPC is a mixture of β-lactoglobulin (57%), α-lactalbumin

(19%), immunoglobulins which are actually some glycoprotein molecules (13%), bovine serum albumin (7%) and specific polypeptides (4%), additional minor protein/peptide components (lactoferrin, lactoperoxidase), glycomacropeptide, carbohydrates such as lactose, minerals, vitamins, fatty acids, and cholesterol (a lipid) [22-25]. The data in the literature highlighted that the whey protein possesses some functional attributes which allowed the encapsulation of molecules such as curcumin, to improve the solubility and bioavailability. In addition, it can form gels, foams, or emulsions when is used in food products [26]. Whey proteins are in 3 forms on the market: concentrates, isolates, and hydrolysates. The difference between them is given by the percentage of protein; the concentrate has fat, lactose, and proteins 29-89%, the isolate 90 % proteins and the hydrolysates represent the partial digested type of proteins. All these forms of whey proteins have some biological activity such as anticancer, antioxidant, antidiabetic, antihypertensive [6, 23, 27, 28].

The benefits of the CCM-WPC complex are highlighted in the literature as: high resistance under gastric conditions; antitumor effects against skin melanoma cells and its ability to decrease blood glucose and liver oxidative stress and inflammatory damage [6, 28, 29]. Some studies use nano-ionization to fabricate curcumin-whey protein composite particles and show that denaturation of whey protein improves the protein-curcumin interactions [30].

According to the fact that whey proteins, such as β-lactoglobulin, have internal and external binding sites for hydrophobic molecules, such as curcumin, and varied interactions, such as hydrophobic and electrostatic interactions, as well as hydrogen bonding can occur between these proteins and curcumin.

The curcumin-whey protein complex in the 1:1 mole ratio was previously investigated by FTIR and XRD, and the encapsulation of CCM in the WPC was revealed [6].

In the present research, our aim was to gain an understanding of the binding between curcumin and whey protein concentrate nanoparticles using the AFM images. To the best of our knowledge, this is the first study with whey protein concentrate as a nano-carrier and curcumin under physiological condition. This investigation could be of support for the stabilization and delivery of curcumin under different environmental conditions to increase its bioavailability and biological effects.

RESULTS AND DISCUSSION

AFM is a useful technology for the characterization of the materials microstructure, nanostructure, and nanomechanical properties [31]. It represents multidisciplinary research in the field of bio nanostructures [32-34], thin films [35, 36], multifunctional biomaterials [37-43], and environmental pollution [44, 45]. AFM is a complex investigation method that allows: measuring surface roughness and characteristics of samples [46-54], analyzing the interaction of the cell membrane with drugs [55-59]. Also, it is useful to visualize the self-assemblies of biomolecules and allows measuring the average particles diameter [60].

AFM may be operated in three modes: contact mode, non-contact, and tapping mode. In this research we use AFM in tapping mode to evaluate the surface morphology and roughness of the samples.

The curcumin powder dispersed in ultrapure water ensures a mobilization of nanoparticles that are in Brownian agitation. Glass slide immersion into the curcumin dispersion for 10 seconds facilitates these nanoparticles to reach the lamella surface and to be adsorbed on it. They remain well fixed, ensuring a very well-formed film after natural drying, as observed from the macroscopic examination of the sample. AFM imaging allows us to observe the nanostructure of this thin film, Figure 1.

The topography of the surface reveals curcumin nanoparticles with spherical shape uniformly adsorbed ensuring a good cohesion of the film, Figure 1a. They are adsorbed in a uniform manner avoiding sticking. This aspect is due to the low solubility of curcumin in aqueous medium. Therefore, the nanoparticles remain sharp and keep their diameter unchanged in contact with water. At the same time, these nanoparticles are very well individualized, appearing well outlined in the phase image, Figure 1b, where they have a brown nuance, and the space between them (the boundary between them) appears with a yellow colour. This is due to the well-defined nanoparticle boundaries. The amplitude image sustains the good structuring of the adsorbed film, Figure 1c, evidencing the uniformity of the adsorbed nanoparticles layer. The profiles in the topographic image show the rounded appearance of the nanoparticles and their diameter around 30 nm, fact confirmed by the particle size distribution histogram in Figure 1f. The regularity of the film leads to very low values of surface roughness expressed as the quadratic mean of the profile height deviations as root mean square, RMS of about 4.76 nm, and arithmetic average roughness, Ra nearby 3.82 nm. The obtained values are comparable to the ones for similar thin films reported in the literature [35, 36].

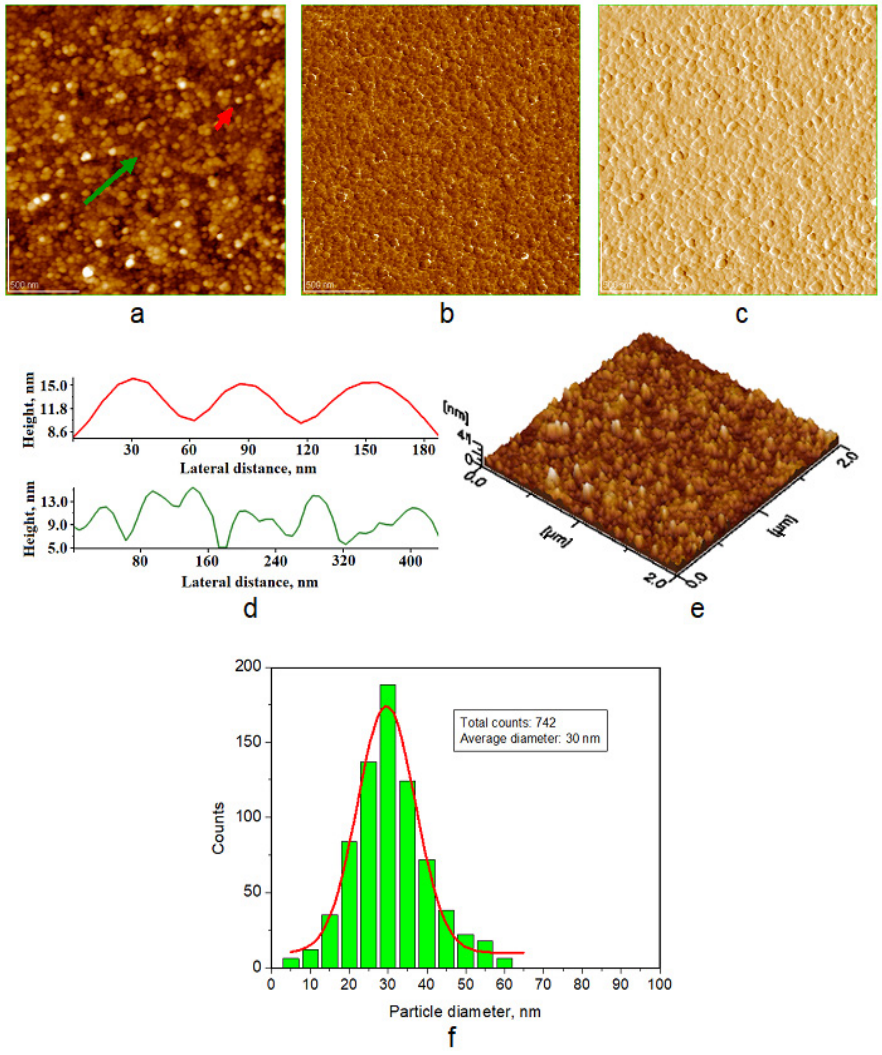

Figure 1. AFM images of CCM NPs adsorbed on glass and naturally dried: a) topographic image, b) phase image, c) amplitude image, d) profiles along the arrows in panel (a), e) tridimensional image and f) histogram of particle size distribution. Scanned area 2 µm x 2 µm.

A prolonged adsorption time could lead to the WPC nanoparticles dissolution due to their particular water solubility. The adsorption time control is one of the most important parameters when working with whey protein.

The whey protein concentrate was successfully dispersed in an aqueous environment, ensuring optimal conditions for the transfer of nanoparticles on the glass support by adsorption for 10 seconds, Figure 2.

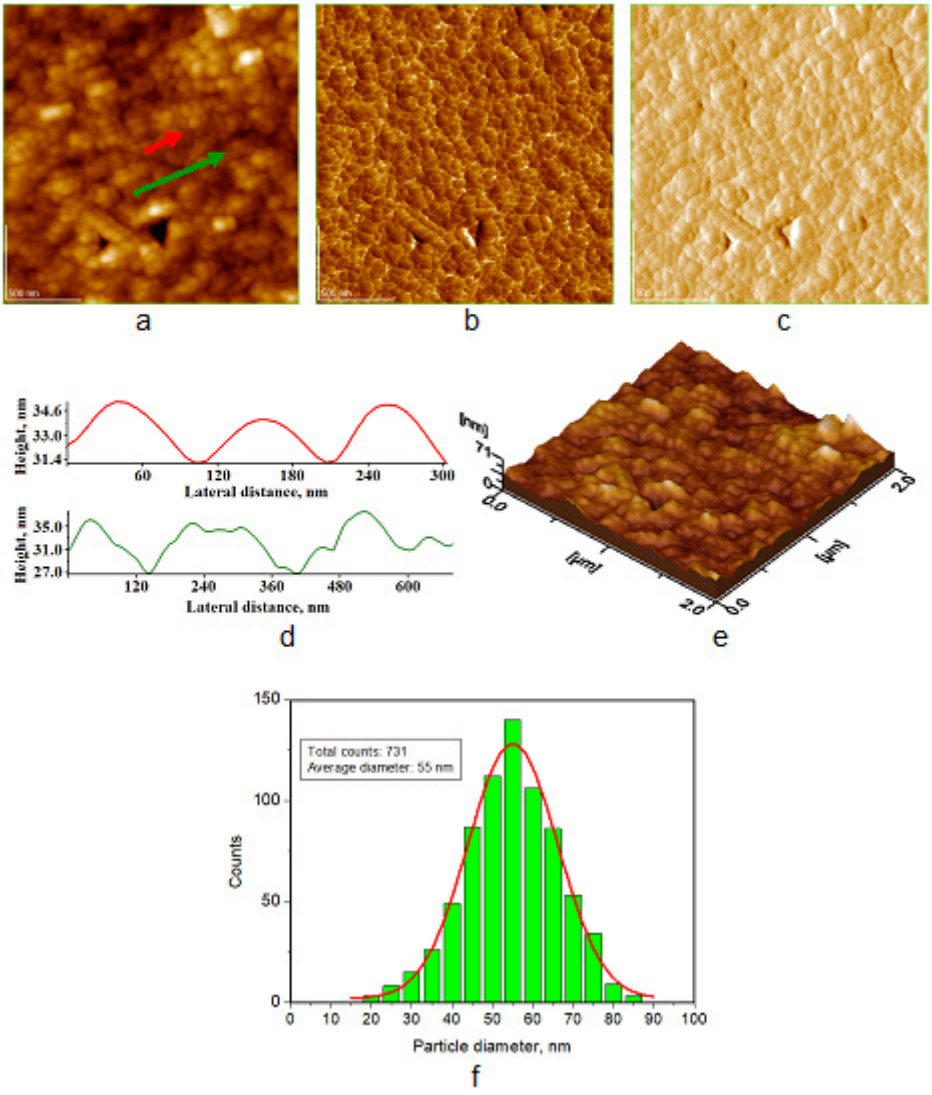

Figure 2. AFM images of WPC NPs adsorbed on glass and naturally dried: a) topographic image, b) phase image, c) amplitude image, d) profiles along the arrows in panel (a), e) tridimensional image and f) histogram of particle size distribution. Scanned area 2 µm x 2 µm.

The topography of the obtained film highlights a uniform adsorption of the nanoparticles. They present a rounded shape and a high agglomeration tendency being adsorbed very close to each other. The revealed topographical aspect in Figure 2a confirms the success of adsorption. On the other hand, the agglomeration tendency is explained by the partial solubility of WPC in aqueous environment. The nanoparticles surface become sticky in such humid conditions and tends to bond them together, forming clusters. Several pores were observed in some places with diameters between 60 and 180 nm as well as a slight tendency to form clusters as can be seen in the upper right corner of the image. Cluster formation is inhibited by the short adsorption time and the dilution in the dispersion; Figure 2a. However, most of the film areas are uniform and show a good individualization of the nanoparticles, although they are very close to each other. This is supported by the phase image, Figure 2b, where the boundary between the nanoparticles is very small and appears yellow, while the nanoparticles are brown. The tendency to form clusters is, however, very weak because they cannot be observed in the amplitude image, Figure 2c, but instead, in this image one can see the porosity of the sample. This leads to a roughness RMS of around 6.53 nm and Ra of about 5.09 nm. These aspects are perfectly correlated with the 3D topographic image in Figure 2e. The cross-section profiles of the topographic image highlight the rounded shape of the nanoparticles and indicate their average diameter around 55 nm. This is in full agreement with the data from the particle size distribution histogram, Figure 2f. It seems that the partial solubility on WPC nanoparticles in aqueous environment determined the appearance of the pores in the adsorbed film topography.

Complexation between curcumin and whey protein concentrate shows significant changes in the morphology and behaviour of the resulting powder. Its dispersion in ultrapure water releases nanoparticles that are adsorbed in a uniform way on the glass surface. AFM images prove to be strong evidence of this effect, Figure 3.

The surface topography shows a thin film of round nanoparticles uniformly adsorbed on the glass slide. The resulted morphology is complex containing elements from both components: from curcumin is observed the good individualization of the nanoparticles and from whey protein the tendency for pore formation is observed (pore size situated in the range of in 60 to 90 nm). The nanoparticles were adsorbed very close to each other, but they are not bonded together, keeping their individuality, fact very well evidenced by the phase and amplitude image, Figures 3b and 3c.

The appearance of the 3D image is smooth and uniform, but the significant presence of pores determines the roughness values of RMS about 6.62 nm and Ra nearby 5.00 nm. The cross-section profiles in Figure 3d show the nanoparticles rounded shape and the average diameter of 40 nm, fact in accordance with the particle size distribution in Figure 3f. Data in the

literature indicates diameters of WPC nanoparticles of about 40 nm [61, 62]. The pores presence in the CCM-WPC thin film is collateral evidence of complex solubility increasing. Pore development within the tin film may occur due to the local dissolution of some WPC nanoparticles in the contact with humid environment.

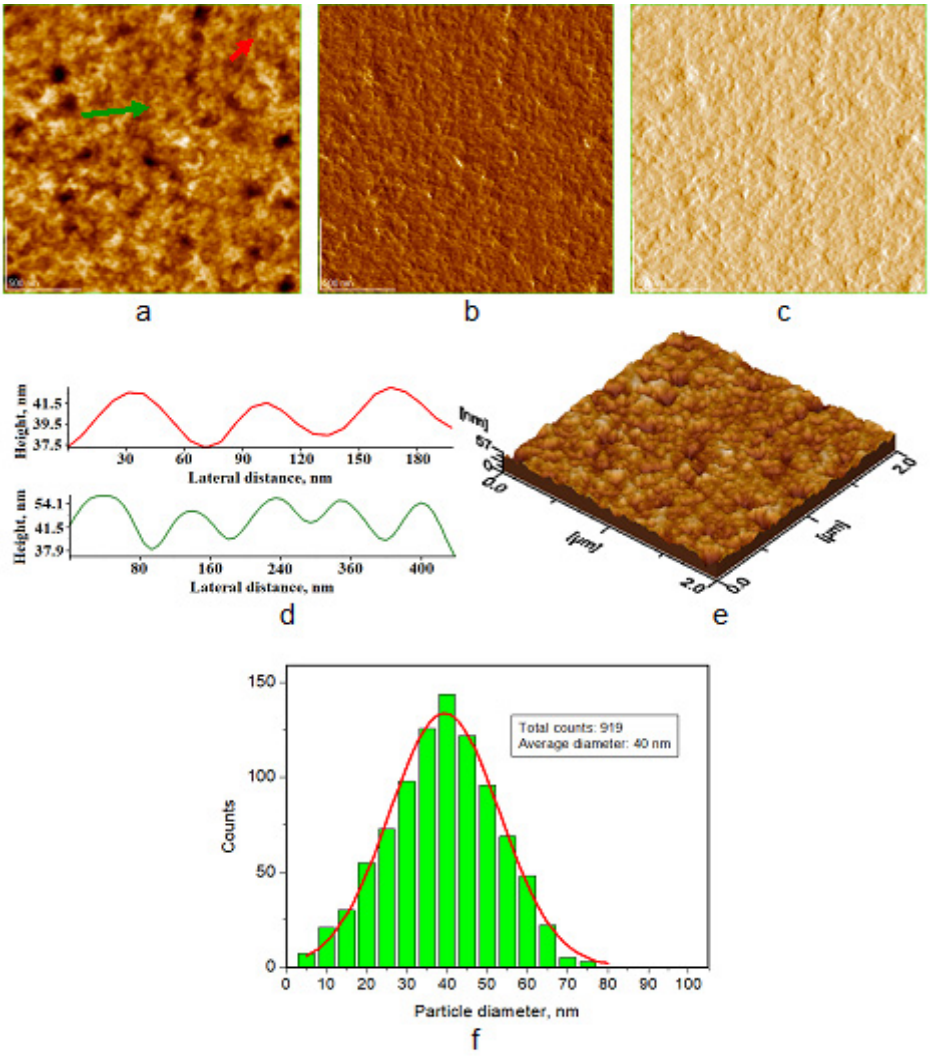

Figure 3. AFM images of the CCM-WPC complex, obtained at pH 7.4, adsorbed on glass and naturally dried: a) topographic image, b) phase image, c) amplitude image, d) profile along the arrow in panel (a), e) tridimensional image and f) histogram of particle size distribution. Scanned area 2 µm x 2 µm.

The nanostructure evolution in the CCM – WPC system reveals that the complex nanoparticles have a larger diameter than that of pure curcumin, but smaller than that of concentrated whey protein. This is a proof of the interpenetration of the CCM and WPC, in good agreement with the microscopically observation in the literature [61]. Therefore, the initial state of the CCM-WPC complex is a dry powder just like many other dietary supplements on the market. The present research evidences the CCM-WPC ability to release nanoparticles into the aqueous environment that is similar to the one release in the stomach medium. AFM investigation sustains the CCM-WPC nanoparticles affinity to be adsorbed on the surfaces. It may be a useful behavior during digestion to enhance contact with the small intestine walls.

The observations within present research allow us to figure out two ways of CCM-WPC delivery into the gastric system: the direct one using a classic dissolvable capsule with complex powder at the proper dosage or a pressed pill; and the indirect delivery which is supposed to encapsulate the complex powder into a microsphere. The CCM-WPC powder encapsulation in a microsphere made of dissolvable material presents the benefit of controlled release during digestion, avoiding premature contact of the nanoparticles with the digestive juice and the intestine wall. These aspects represent a challenge for the future.

CONCLUSIONS

The nanostructures of the CCM-WPC system were successfully investigated by atomic force microscopy which is a fundamental method for the nano characterization of materials. Both initial CCM and WPC powders were able to form nanoparticles into aqueous environment. These nanoparticles were adsorbed onto a glass substrate, forming thin films. Their shape is rounded, and their diameter differs on each sample: about 30 nm for CCM, around 55 nm for WPC.

The complexation involved between CCM and WPC leads to an intermediary diameter of approximately 40 nm. CCM nanoparticles are uniformly adsorbed on the glass surface, generating a smooth film with low roughness. WPC tends to generate pores on the adsorbed film, which leads to relatively higher values of the roughness. The CCM-WPC complex forms a smooth thin film, but the influence of WPC within the composition still generates some pores that affect the roughness value.

These results might support the development of functional foods including curcumin and whey protein, with new uses in yoghourt and nutritional supplements.

EXPERIMENTAL SECTION

Materials

Curcumin from *Curcuma longa* powder ≥ 65%, ethanol (CH_3CH_2OH) 95%, were purchased from Sigma-Aldrich, Darmstadt, Germany; Whey protein concentrate (WPC) contains about 80% protein and it was purchased from Foodcom S.A. Warsaw, Poland. Ammonia solution 25% was purchased from Merck, Darmstadt, Germany. Ultrapure water (resistivity of 18.2 MΩ x cm) was used in all experiments.

Preparation of the CCM-WPC complex

A solution containing 0.50 g CCM (1.36 mmol) in 50 mL ethanol and a solution of 24.97 g WPC (1.36 mmol) in 1 L of water with NH_3 solution added dropwise to adjust the pH at 7.4 were prepared. The molar mass of β-lactoglobulin (18400 g/mol) was taken for the molar mass of WPC. The two solutions were mixed and stirred magnetically for 4 hours in dark condition, at room temperature. The resulting CCM and WPC (1:1 mole ratio) complex was dried using a Pilotech YC-018A spray dryer, at T_{in} of about 165 ^oC and T_{out} of around 49 ^oC, with ventilator frequency 58 Hz and solution flow rate 5 mL/min.

Samples preparation for AFM investigation

Curcumin was dispersed in ultrapure water, followed by homogenization with a magnetic stirrer at 500 rpm for 15 minutes. The CCM film adsorption was done in vertical plane on glass, 10 seconds, followed by natural drying at room temperature. For whey protein concentrate (WPC) and for the CCM-WPC complex, the process was similar.

Atomic Force Microscopy

AFM, JEOL JSPM 4210 model (Tokyo, Japan) was used to determine the NPs size and morphology of the layer of curcumin, whey protein concentrate and the CCM-WPC complex. The surface of the sample is scanned with a sharp tip (cantilever) that is brought as close as possible to its surface with optical technique so that AFM images are obtained by monitoring the change in amplitude of the cantilever oscillation during scanning. The measurements were performed in tapping mode (the most common mode of obtaining surface morphology) using a silicon nitride cantilever (NSC 15 Hard) purchased from MikroMasch, Sofia, Bulgaria, with a resonant frequency of 325 kHz and a force constant of 40 N/m.

The topographic, phase and amplitude images were obtained simultaneously at a scanning speed of about 1.2 Hz and their processing was performed with Win SPM2.0 Processing software, JEOL, Japan.

ACKNOWLEDGMENTS

This work was supported by grants of the Ministry of Research, Innovation and Digitization, CNCS/CCCDI-UEFISCDI, project number 186 and 481, within PNCDI III.

REFERENCES

1. B. Zheng; D.J. McClements; *Molecules*, **2020**, *25*, 2791.
2. V. Furlan; J. Konc; U. Bren; *Molecules*, **2018**, *23*, 3351.
3. S.S. Hettiarachchi; S.P. Dunuweera; A.N. Dunuweera; R.M.G. Rajapakse; *ACS Omega*, **2021**, *6*, 8246−8252.
4. M.U. Akbar; K. Rehman; K.M. Zia; M.I. Qadir; M.S.H. Akash; M. Ibrahim; *Crit. Rev. Eukaryot. Gene Expr.*, **2018**, *28*(1), 17–24.
5. M.L. Del Prado-Audelo; I.H. Caballero-Floran; J.A. Meza-Toledo; N. Mendoza-Munoz; M. Gonzalez-Torres; B. Floran; H. Cortes; G. Leyva-Gomez; *Biomolecules*, **2019**, *9*, 56.
6. L. Racz; M. Tomoaia-Cotisel; Cs.P. Racz; P. Bulieris; I. Grosu; S. Porav; A. Ciorita; X. Filip; F. Martin; G. Serban; I. Kacso; *Studia UBB Chemia*, **2021**, *66*(3), 209-224.
7. G.A. Paltinean; S. Riga; Gh. Tomoaia; A. Mocanu; M. Tomoaia-Cotisel; *Academy of Romanian Scientists Annals Series on Biological Sciences,* **2021**, *10*(2), 103-141.
8. K.I. Priyadarsini; *Molecules*, **2014**, *19*(12), 20091-20112.
9. B.H. Ali; H. Marrif; S.A. Noureldayem; A.O. Bakheit; G. Blunden; *Nat. Prod. Commun*., **2006**, *1*(6), 509-521.
10. S. Solghi; Z. Emam-Djomeh; M. Fathi; F. Farahani; *J. Food Process Eng*., **2020**, *43*(6), e13403.
11. V.S Ipar; A. Dsouza; P.V. Devarajan; *Eur. J. Drug Metab. Pharmacokinet*., **2019**, *44*(4), 459-480.
12. M. Kharat; D.J. McClements; *J. Colloid Interface Sci.,* **2019**, *557*, 506–518.
13. A.D. Moghaddam; M. Mohammadian; A. Sharifan; S. Hadi; *J. Food Bioprocess Eng.*, **2019**, *2*(1), 55-60.
14. A.H. Sneharani; J.V. Karakkat; S.A. Singh; A.G.A. Rao; *J. Agric. Food Chem*., **2010**, *58*(20), 11130–11139.

15. M. Li; Y. Ma; M. O. Ngadi; *Food Chem*., **2013**, *141*(2), 1504-1511.
16. P. Arya; N. Raghav; *J. Mol. Struct*., **2021**, *1228*, 129774.
17. H. Mashaqbeh; R. Obaidat; N. Al-Shar'I; *Polymers*, **2021**, *13*(23), 4073.
18. Cs.P. Racz; R.D. Pasca; S. Santa; I. Kacso; Gh. Tomoaia; A. Mocanu; O. Horovitz; M. Tomoaia-Cotisel; *Rev. Chim. (Bucharest*), **2011**, *62*(10), 992-997.
19. Cs.P. Racz; G. Borodi; M.M. Pop; I. Kacso; S. Santa; M. Tomoaia-Cotisel; *Acta. Crystallogr. B. Struct. Sci. Cryst. Eng. Mater*., **2012**, *68*(2), 164-170.
20. Cs.P. Racz; S. Santa; M. Tomoaia-Cotisel; G. Borodi; I. Kacso; A. Pirnau; I. Bratu; *J. Incl. Phenom. Macrocycl. Chem.,* **2013***, 76*(1), 193-199.
21. J. Burgain; R. El Zein; J. Scher; J. Petit; E.A. Norwood; G. Francius; C. Gaiani; *J. Food Eng*., **2016**, *178*, 39-46.
22. P.S. de P. Herrmann; C.M.P. Yoshida; A.J. Antunes; J.A. Marcondes; *Packag. Technol. Sci*., **2004**, *17*, 267–273.
23. P.X. Qi; C.I. Onwulata; *J. Dairy Sci*., **2011**, *94*(5), 2231–2244.
24. G.T. D. Sousa; F.S. Lira; J.C. Rosa; E.P. de Oliveira; L.M. Oyama; R.V. Santos; G.D. Pimentel; *Lipids Health Dis*., **2012**, *11*, 67.
25. U.S. Dairy Export Council; *Reference Manual for U.S. Whey and Lactose Products*, edited by V. Lagrange; U.S. Dairy Export Council, Arlington, USA, **2003**, pp. 1-226.
26. G.K. Gbassi; F.S. Yolou; S.O. Sarr; P.G. Atheba; C.N. Amin; M. Ake*; Int. J. Biol. Chem. Sci.,* **2012**, *6*(4), 1828-1837.
27. S. Patel; *J. Funct. Foods*, **2015**, *19*, 308–319.
28. S. Minj; S. Anand; *Dairy*, **2020**, *1*, 233–258.
29. A.R. da Conceicao; K.A. Dias; S.M.S. Pereira; L.C. Saraiva; L.A. Oliveira; E.C. Gomes de Souza; R.V. Goncalves; S.L.P. da Matta; A.J. Natali; H.S.D. Martino; C.M. Della Lucia; *Br. J. Nutr*., **2022**, *127*, 526–539.
30. A. Nayak; C. Genot; A. Meynier; A. Dorlando; I. Capron; *LWT,* **2022,** *153*, 112421.
31. Y. Wen; Z. Xu, Y. Liu; H. Corke; Z. Sui; *Compr. Rev. Food Sci. Food. Saf*., **2020**, 1–24.
32. R.D. Pasca; Gh. Tomoaia; A. Mocanu; I. Petean; A.G. Paltinean; O. Soritau; M. Tomoaia-Cotisel; *Studia UBB Chemia*, **2015**, *60*(3), 257-264.
33. Gh. Tomoaia; O. Soritau; M. Tomoaia-Cotisel; L.B. Pop; A. Pop; A. Mocanu; O. Horovitz; L.D. Bobos; *Powder Technol*., **2013**, *238*, 99-107.
34. Gh. Tomoaia; M. Tomoaia-Cotisel; L.B. Pop; A. Pop; O. Horovitz; A. Mocanu; N. Jumate; L.D. Bobos; *Rev. Roum. Chim*., **2011**, *56*(10-11), 1039-1046.
35. A. Mocanu; I. Cernica; Gh. Tomoaia; L.D. Bobos; O. Horovitz; M. Tomoaia-Cotisel; *Colloid Surf. A*, **2009**, *338*(1-3), 93-101.
36. Gh. Tomoaia; O. Horovitz; A. Mocanu; A. Nita; A. Avram; Cs.P. Racz; O. Soritau; M. Cenariu; M. Tomoaia-Cotisel; *Colloids Surf. B*, **2015**, *135*, 726-734.

37. A. Mocanu; O. Cadar; P.T. Frangopol; I. Petean; Gh. Tomoaia; G.A. Paltinean; Cs.P. Racz; O. Horovitz; M. Tomoaia-Cotisel; *R. Soc. Open Sci.*, **2021**, *8*(1), 201785.
38. C. Garbo; J. Locs; M. D'Este; G. Demazeau; A. Mocanu; C. Roman; O. Horovitz; M. Tomoaia-Cotisel; *Int. J. Nanomed*., **2020**, *15*, 1037-1058.
39. D. Oltean-Dan; G.B. Dogaru; M. Tomoaia-Cotisel; D. Apostu; A. Mester; H.R. C. Benea; M.G. Paiusan; E.M. Jianu; A. Mocanu; R. Balint; C.O. Popa; C. Berce; G.I. Bodizs; A.M. Toader; Gh. Tomoaia; *Int. J. Nanomed*., **2019**, *14*, 5799-5816.
40. D. Oltean-Dan; G.B. Dogaru; E.M. Jianu; S. Riga; M. Tomoaia-Cotisel; A. Mocanu; L. Barbu-Tudoran; Gh. Tomoaia; *Micromachines*, **2021**, *12*(11), 1352.
41. A. Mocanu; G. Furtos; S. Rapuntean; O. Horovitz; F. Chirila; C. Garbo; A. Danisteanu; G. Rapuntean; C. Prejmerean; M. Tomoaia-Cotisel; *Appl. Surf. Sci.*, **2014**, *298*, 225-235.
42. C. Garbo; M. Sindilaru; A. Carlea; Gh. Tomoaia; V. Almasan; I. Petean; A. Mocanu; O. Horovitz; M. Tomoaia-Cotisel; *Part. Sci. Technol*., **2017**, *35*(1), 29-37.
43. G. Furtos; M. Tomoaia-Cotisel; C. Garbo; M. Senila; N. Jumate; I. Vida-Simiti; C. Prejmerean; *Part. Sci. Technol*., **2013**, *31*(4), 392-398.
44. G.A. Hosu-Prack; I. Petean; G. Arghir; L.D. Bobos; I. Iurcut; M. Tomoaia-Cotisel; *Carpathian J. Earth Environ. Sci*., **2013**, *8*(4), 75-82.
45. G.A. Paltinean; I. Petean; G. Arghir; D.F. Muntean; L.D. Bobos; M. Tomoaia-Cotisel; *Partic. Sci. Technol*., **2016**, *34*(5), 580-585.
46. M. Tomoaia-Cotisel; A. Tomoaia-Cotisel; T. Yupsanis; Gh. Tomoaia; I. Balea; A. Mocanu; Cs.P. Racz; *Rev. Roum. Chim*., **2006**, *51*(12),1181-1185.
47. O. Horovitz; Gh. Tomoaia; A. Mocanu; T. Yupsanis; M. Tomoaia-Cotisel; *Gold Bull*., **2007**, *40*(3), 213-218.
48. O. Horovitz; A. Mocanu; Gh. Tomoaia; L.D. Bobos; D. Dubert; I. Daian; T. Yupsanis; M. Tomoaia-Cotisel; *Studia UBB Chemia*, **2007**, *52*(1), 97-108.
49. O. Horovitz; A. Mocanu; Gh. Tomoaia; M. Crisan; L.D. Bobos; Cs.P. Racz; M. Tomoaia-Cotisel; *Studia UBB Chemia*, **2007**, *52*(3), 53-71.
50. M. Tomoaia-Cotisel; A. Mocanu; *Rev. Chim. (Bucharest)*, **2008**, *59*(11), 1230-1233.
51. P.T. Frangopol; D.A. Cadenhead; M. Tomoaia-Cotisel; A. Mocanu; *Studia UBB Chemia*, **2009**, *54*(1), 23-35.
52. I. Balea; M. Tomoaia-Cotisel; O. Horovitz; Gh. Tomoaia; A. Mocanu; *Studia UBB Chemia*, **2009**, *54*(1), 151-163.
53. Gh. Tomoaia; C. Borzan; M. Crisan; A. Mocanu; O. Horovitz; L.D. Bobos; M. Tomoaia-Cotisel; *Rev. Roum. Chim*., **2009**, *54*(5), 363-372.
54. O. Monfort; L.C. Pop; S. Sfaelou; T. Plecenik; T. Roch; V. Dracopoulos; E. Stathatos; G. Plesch; P. Lianos; *Chem. Eng. J*., **2016,** *286,* 91-97.
55. M. Tomoaia-Cotisel; D.V. Pop-Toader; U.V. Zdrenghea; Gh. Tomoaia; O. Horovitz; A. Mocanu; *Studia UBB Chemia*., **2009**, *54*(4), 285-296.

56. U.V. Zdrenghea; Gh. Tomoaia; D.V. Pop-Toader; A. Mocanu; O. Horovitz; M. Tomoaia-Cotisel; *Comb. Chem. High Throughput Screen*., **2011**, *14*(4), 237-247.
57. P.T. Frangopol; D.A. Cadenhead; Gh. Tomoaia; A. Mocanu; M. Tomoaia-Cotisel; *Rev. Roum. Chim*., **2015**, *60*(2-3), 265-273.
58. A. Mocanu; P.J. Quinn; C. Nicula; S. Riga; Gh. Tomoaia; C.A. Bardas; M. Tomoaia-Cotisel; *Rev. Roum. Chim*., **2021**, *66*(10-11), 855-869.
59. Gh. Tomoaia; M. Tomoaia-Cotisel; A. Mocanu; O. Horovitz; L.D. Bobos; M. Crisan; I. Petean; *J. Optoelectron. Adv. Mater*., **2008**, *10*(4), 961-964.
60. A.G. Hosu-Prack; I. Petean; G. Arghir; L.D. Bobos; M. Tomoaia Cotisel; *Carpathian J. Earth Environ. Sci.,* **2016**, *11*(2), 539-546.
61. M. Mohammadian; M. Salami; F. Alavi; S. Momen; Z. Emam-Djomeh; A.A. Moosavi-Movahedi; *Food Biophys*., **2019**, *14*, 425–436.
62. M. Mohammadian; A.D. Moghaddam; A. Sharifan; P. Dabaghi; S. Hadi*; J. Iran Chem. Soc.*, **2020**, *17*, 2481–2492.

STUDIA UBB CHEMIA, LXVII, 3, 2022 (p. 75-99)
(RECOMMENDED CITATION)
DOI:10.24193/subbchem.2022.3.06

COMPLEXATION OF CURCUMIN USING WHEY PROTEINS TO ENHANCE AQUEOUS SOLUBILITY, STABILITY AND ANTIOXIDANT PROPERTY

LEVENTE ZSOLT RACZ[a], CSABA-PAL RACZ[a], OSSI HOROVITZ[a], GHEORGHE TOMOAIA[b,c], AURORA MOCANU[a], IRINA KACSO[d], MELINDA SARKOZI[e], MONICA DAN[d], SEBASTIAN PORAV[d], GHEORGHE BORODI[d], MARIA TOMOAIA-COTISEL[a,c,*]

ABSTRACT. The stability and solubility of curcumin, CCM, can be enhanced by complexation with whey protein concentrate (WPC). The CCM-WPC of 1:1 and 1:0.5 molar ratio complexes were encapsulated by two methods, namely spray drying (SD) and freeze drying (FD). The major objective of this work is to determine the stability and solubility of the CCM-WPC complexes encapsulated by SD and FD method. The X-ray diffraction and thermogravimetric analysis were performed on raw CCM and WPC, and on their complexes. The changes in thermal degradation and in crystallinity suggest the formation of these CCM-WPC complexes. Scanning electron microscopy images showed that the used methods influenced the morphology and the properties of the formed complexes. The stability and solubility of curcumin are enhanced by complexation in both encapsulation methods. However, comparing the used molar ratio and drying methods, the results are various. The solubility of samples obtained by FD method was higher than in the case of the SD method, which can explain the difference of their morphology (FD samples are more amorphous than SD samples). The antioxidant property of curcumin and its protein-complexes compared to vitamin C showed that CCM and its complexes have a lower IC_{50} value than vitamin C, i.e., the antioxidant effect of CCM is higher. The addition of WPC improved the antioxidant activity of CCM, probably due to its encapsulation in the protein. Our results suggest that the 1CCM-1WPC_SD complex is the best antioxidant from these studied CCM-WPC complexes.

Keywords: *curcumin, whey protein concentrate, spray drying, freeze drying, solubility, half-life time, antioxidant property*

[a] *Babeş-Bolyai University, Research Center of Physical Chemistry, Faculty of Chemistry and Chemical Engineering, 11 Arany Janos str., RO-400028, Cluj-Napoca, Romania*
[b] *Iuliu Hatieganu University of Medicine and Pharmacy, Department of Orthopedics and Traumatology, 47 Gen. Traian Mosoiu str., RO-400132, Cluj-Napoca, Romania*
[c] *Academy of Romanian Scientists, 3 Ilfov str., RO-050044, Bucharest, Romania*
[d] *National Institute for Research and Development of Isotopic and Molecular Technologies, Department of Molecular and Biomolecular Physics, 67-103 Donath Str., RO-400293, Cluj-Napoca Romania*
[e] *SC. Parapharm SRL, 9 Dacilor Str., RO-335200, Brad, Romania*
** Corresponding author: mcotisel@gmail.com*

INTRODUCTION

As a naturally occurring polyphenol, curcumin (CCM) is an active component of the dietary spice turmeric (Curcuma longa), which possesses physiological and pharmacological properties [1]. CCM's health-promoting properties include like anti-Alzheimer [2, 3], anticancer [4-8], anti-inflammatory [9, 10], antidiabetic [11, 12], antiproliferative [13], antioxidant [14] and antimicrobial effects [15, 16]. However, the therapeutic application is contained by its low water solubility, instability and bio-accessibility [17-19]. To improve these limiting factors, β-Lactoglobulin (βLG), the major protein from whey protein concentration (WPC), can be used, due to its properties to solubilize and bind small hydrophobic molecules [20, 21].

Microencapsulation is a widely used technology for improving stability or solubility, is a process in which tiny insoluble particles are surrounded by a coating to give small capsules, with useful properties. In this case CCM is capsulated with WPC [22]. Various microencapsulation techniques have been applied, such as physical, or physico-mechanical techniques as spray drying, freeze drying, extrusion, and centrifugal extrusion [23] or physico-chemical ones as coacervation or chemical techniques as matrix polymer. Spray drying is an efficient and cheap drying method. It can be used for drying liquid mixtures where the dry matter content is dissolved or suspended. The liquid is broken down into small droplets by the spray head, and the moisture content by the drying air evaporates. The speed of the process is due to the increased evaporation surface. Freeze-drying, also known as lyophilization, is a method in which the humidity is removed by freezing and sublimation. During the process, the material is first frozen, the pressure is reduced, and then the heat loss due to drying is compensated by heating the material, otherwise this would significantly slow down the process. The disadvantage is that the procedure is time consuming and comes with a high price [24].

The aim of this paper was to enhance the solubility and stability of CCM by encapsulation with WPC. Moreover, the comparison of the two used drying methods and their effects on the CCM's thermal stability, antioxidant activity, crystallinity and morphology were also explored in this work.

RESULTS AND DISCUSSION

Thermogravimetric analysis (TG/DTG)

In our research, we performed TG/DTG measurements of CCM, WPC and their complexes (Figures 1-6) prepared by two different methods.

During the measurements, different thermal decomposition of the substances was observed, which provides evidence for the formation of the curcumin and whey protein complex.

Derivation of the curves allows the evaluation of fine details. The weight loss of CCM takes place in two steps between 200-410°C (42.34%) and 410-550°C (58.42%). In the keto form of CCM, a highly activated carbon atom leads to the loss of hydrogen atoms, which initiates the degradation of it [1].

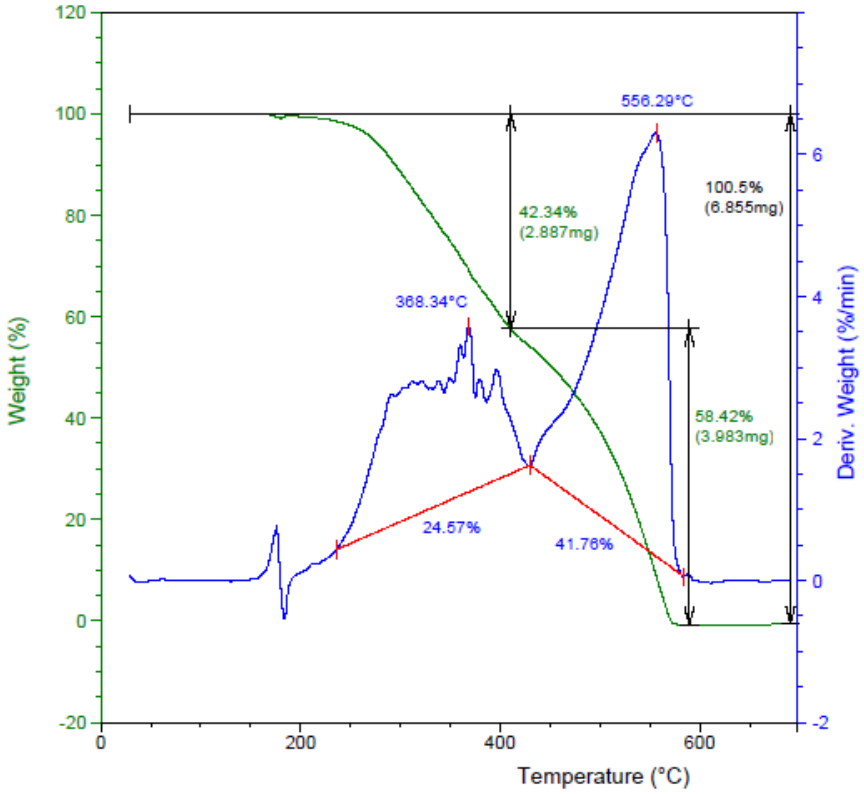

Figure 1. TG/DTG analysis of CCM

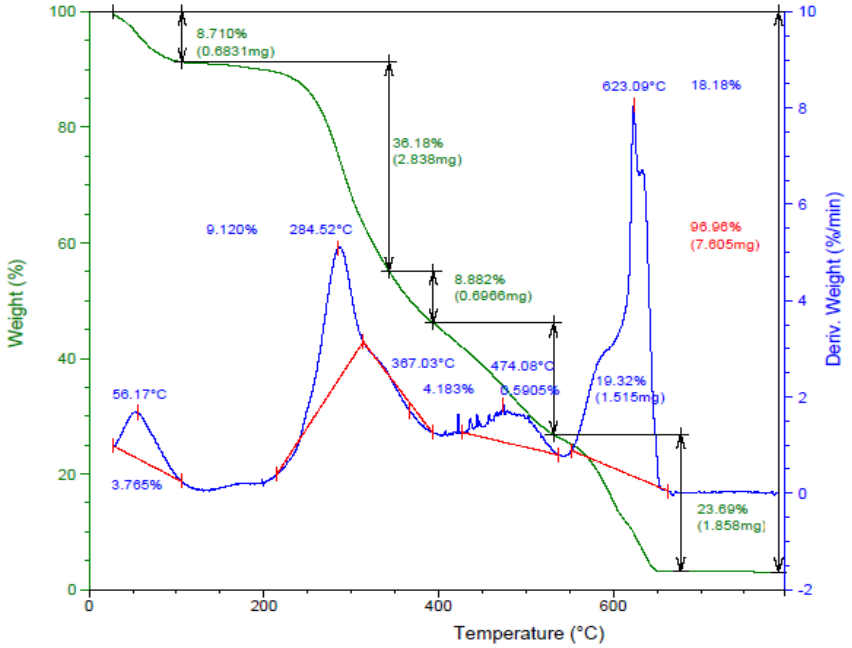

Figure 2. TG/DTG analysis of WPC

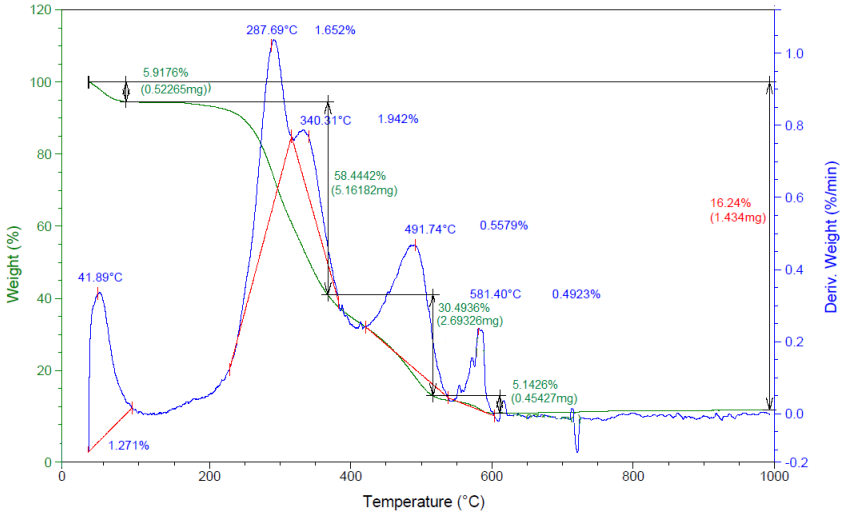

Figure 3. TG/DTG analysis of 1CCM-0.5WPC_SD

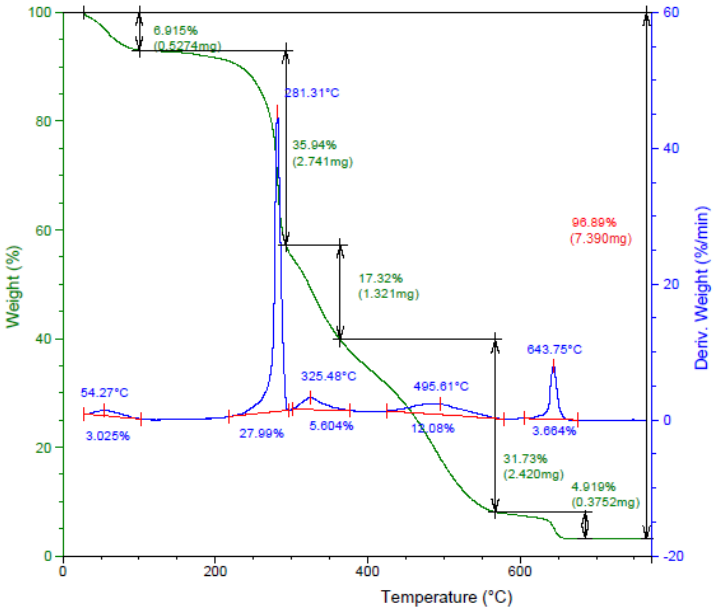

Figure 4. TG/DTG analysis of 1CCM-1WPC_SD

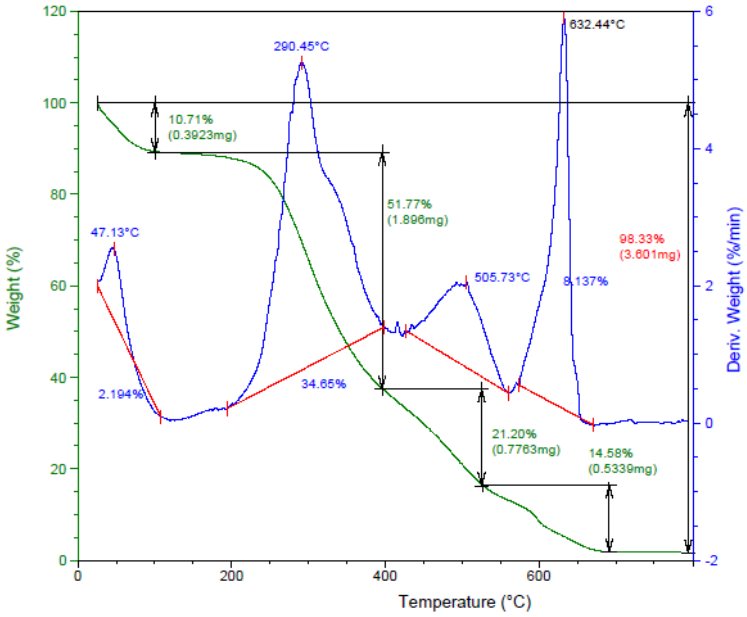

Figure 5. TG/DTG analysis of 1CCM-1WPC_FD

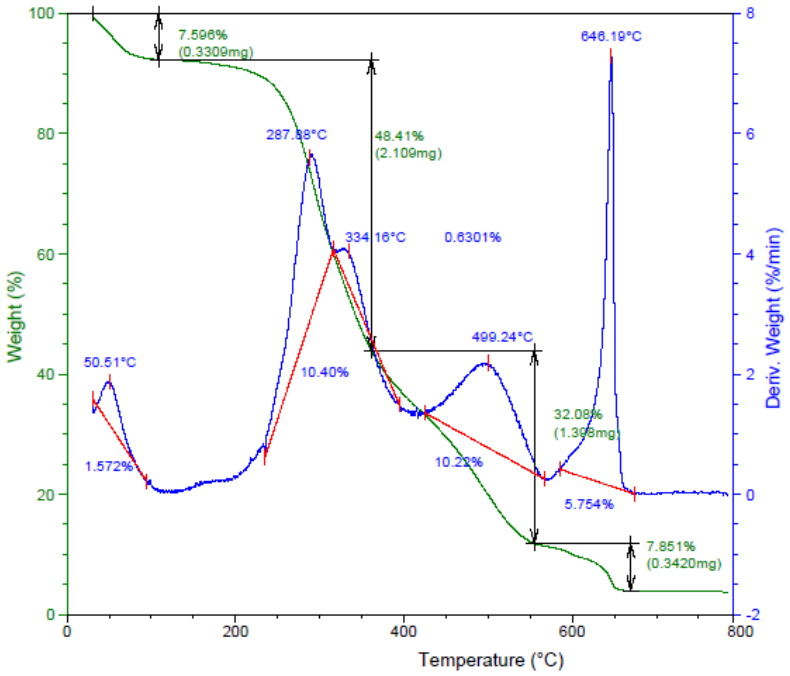

Figure 6. TG/DTG analysis of 1CCM-0.5WPC_FD

The thermal decomposition of WPC takes place in 5 steps between 50-110°C (8.71%), which is attributed to water evaporation, ~200-350°C (36.18%), 350-400°C (8.88%), 400-540°C (19.32%) and 540-670°C (23.69%), similarly in cases of its complexes.

X-ray diffraction analysis (XRD)

The XRD patterns of CCM, WPC and their complexes for studying their crystallinity are shown in Figure 7 WPC showed classic amorphous XRD patterns indicating that the amorphous nature of WPC was not changed by complexation with CCM.

On the contrary, the XRD pattern of free curcumin displayed different intense diffraction peaks between 5° and 39° attributed to its highly crystallized structure [20, 25]. However, as represented in the diffractograms of CCM-WPC samples, most of the characteristic peaks related to the crystalline structure of curcumin disappeared in the complexes, which suggest that the complexation process occurs [19].

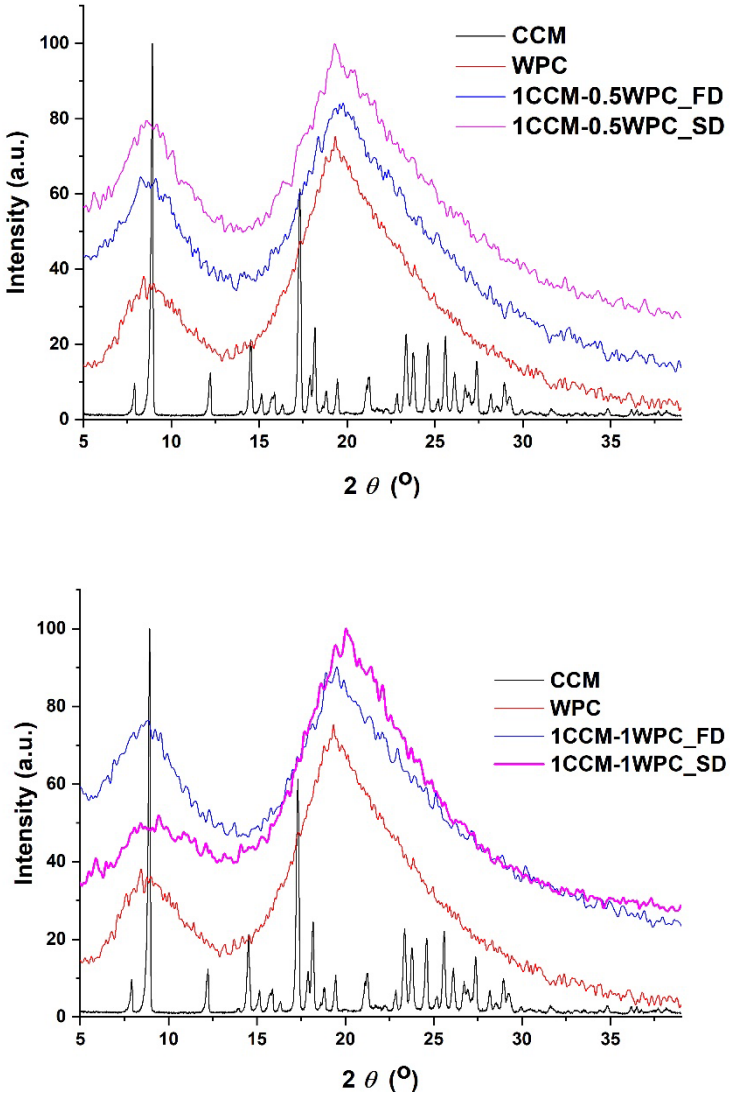

Figure 7. XRD diffractograms of CCM, WPC and their complexes.

Scanning electron microscopy (SEM)

The morphological structures of microparticles examined by SEM are presented in *Figure 8*.

Following the two drying methods, different morphological characteristics resulted. Spray dried microparticles were more spherical and regular in shape, which are typical of spray-dried powders, and their surface appeared relatively smoother than the freeze-dried ones, which exhibited more cracks or fractures [23]. The SEM images of the complexes shown that the curcumin was protected within the wall matrix, which is based on the fact, that the scaly and abrupt-edged structure of CCM it is absent in the microcapsules [19].

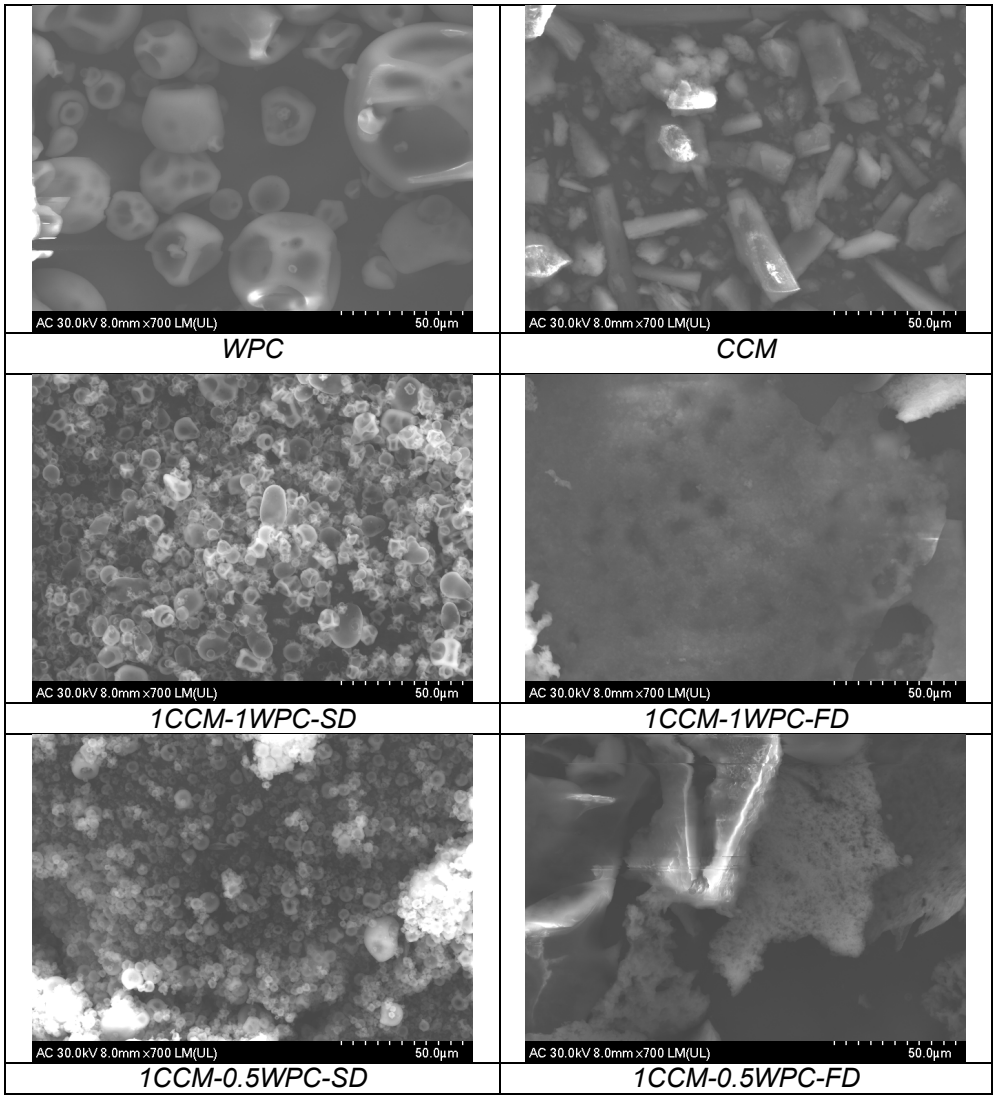

Figure 8. SEM images of WPC, CCM, and CCM-WPC complexes

Solubility in water

For the solubility measurements the absorbance of CCM-WPC complexes was measured by an UV-Vis spectrometer at 425 nm (see in Figure 9).

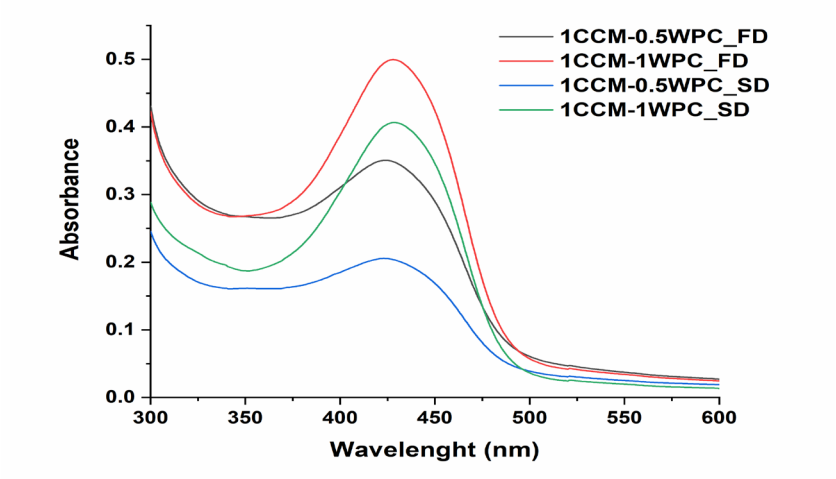

Figure 9. The UV-Vis spectra of complexes.

The CCM concentration was calculated using calibration curve of CCM in ethanol (Figure 10). Absorbance is given in arbitrary units.

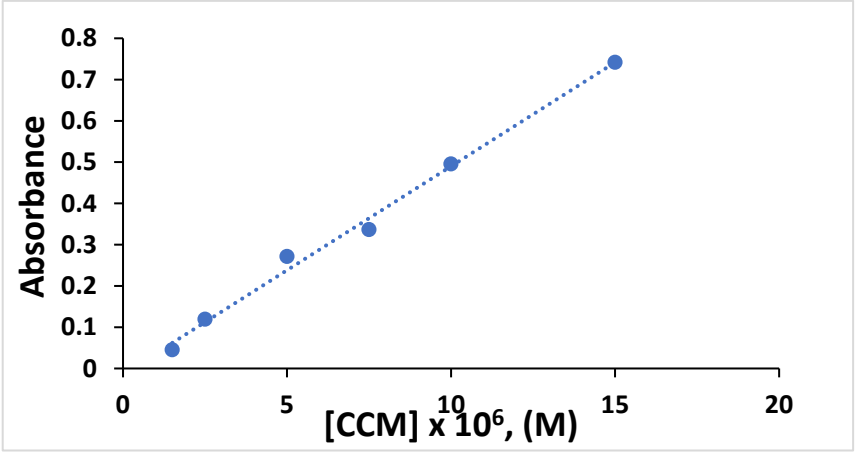

Figure 10. Calibration curve of CCM in ethanol. Characteristics of regression line are: $y = 50361x - 0.0137$, where x is curcumin concentration, and $R^2 = 0.9932$.

Water solubility of curcumin is very low, just 0.00262 mg/ml (Table 1). Complexation of CCM with WPC increases the water solubility of CCM, in all cases and the CCM-WPC complexes (particularly of 1:1 molar ratio) have the higher solubility (Table 1). Comparing the spray drying (SD) and freeze-drying (FD) methods, the prepared complexes with the latter method have shown a higher solubility, namely SD method showed 7.5x increase, while FD method exhibited an 8.9x increase in CCM solubility. SEM images (Figure 8) suggest that FD methods resulted in amorphous particles, which are markedly more soluble than their crystalline counterparts obtain by the SD method, which is supported by the XRD diffractograms too [26].

Table 1. Water solubility (μg/mL) of curcumin and its complexes

Materials	Solubility (μg/mL)
CCM	2.6
1CCM-1WPC_SD	19.5
1CCM-0.5WPC_SD	12.9
1CCM-1WPC_FD	23.1
1CCM-0.5WPC_FD	15.3

Stability and degradation of curcumin and its complexes in different aqueous solutions of various pH values

The chemical instability of curcumin is widely known [27]. In order to investigate the protective effects of the WPC and the influence of the drying methods on the degradation kinetics of curcumin, the kinetic profile of water-mediated curcumin degradation, CCM-WPC complexes were dissolved in buffers with pH values as in simulated gastric (1.5), in intestinal (8.0) or in physiological (7.4) [28] simulated fluids without enzymes. Therefore, beside the protective effect of WPC and preparation technique, the effect of pH was also studied on the stability of CCM. Depending of the used medium, the degradation products and mechanism of CCM are different because of its structure [29, 30].

Consequently, in the following two examples are given as the UV-vis spectra of the decrease in time of CCM absorbance (noted A, a.u.) for 1CCM-0.5WPC_SD and 1CCM-1WPC_FD complexes at pH 7.4 in Fig. 11A and Fig. 11B, respectively.

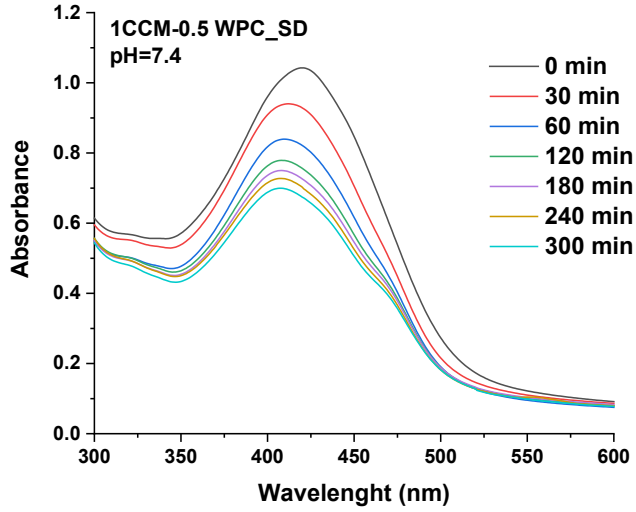

Figure 11.A. The UV-vis spectra of the decrease in time of CCM absorbance in 1CCM-0.5WPC_SD at pH 7.4

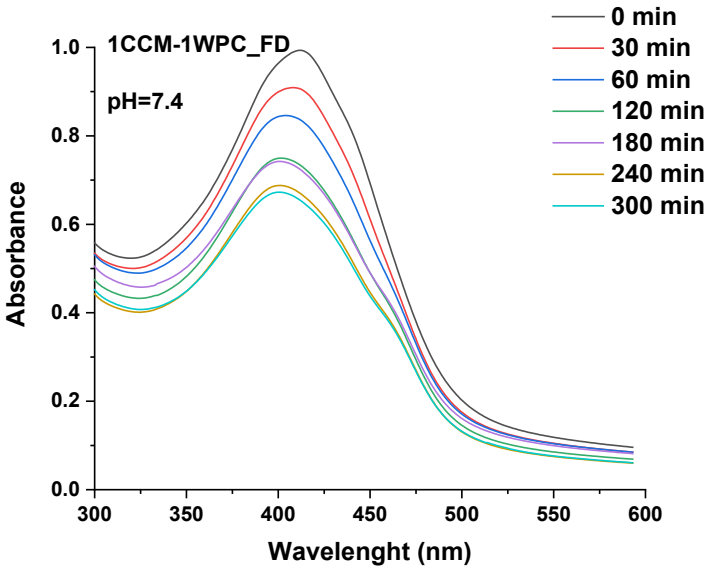

Figure 11.B. The UV-vis spectrum of the decrease in time of CCM absorbance in 1CCM-1WPC_FD complex at pH 7.4

The half-life ($t_{1/2}$) is the time moment on which the initial concentration of CCM is decreased by half of its original value. Depending on the reaction type, the half-life can be calculated with different equations:

- For *first order* reaction:

  R→ $\boldsymbol{Products}$

$$\text{rate} = k[R]$$

where k is the rate constant, and [R] is the molar concentration of the reactant. Since the absorbance, A, is proportional to the concentration, absorbance values can be used in the kinetic equations instead of concentration values.

The integrated form of the *first order* kinetic equation can thus be written as:

$$\ln A = \ln A_o - kt$$

where A values are the absorbance values at different moments and A_o is the initial value (at t = 0).

The rate constant k was determined by plotting of ln(A) versus time;

$$k = -a,$$

where a is the slope of the regression line: y = ax + b, and $t_{1/2}$ was calculated as:

$$t_{1/2} = \frac{0.693}{k}$$

- For *second order* reaction:

  2R→ $\boldsymbol{Products}$ or R + S → $\boldsymbol{Products}$; when [R] = [S]:

$$\text{rate} = k[R]^2$$

Using absorbance values instead of concentrations, the integrated 2nd order kinetic equation is:

$$1/A = 1/A_o + kt$$

The k value was determined, by plotting 1/A versus time, as the slope a of the regression line,

$$k = a.$$

Then, $t_{1/2}$ was obtained from the relation:

$$t_{1/2} = \frac{1}{kA_0}$$

The measured and calculated values are given in Table 2, together with the coefficients of determination, R^2, for the linear regression, represented, as examples, in Fig.12A and Fig.12B.

Table 2. The stability measurements (e.g., absorbance, a.u.) of the 1CCM-1WPC_FD complex in different (1.5, 7.4 and 8.0 pH) buffer solutions

pH 8.0									
t(sec)	Absorb-ance, A	1st order kinetics				2nd order kinetics			
		ln A	a = -k (s^{-1})	b	R^2	1/A	a= k (s^{-1})	b	R^2
0	0.9834	-0.017	-0.0006± 1.22E-4	-0.102± 0.089	0.8518	1.017	0.0009± 1.62E-4	1.1025± 0.117	0.8789
240	0.8358	-0.179				1.196			
480	0.5859	-0.535				1.707			
720	0.5292	-0.636				1.890			
960	0.5131	-0.667				1.949			
1200	0.5021	-0.689				1.992			
pH 7.4									
t(min)	Absorb-ance, A	1st order kinetics				2nd order kinetics			
		ln A	a = -k (min^{-1})	b	R^2	1/A	a = k (min^{-1})	b	R^2
0	0.9423	-0.059	-0.0012± 2.6E-4	-0.138± 0.044	0.8401	1.061	0.0015± 3.23E-4	1.1479± 0.054	0.8653
30	0.8508	-0.162				1.175			
60	0.7885	-0.238				1.268			
120	0.6917	-0.369				1.446			
180	0.6905	-0.370				1.448			
240	0.6596	-0.416				1.516			
300	0.6506	-0.430				1.537			
pH 1.5									
t(min)	Absorb-ance, A	1st order kinetics				2nd order kinetics			
		ln A	a = -k (min^{-1})	b	R^2	1/A	a= k (min^{-1})	b	R^2
0	1.019	0.019	-0.0007± 3.1E-5	0.0082± 0.005	0.9809	0.981	0.0007± 3.48E-5	0.9891± 0.0059	0.9897
30	0.9804	-0.020				1.020			
60	0.9629	-0.038				1.039			
120	0.9291	-0.074				1.076			
180	0.9022	-0.103				1.108			
240	0.8660	-0.144				1.155			
300	0.8229	-0.195				1.215			

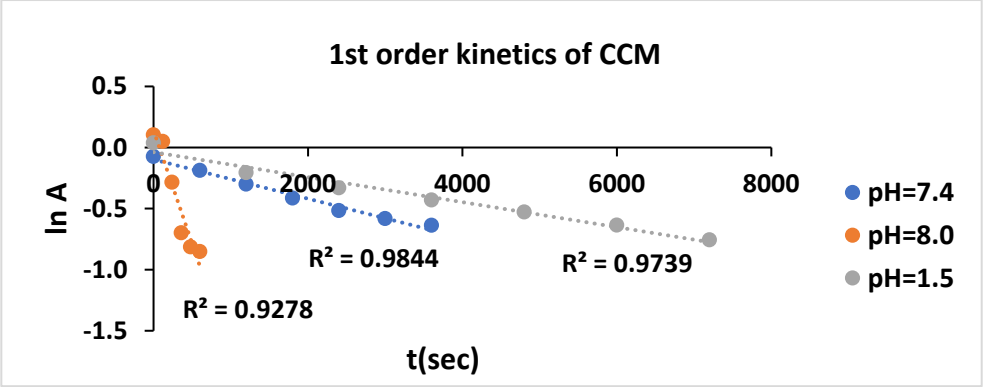

Figure 12 A. The first order degradation plot of CCM at different pH values and at 37°C.

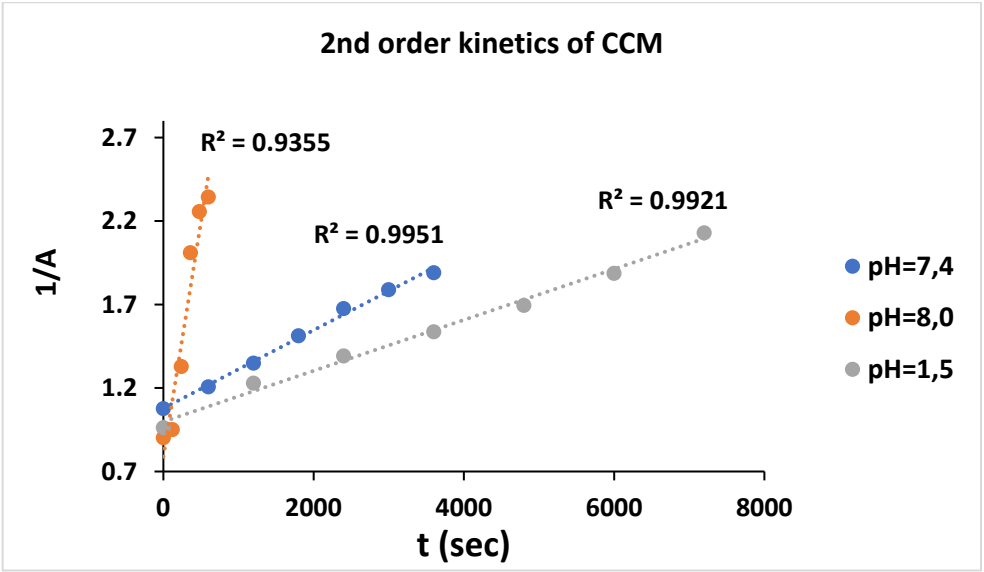

Figure 12 B. The second order degradation plot of CCM at different pH values and at 37°C.

Since correlations are better according to the 2nd order kinetics, in Table 3 the $t_{1/2}$ values were calculated assuming the process to follow this kinetic law.

Table 3. The half-life ($t_{1/2}$) time of CCM and its complexes by using of second order kinetics model.

Materials	$t_{1/2}$ (min)		
	pH 1.5	pH 7.4	pH 8.0
CCM	78±13.37	74±18.11	4±0.58
1CCM-1WPC_SD	397±33.42	1069±88.48	36±5.31
1CCM-0.5WPC_SD	237±9.11	742±102.36	17±0.22
1CCM-1WPC_FD	1656±211.61	784 ±125.3	22±2.65
1CCM-0.5WPC_FD	725±270.78	739±113.6	7±0.81

Under alkaline conditions (pH ≥8.0) a rapid decrease in absorbance was observed, and the half-life time of CCM was just 4 minutes (see in Table 3). The CCM solution has higher stability in acidic media than in alkaline ones, which has shown that curcumin is more chemically stable under acidic conditions [31]. The $t_{1/2}$ of CCM increased in all tested media by complexation of CCM with WPC. During the study first and second order kinetics model was fitted as shown in Fig. 12A and Fig. 12B, respectively. These results suggested that the second order kinetics described more exactly the degradation kinetics of CCM, thereby the degradation of CCM depends on the initial concentration.

Antioxidant activity determined by DPPH• free radical scavenging activity

Free radical scavenging activity of ascorbic acid, curcumin and its complexes were tested using the DPPH method. DPPH• method is highly reproducible and was applied on the study of antioxidant activity of food products [32].

The UV-vis spectra of the decrease of absorbance of DPPH by addition of different quantity of CCM solution, ascorbic acid (Vitamin C) solution, 1CCM-1WPC_SD solution, 1CCM-1WPC_FD solution, 1CCM-0.5WPC_SD solution, and 1CCM-0.5WPC_FD solution are shown in Figs. 13-18, respectively.

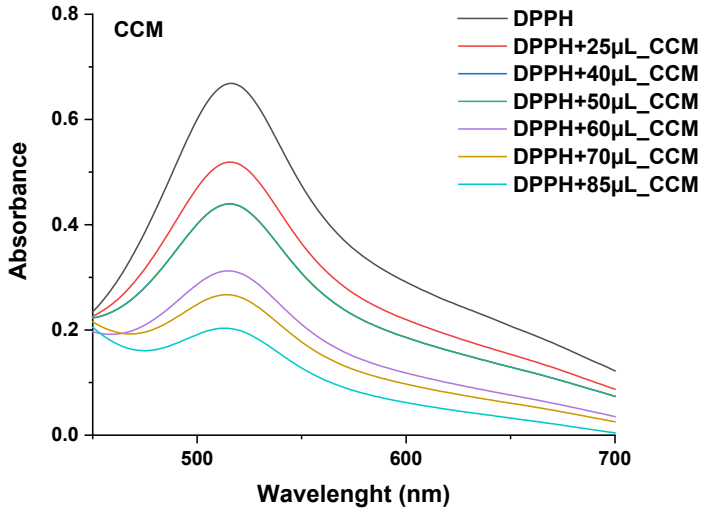

Figure 13. The UV-vis spectrum of the decrease of absorbance of DPPH by addition of different quantity of CCM solution

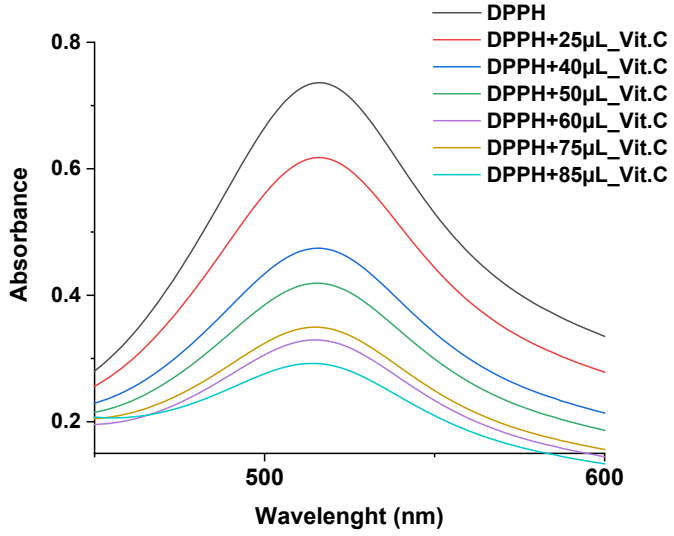

Figure 14. The UV-vis spectrum of the decrease of absorbance of DPPH by addition of different quantity of ascorbic acid (Vitamin C, Vit.C) solution

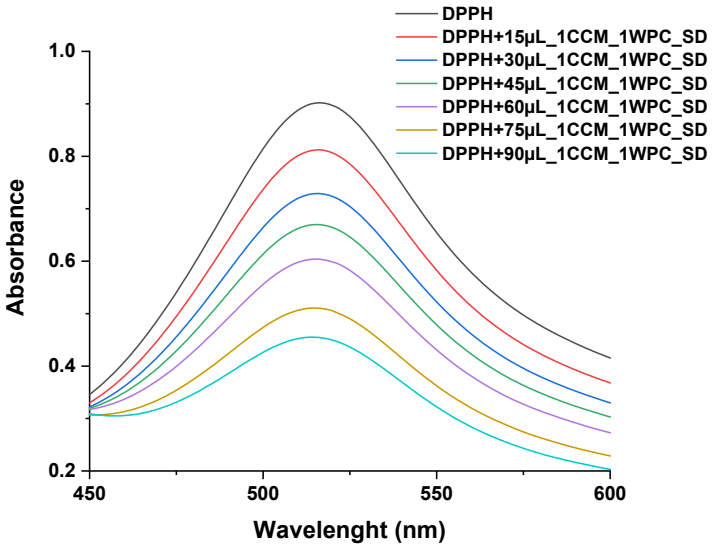

Figure 15. The UV-vis spectrum of the decrease of absorbance of DPPH by addition of different quantity of 1CCM-1WPC_SD solution

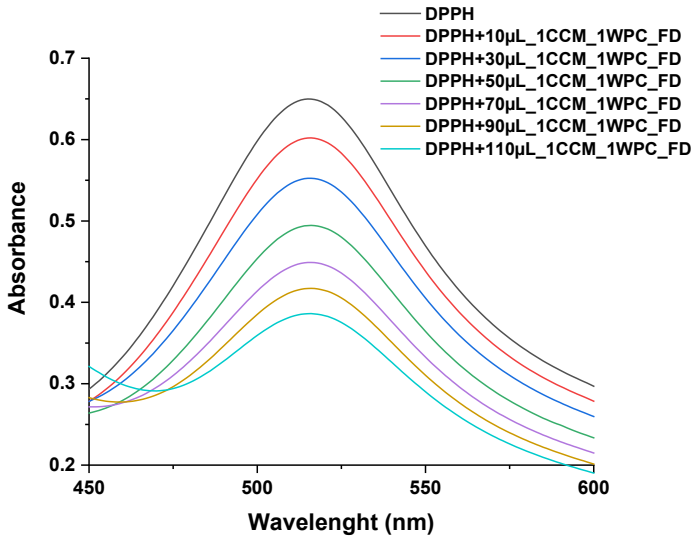

Figure 16. The UV-vis spectrum of the decrease of absorbance of DPPH by addition of different quantity of 1CCM-1WPC_FD solution

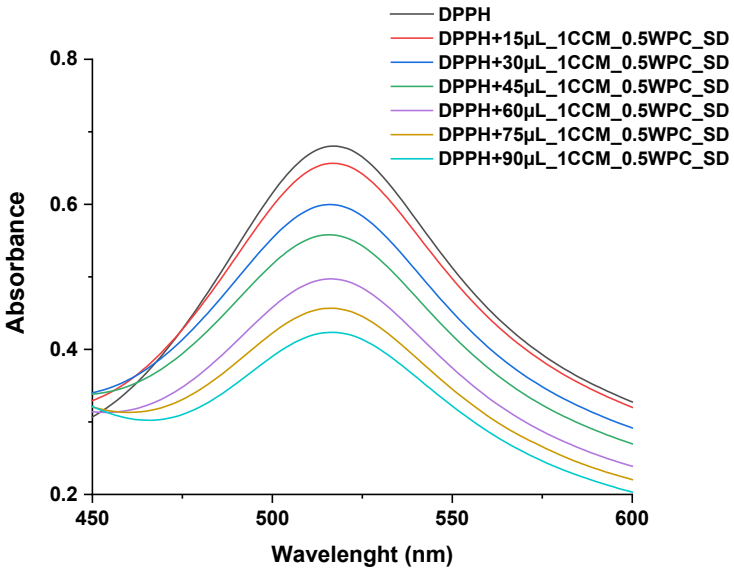

Figure 17. The UV-vis spectrum of the decrease of absorbance of DPPH by addition of different quantity of 1CCM-0.5WPC_SD solution

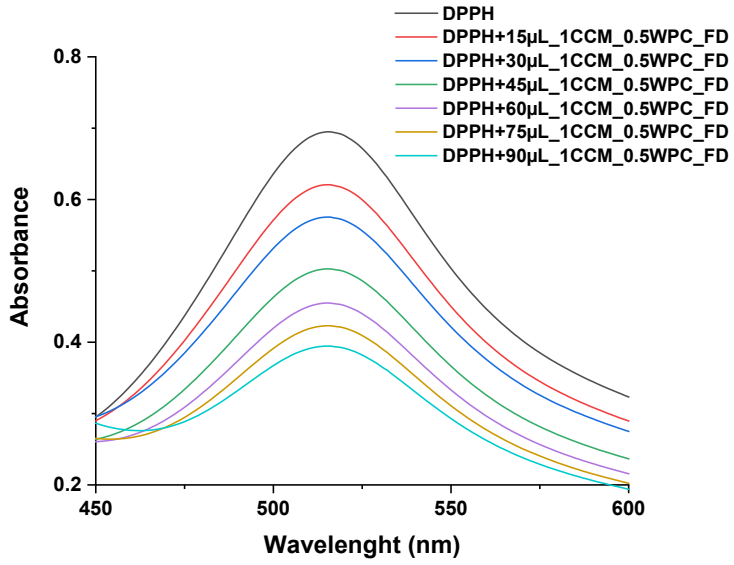

Figure 18. The UV-vis spectra of the decrease of absorbance of DPPH by addition of different quantity of 1CCM-0.5WPC_FD solution

The use of DPPH• method provides an easy, quick path to assess the *antioxidant properties of curcumi*n [33, 34]. The antioxidant effect of CCM was measured by the discoloration of a purple-colored methanol solution of the stable DPPH• radical.

The %DPPH radical scavenging activity = $\{(A_0-A_t)/A_0\} * 100$

where A_0 is the absorbance of DPPH solution without antioxidant, and A_t is absorbance of DPPH with different (test, t) concentrations of antioxidant.

By plotting of %DPPH radical scavenging activity in function of antioxidant concentrations (e.g., Fig. 19 and Fig. 20), and from the characteristic regression line equation, the value of IC_{50} can be determined:

IC_{50} = (50-y intercept) / slope

IC_{50} is the concentration, which is effective in producing 50% of the maximal effect of DPPH solution, without antioxidant.

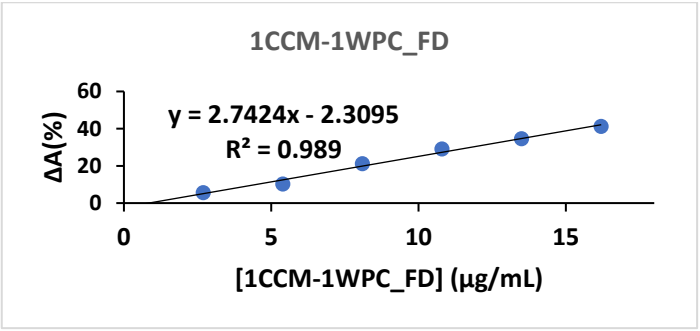

Figure 19. The plot of %DPPH radical scavenging activity in function of 1CCM-1WPC_FD concentration (µg/mL)

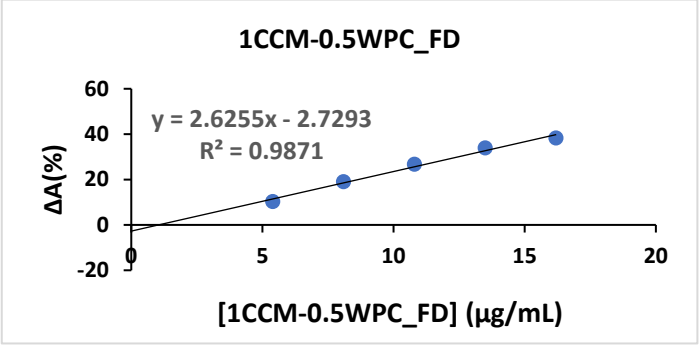

Figure 20. The plot of %DPPH radical scavenging activity in function of 1CCM-0.5WPC_FD concentration (µg/mL)

The result IC_{50} was expressed in molar concentration, M, of consumed sample per gram of DPPH• free radical.

The scavenging effect of complexed curcumin and standards on the DPPH radical decreased in the order of 1CCM:1WPC_SD ≥ 1CCM:1WPC_FD ≥ 1CCM:0.5WPC_SD ≥ 1CCM:0.5WPC_FD ≥ CCM ≥ ascorbic acid (Table 4).

Table 4. Half-maximal inhibitory concentrations (IC_{50}) of ascorbic acid, CCM, and obtained CCM-WPC complexes

Materials	IC_{50} (M)	Materials	IC_{50} (M)
Ascorbic acid	$3.71x10^{-5}$	CCM	$2.95x10^{-5}$
1CCM:1WPC_SD	$8.48\ x10^{-7}$	1CCM:0.5WPC_SD	$1.83x10^{-6}$
1CCM:1WPC_FD	$1.04x10^{-6}$	1CCM:0.5WPC_FD	$1.88x10^{-6}$

Comparing the used molar ratios of CCM and WPC within their complexes, the 1CCM-1WPC (1:1 mole ratio) complexes had higher antioxidant effect (Table 4) than the 1CCM-0.5 WPC (1:0.5 mole ratio) complexes. On the other hand, the 1CCM-0.5WPC (1:0.5 mole ratio) complexes were not affected by the used preparation spray drying, SD, or freeze drying, FD, method. However, the 1CCM:1WPC_SD complex had the highest antioxidant effect (about 35x improvement, compared to CCM antioxidant effect). Certainly, the encapsulation of CCM in whey protein leads to an enhanced antioxidant effect of CCM, and thus, these complexes are potential carriers for CCM in vitro and in vivo.

CONCLUSIONS

During our study the 1CCM-1WPC and 1CCM-0.5WPC complexes were prepared by spray drying and lyophilization methods. The resulted complexes and the raw materials were analyzed by TG, XRD and SEM techniques and their solubility and stability were comparatively examined. Moreover, the antioxidant properties of CCM and its protein complexes are evaluated and discussed in comparison with the antioxidant activity of vitamin C. The pure curcumin has a crystalline structure, which by complexation becomes a compound (material) which is amorphous, and this amorphous nature of complexes also contributes to the significant increase of CCM solubility. The morphology of CCM, WPC and their complexes is different depending on the used drying techniques. The antioxidant properties, solubility and stability of curcumin increased by complexation with whey protein

concentrate. Therefore, the complexes of curcumin-whey protein concentrate stabilized curcumin from degradation improving the solubility and stability as well as the anti-oxidant ability of curcumin.

EXPERIMENTAL SECTION

Materials and methods

Curcumin of high purity (95%) and ethanol were purchased from Sigma-Aldrich (Darmstadt, Germany), while whey protein concentrate (80%) was bought from Foodcom (Warsaw, Poland), disodium hydrogen phosphate (Na_2HPO_4) and DPPH (2,2-diphenyl-1-picrylhydrazyl) were obtained from Merck (Darmstadt, Germany), and the methanol from VWR chemicals (Fontenay-sous-Bois, France). Potassium dihydrogen phosphate, NaCl and HCl (36%) were obtained from Sigma-Aldrich (Darmstadt, Germany). During the experiment ultrapure water was used, which was purified with Milli-Q® IQ 7003. All compounds were used without further purification.

Preparation of samples

During our research spray drying and lyophilization methods were applied as preparation of the samples [8]. In the two cases mol ratios were 1CCM:1WPC and 1CCM:0.5WPC. CCM in ethanol and WPC in purified water were dissolved according to the molar ratios. After mixing of CCM and WPC solutions, the obtained solution was stirred for 4 hours in dark conditions and room temperature. In the final solutions the ethanol portion does not exceed 5% of the protein solution [35]. After 4 hours stirring the solutions were dried with two different methods:

- Spray drying (Pilotech, YC-018A) parameters were: T_{inlet} =165ºC, T_{outlet}= 49ºC, ventilator frequency 58 Hz, solution flow rate 5 mL/min. In the end a fine, homogeneous yellow-orange, powder was obtained (1CCM-1WPC_SD and 1CCM-0.5WPC_SD).
- Freeze drying (Alpha 1-2 LD plus) parameters were: -55ºC temperature, 0,06 mbar pressure, duration of the operation was 24 h (1CCM-1WPC_FD and 1CCM-0.5WPC_FD)

Solubility in water

Samples equivalent to 0.53 mg of CCM were added to screw-capped vessels containing 5 mL distilled water and were treated by sonication (Elmasonic S300/H) at 36ºC for 2 hours. The solutions were filtered with a

0.45 μm disc filter. Filtered 200 μl solution was diluted with 1800 μl ethanol and the absorption of CCM was measured by an UV-Vis spectrometer (*Jasco 670*) at 425 nm.

Stability measurement of CCM and its complexes at different pH values

For determination of CCM stability, a CCM was dissolved in ethanol ($2x10^{-3}$ M stock solution) and dropped in buffer solutions (1.5; 7.4 and 8.0 pH), which are given in Table 5, at 37 ºC and the variation of the absorbance was measured around 425 nm at different time intervals with UV-Vis spectrophotometer, *Jasco V-670*. The constant temperature was provided by a heating circulator, *Julabo MA 4*. In case of complexes, the powders were dissolved in buffers and the decrease of absorbance was measured as in case of CCM.

Table 5. The recipe of used buffer solutions

BUFFER SOLUTION	USED MATERIALS	Used quantity for 1 L	M (g/mol)	Reference
pH 7.4	Na_2HPO_4	17.9 g	141.96	[37]
	KH_2PO_4	3.6 g	136.086	
	NaCl	4.3 g	58.44	
pH 1.5	HCl (2N)	50 mL	36.46	
pH 8.0	Na_2HPO_4	14.2 g	141.96	
	HCl (0.1M)	44.9 mL	36.46	

The used buffers were prepared based on the recipe in Table 5 using purified water as solvent.

The daylight and artificial lighting can affect remarkably the degradation of CCM [36], as the measurements were carried out in the absence of light.

DPPH• free radical scavenging activity

The DPPH method (2.2-diphenyl-1-picryl hydrazyl) is based on the catching of the DPPH free radical by antioxidants, causing a decrease in absorbance at 517 nm wavelength [38]. The course of the reaction can also be seen with the naked eye, as the dark purple radical loses its color when reacting with antioxidants.

Table 6. The used stock solutions for antioxidant activity measurements

Stock solution	Solvent	Concentration (mol/L)
DPPH	Methanol	$1.01x10^{-7}$
Ascorbic acid	Purified water	$1.13x10^{-7}$
CCM	Methanol	$9.77x10^{-7}$
1CCM-1WPC_SD	Methanol	$4.78x10^{-6}$
1CCM-1WPC_FD	Methanol	$4.78x10^{-6}$
1CCM-0.5WPC_FD	Methanol	$2.43x10^{-6}$
1CCM-0.5WPC_SD	Methanol	$2.43x10^{-6}$

A series of solutions was prepared by adding different concentrations of antioxidant (0-90 µL) solution to 3 mL of DPPH stock solution and diluting it with methanol to a final volume of 5 mL. The reference solution was without antioxidants (Table 6). Ascorbic acid was used as standard. The solutions must be stored in the dark for half an hour before the measurement. The measurements were made by a UV-Vis spectrophotometer, Jasco V-670, at 517 nm.

X-ray powder diffraction (XRD)

The crystallographic structure of curcumin and its complexes were studied by XRD analysis as presented elsewhere [39, 40]. The patterns of WPC, CCM, 1CCM:1WPC_SD, 1CCM:0.5WPC_SD, 1CCM:1WPC_FD and 1CCM:0.5WPC_FD after freeze drying or spray drying were obtained by a Bruker D8 Advance diffractometer equipped with a goniometer and graphite bent crystal monochromator (CuKα1 radiation). The measurements were done at a filament current of 40 mA and operating voltage of 40 kV using Ge 111 monochromator. The scanned angle was set from 2θ of 5°–39° and the scan rate was 1° s^{-1}.

Scanning electron microscopy (SEM)

The samples were spread over the double-sided conductive tape (12 mm) fixed on aluminum stubs and coated with a 10 nm layer of gold. SEM images were done on a Hitachi SU8230 High Resolution Scanning Electron Microscope equipped with a cold field emission gun and an 80 X-Max system from Oxford Ins. for EDS analysis.

For this analysis the microscope was operated at 30 kV in high mag. mode. Approximately 85% of the carbon disk was scanned to give a realistic overview of the sample and only a few representative areas were captured.

Thermogravimetric analysis (TG)

Thermogravimetric analysis was performed with SDT Q600 TA Instruments thermogravimeter, in air (with 12% oxygen) flow of 20 mL min^{-1}, heating rate 10 °C min^{-1} and temperature range of 30–600 °C. The sample mass used was 8.0 ± 1.0 mg in an alumina cell.

ACKNOWLEDGMENTS

This work was supported by grants of the Ministry of Research, Innovation and Digitization, CNCS/CCCDI-UEFISCDI, project number 186 and 481, within PNCDI III.

REFERENCES

1. J. Yi; G. Peng; S. Zheng; Z. Wen; C. Gan; Y. Fan; *Food Chem*, **2021**, *348*, 129102.
2. M. Chen; Z. Y. Du; X. Zheng; D. L. Li; R. P. Zhou; K. Zhang; *Neural Regen Res*, **2018**, *13*, 742-752.
3. K. G. Goozee; T. M. Shah; H. R. Sohrabi; S. R. Rainey-Smith; B. Brown; G. Verdile; R. N. Martins; *Br J Nutr*, **2016**, *115*, 449-465.
4. M. A. Tomeh; R. Hadianamrei; X. Zhao; *Int J Mol Sci,* **2019**, *20*(5),1033.
5. M. Pricci; B. Girardi; F. Giorgio; G. Losurdo; E. Ierardi; A. Di Leo; *Int J Mol Sci*, **2020**, *21*(7), 2364.
6. S. Zhou; D. Yao; L. Guo; L. Teng; *FEBS Open Bio*, **2017**, *7*, 1078-1084.
7. R. Ramakrishna; T. H. Diamond; W. Alexander; A. Manoharan; T. Golombick; *Clin Case Rep*, **2020**, *8*, 739-744.
8. L. Racz; M. Tomoaia-Cotisel; Cs.-P. Racz; P. Bulieris, I. Grosu, S. Porav, A. Ciorita, X. Filip, F. Martin, G. Serban, I. Kacso; *Studia UBB Chemia,* **2021**, *66*(3), 209-224.
9. M. C. Fadus; C. Lau; J. Bikhchandani; H. T. Lynch; *J Tradit Complement Med*, **2017**, *7*, 339-346.
10. S. Ahmadabady; F. Beheshti; F. Shahidpour; E. Khordad; M. Hosseini; *Biochem Biophys Rep*, **2021**, *25*, 100908.
11. D. J. Den Hartogh; A. Gabriel; E. Tsiani; *Nutrients*, **2019**; *12*:E58.
12. D. J. Den Hartogh; A. Gabriel; E. Tsiani; *Nutrients*, **2020**; *12*:E118.
13. L. Cianfruglia; C. Minnelli; E. Laudadio; A. Scire; T. Armeni; *Antioxidants (Basel)*, **2019**, *8*, 382.
14. V. P. Menon; A. R. Sudheer; *Adv. Exp. Med. Biol*, **2007**, *595*, 105-125.
15. S. Meena; W. Prasad; K. Khamrui; S. Mandal; S. Bhat; *Food Bioscience*, **2021**, *41*:100990.

16. Q. Ye; F. Ge; Y. Wang; M. W. Woo; P. Wu; X. D. Chen; C. Selomulya; *Food Chem*, **2021**, *346*, 128900.
17. S. R. Adsare; U. S. Annapure; *J. Food Eng*, **2021**, *298*, 110502.
18. L. Xie; X. Ji; Q. Zhang; Y. Wei*; Biomed Pharmacother*, **2022**, *146*, 112567.
19. U. Kannamangalam Vijayan; N. N. Shah; A. B. Muley; R. S. Singhal; *J. Food Eng*., **2021**, *292*, 110258.
20. W. Liu; X. D. Chen; Z. Cheng; C. Selomulya; *J. Food Eng*., **2016**, *169*, 189-195.
21. S. Solghi; Z. Emam-Djomeh; M. Fathi; F. Farahani; *J. Food Process Eng*., **2020**, *43*(6), e13403.
22. M. Rosen, *Delivery System Handbook for Personal Care and Cosmetic Products*; Publisher: William Andrew, Norwich, New York, USA, **2005**.
23. J. Guo; P. Li; L. Kong; B. Xu; *Lwt,* **2020**, *132,* 109892.
24. O. I. Parisi; F. Puoci; D. Restuccia; G. Farina; F. Iemma; N. Picci, Polyphenols and Their Formulations, in *Polyphenols* in *Human Health and Disease*, R.R. Watson, V. D. Preedy, S. Zibadi Eds. Academic Press, **2014**, Chapter 4, pp. 29-45.
25. F. Mohammadi; A. K. Bordbar; A. Divsalar; K. Mohammadi; A. A. Saboury; *Protein J*, **2009**, *28*, 189-196.
26. B. C. Hancock; M. Parks; *Pharm Res,* **2000**, *17*, 397-404.
27. C. Schneider; O. N. Gordon; R. L. Edwards; P. B. Luis; *J Agric Food Chem,* **2015**, *63*(35), 7606-7614.
28. A. Maltais; G. E. Remondetto; M. Subirade; *Food Hydrocolloids,* **2009**, *23,* 1647-1653.
29. S. A. Rege; M. Arya; S. A. Momin; *Ukrainian Food Journal,* **2019**, *8*, 45-60.
30. F. Mirzaee; L. Hosseinzadeh; M. R. Ashrafi-Kooshk; S. Esmaeili; S. Ghobadi; M. H. Farzaei; M. R. Zad-Bari; R. Khodarahmi; *Protein Pept Lett,* **2019**, *26*, 132-147.
31. M. Kharat; Z. Du; G. Zhang; D. J. McClements; *J Agric Food Chem,* **2017**, *65*, 1525-1532.
32. D. Villano, M. S. Fernandez-Pachon, M. L. Moya, A. M. Troncoso, M. C. Garcia-Parrilla, *Talanta*, **2007**, *71*(1), 230-235.
33. D. de M. Carvalho; K. P. Takeuchi; R. M. Geraldine; C. J. de Moura; M. C. L. Torres; *Food Science and Technology* (Campinas), **2015**, *35*, 115-119.
34. T. Chumroenphat; I. Somboonwatthanakul; S. Saensouk; S. Siriamornpun; *Food Chem,* **2021**, *339*, 128121.
35. E. Ghorbani Gorji; E. Rocchi; G. Schleining; D. Bender-Bojalil; P. G. Furtmüller; L. Piazza; J. J. Iturri; J. L. Toca-Herrera; *J. Food Eng.*, **2015**, *167*, 217-225.
36. J. Jankun; M. Wyganowska-Swiatkowska; K. Dettlaff; A. Jelinska; A. Surdacka; D. Watrobska-Swietlikowska; E. Skrzypczak-Jankun; *Int J Mol Med,* **2016**, *37*(5), 1151-1158.
37. J. Lurie, *Handbook of analytical chemistry,* 1975, Mir Publisher: Moscow.
38. T. Ak; I. Gulcin; *Chem Biol Interact,* **2008**, *174*, 27-37.
39. Cs-P. Racz; G. Borodi; M.M. Pop; I. Kacso; S. Santa; M. Tomoaia-Cotisel; *Acta Cryst.,* **2012**, *B68*, 164-170.
40. Cs-P. Racz; Sz. Santa; M. Tomoaia-Cotisel; Gh. Borodi; I. Kacso; A. Pirnau; I. Bratu; *J. of Incls. Phenomena and Macrocyclic Chem.,* **2013**, *76*(1), 193-199.

STUDIA UBB CHEMIA, LXVII, 3, 2022 (p. 101-108)
(RECOMMENDED CITATION)
DOI:10.24193/subbchem.2022.3.07

A NEW HIGH PERFORMANCE LIQUID CHROMATOGRAPHY METHOD FOR THE DETERMINATION OF INDOMETHACIN FROM TRANSDERMAL THERAPEUTIC SYSTEMS

PAULA ANTONOAEA[a], ADRIANA CIURBA[a*], ROBERT-ALEXANDRU VLAD[a], EMŐKE RÉDAI[a], NICOLETA TODORAN[a], ANCA GABRIELA CÂRJE[b]

ABSTRACT. This study aimed to develop and validate an HPLC method in order to assay the indomethacin from therapeutic transdermal systems (TTS). A TTS with indomethacin and $HPMC_{15k}$ as a film-forming agent was developed. The performance of the method was verified in terms of specificity, linearity, detection limit, quantification limit, and precision. The results proved the developed method specificity no interference being observed in a placebo sample at the retention time corresponding to indomethacin. To evaluate the linearity, concentrations in the range of 1-100 µg/mL were used, proving the existence of a linear relationship between the selected points. The detection limit was 0.93 µg/mL and the quantification limit was 2.80 µg/mL. Indomethacin concentration in the analysed samples indicated a concentration of 95.15±4.15% respecting the official data. The statistical parameter used to evaluate the precision was the relative standard deviation, being used in the case of the evaluated concentrations smaller than 2%. In conclusion, the developed method is specific, reproducible and precise. An advantage of the developed method consists of the short analysis time of 3.53 min, whilst the presence of a single characteristic signal in the TTS samples chromatograms certifies that the indomethacin was quantified successfully from the TTS.

Keywords: *HPLC, TTS, indomethacin*

[a] *George Emil Palade University of Medicine, Pharmacy, Science, and Technology of Targu Mures, Faculty of Pharmacy, Pharmaceutical Technology and Cosmetology Department, 38th Gheorghe Marinescu street, RO-540142, Targu Mures, Romania*

[b] *George Emil Palade University of Medicine, Pharmacy, Science, and Technology of Targu Mures, Faculty of Pharmacy, Analytical Chemistry and Drug Analysis Department, 38th Gheorghe Marinescu street, RO-540142, Targu Mures, Romania*

* *Corresponding author adriana.ciurba@umfst.ro*

INTRODUCTION

Due to the advantages that the therapeutic transdermal systems (TTS) give, developing this type of pharmaceutical product represents a high-interest alternative to conventional formulations. Developing TTS aims to improve the clinical efficiency of a medicinal molecule and to increase the treatment acceptability and the patient's compliance through the capacity of a system to release a small amount of a drug at a pre-established liberation release. Furthermore, the transdermal patches present advantages when a lack of tolerance regarding oral administration occurs [1-6].

Indomethacin (IND), is indole acetic acid derived chemically named 2-[1-(4-chlorobenzoyl)-5-methoxy-2-methylindol-3-yl] acetic acid, belonging to the first generation of nonsteroidal anti-inflammatory drugs (NSAIDs), that act through the inhibition of the cyclooxygenase enzymes. It is well known fact that the NSAIDs through their mechanism of action significantly decrease the pain experienced in particular conditions while administrated orally, in addition, gastric side effects might be exhibited. To reduce the NSAIDs side-effects and taking into consideration the high number of patients that require chronically this type of medication, developing TTS gained a high interest, especially related to the ease of administration [7-12].

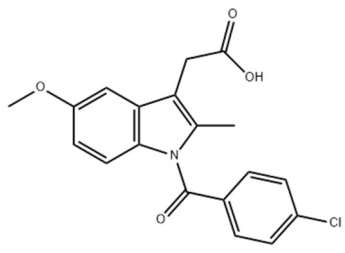

Molecular formula:
$C_{19}H_{16}ClNO_4$
Molecular weight:
357.8
Physical description:
- pale-yellow to yellow-tan, crystalline powder, odorless
- crystals exhibit polymorphism
Melting point:
158°C
Solubility:
- in water, 0.937 mg/L (at 25°C)
- soluble in ethanol, ether, acetone
Log P:
4.27
Stability:
- sensitive to light
- stable in neutral or slightly acidic media
- it is decomposed by strong alkali

Figure 1. Indomethacin: physical and chemical properties [13]

Considering its applicability, whilst developing TTS it is very important to quantify the active pharmaceutical ingredient from the proposed pharmaceutical formulation. In this regard, the main objective of this study consisted of developing and validating an analytical method for quantifying the IND from the polymeric TTS, through an HPLC method.

RESULTS AND DISCUSSION

To develop and validate an HPLC method to assay IND from the polymeric matrices, the specification found in the literature were considered [14-17]. To optimize the method and the chromatographic conditions, multiple compositions of the mobile phase, wavelength, and flow rate were studied. Thus, respecting the conditions outlined in the Material and Methods chapter, a characteristic signal was obtained at 3.53 minutes.

Method specificity and linearity

Developing and validating an HPLC method to quantify IND from polymeric TTS

Specificity. The comparative evaluation of the results based on the chromatograms registered for the placebo sample and a sample solution proved the lack of interference at the IND retention time.

Linearity. The evaluation of this parameter was obtained in the concentration range of 1-100 µg/mL, the measurements being conducted in triplicate for five levels of concentration. The statistical data included in **Table 1**, proved the linear relations between the variables.

Table 1. Linearity parameters

Concentration level (µg/mL)	Area ± SD	Statistical parameters
		Mean equation: y=4.9722x+0.0241 Slope = 4.9722; Intercept = 0.0241; R^2 = 0.9999
1	5.6±0.36	**Student's t test:** $t_{calculated}$= -0.162; $t_{tabulated}$= 2.160 If $t_{calculated} < t_{tabulated}$, ordonate at origin does not differ significantly of 0
5	25.3±0.73	
25	124.3±0.40	
50	248.3±1.30	**Cochran test:** $C_{calculated}$= 0.498; $C_{tabulated}$= 0.680 If $C_{calculated} < C_{tabulated}$, determination groups variants are homogeneous
75	372.1±0.46	
100	498.1±0.75	**Fischer test:** $F_{calculated}$= 1.171; $F_{tabulated}$= 3.710 If $F_{calculated} < F_{tabulated}$, equation is valid

Detection and quantification limit. By the ICH guide [15], the calculation of the parameters was done considering the following formulas:

*LOD = (3.3*σ)/S,* where: LOD - detection limit; σ - was calculated based on the calibration curve (intercept standard deviation) (y's standard deviation) y, calculated through simple linear regression); S - calibration curve slope.

*LOQ = 10*σ/S,* where: LOQ - quantification limit.

For IND, LOD was 0.93 µg/mL, whilst LOQ was 2.8 µg/mL, the results being similar to the ones found in the literature [14].

Accuracy and precision

Accuracy. Evaluation of this parameter was made through the quantification of IND found in the sample compared to a standard solution with a previously established concentration of 40 µg/mL. The determinations were made in triplicate. The obtained results of the IND average concentration in the analyzed samples indicated a concentration of 95.15±4.15% respecting the Ph. Eur. 10.0 stipulations [19]. A characteristic chromatogram for the IND-TTS samples can be observed in **Figure 2**.

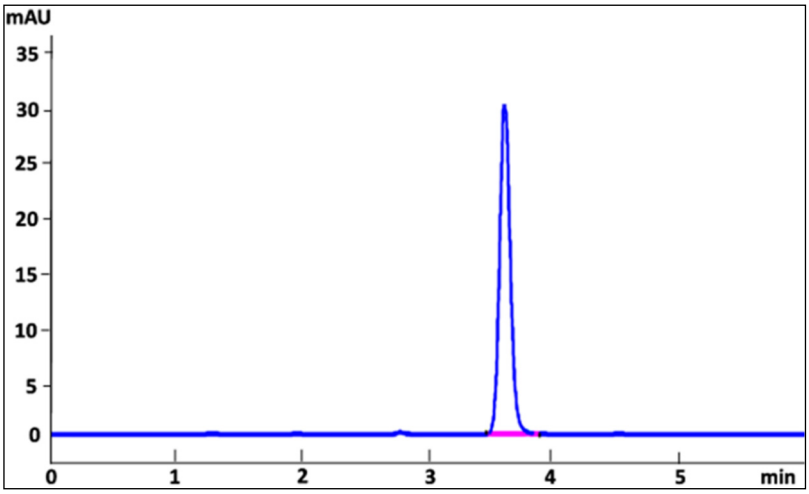

Figure 2. Typical chromatogram for IND assay from a TTS sample

Precision. Two parameters were evaluated (repeatability - intraday precision) and repeatability on different days (interday precision). All determinations were conducted in triplicate.

The precision was verified on three levels of concentrations belonging to the standard solutions: 25, 50, and 100 µg/mL. According to the results found in **Table 2**, RSD% showed values between 0.043-0.601%, corresponding to the pre-established acceptability criteria.

Table 2. Precision intraday and interday

	Precision intraday				**Precision interday**		
Concentration level (µg/mL)	**100**	**50**	**25**		**100**	**50**	**25**
Area±SD	496.9 ±1.4	248.7 ±1.0	124.8 ±0.7		497.2 ±0.9	248.5 ±0.5	124.9 ±0.6
RSD%	0.287	0.419	0.601		0.181	0.221	0.455
			Retention time (min) - T_R -				
$T_{RAverage}$ ±SD	3.530 ±0.007	3.529 ±0.001	3.536 ±0.012		3.530 ±0.003	3.536 ±0.011	3.533 ±0.006
RSD%	0.216	0.043	0.360		0.098	0.327	0.176

Application of the method to in vitro *release study*

The developed method can be successfully applied to study the release profiles of drug and to determine the release rate pattern of the IND from the TTS in dissolution rate studies, without interference.

CONCLUSIONS

The obtained results proved that the method developed to quantify IND is specific, reproducible, and precise. An advantage of this method consists of the short analysis time (t_R=3.53 min). The presence of only one characteristic signal in the chromatograms of the IND-TTS sample certifies the success of the assay for evaluating the drug from the polymeric matrix.

EXPERIMENTAL SECTION

Formulation and development of IND-TTS

Materials: indomethacin (IND) (Sigma Aldrich, Milan, Italy), hydroxypropyl methylcellulose 15k ($HPMC_{15k}$) (Metolose 90SH - 15000 mPa·s, Shin-Etsu Chemical Co., Ltd. Tokyo, Japan), propylene glycol (Scharlau Chemie, Barcelona, Spain), Tween 20 (Sigma Aldrich Co., France), ethanol (Chemical Company, Romania), ultrapure water (Millipore Direct-QS distiller).

Preparation method: solvent casting method (**Table 3**). Steps:

1. IND will be dissolved in a mixture of ethanol and propylene glycol under continuous stirring (500 rpm, Heidolph RYR1 stirrer, Germany) for 30 minutes.
2. The Tween will be dissolved in the available water amount, then the Tween solution will be mixed with the IND solution.
3. The chosen polymer will be dispersed in the formed solution and will be stirred continuously for 1 hour.
4. The formed dispersion will be kept in the water bath to eliminate the air bubbles.
5. The mixture will be cast in Petri dishes (diameter 9.8 cm).
6. Subsequently, the solvent will evaporate and a polymeric film will be formed by keeping the Petri dishes, at 40°C for 24 h.
7. The polymeric films will be packed individually in aluminum foil and will be kept in constant conditions of temperature and humidity constant (20ºC±2ºC, RH≈40%)

Table 3. TTS polymeric matrix type composition

Ingredients (% w/w)	**IND**	**$HPMC_{15k}$**	**Ethanol**	**Propylene glycol**	**Tween**	**Water**
	0.5	1.0	30.0	10.0	1.0	57.5

Similarly, a placebo TTS was prepared, without IND.

Development and validation of the HPLC method

Apparatus: HPLC Agilent Technologies 1100 Series (USA) features a quaternary pump, degasser, automatic injector, thermostated column, UV detector, data acquisition software (ChemStation), AB54S (Mettler Toledo, Sweden), ultrasonic bath T700H (Elma Transsonic).

Solvents for HPLC: acetonitrile (Merck, Germany), methanol (Merck, Germany) with analytical purity, ultrapure water (Millipore Direct-Q S distillation system); phosphate buffer KH2PO4 (Merck, Germany) 20 mM with pH adjusted at 3 using a phosphoric acid solution of 10 % (Merck, Germany)

Calibration and validation protocol

1. Phosphate buffer (KH_2PO_4 20 mM) was prepared by dissolving the KH_2PO_4 in ultrapure water, in a volumetric flask of 1000 mL.
2. Stationary phase: Waters Symmetry Column C8 (4.6x150 mm, 5 µm)
3. Chromatographic conditions:

a. Mobile phase (sonicated 10 min for degassing) composed from: phosphate buffer KH_2PO_4 20 mM, pH=3.0 and acetonitrile 35:65 (v/v%).
b. Flow rate: 1 mL/min.
c. Detection: UV 320 nm.
d. Column temperature: 35°C.
e. Injection volume: 5 µL.

Stock solution - preparation steps:

- 0.0100 g IND were dissolved in 5 mL methanol, subsequently, the solution formed is diluted with phosphate buffer (pH=7.4) until 100 mL using a volumetric flask of 100 mL. Preparation of the stock solution was made daily before starting the chromatographic analysis.
- Preparation of phosphate buffer, pH=7.4: 2.28 g of $NaH_2PO_4 \cdot H_2O$) (Fisher Scientific, UK) and 9.146 g ($Na_2HPO_4 \cdot 2H_2O$) (Merk, Germany) are dissolved in ultrapure water in a 1000 mL volumetric flask.

Preparation of the standard solutions:

Standard solutions were prepared using the stock solution making suitable dilution in order to obtain the following concentrations: 1 µg/mL, 5 µg/mL, 25 µg/mL, 50 µg/mL, 75 µg/mL, 100 µg/mL. The stock solution was diluted with phosphate buffer (pH=7.4).

Preparation of IND-TTS:

IND-TTS polymeric matrices with a surface of 0.7539 cm^2 and a theoretical concentration of 1.33 mg/cm^2 of IND were dissolved in phosphate buffer (pH=7.4), in a volumetric flask of 25 mL, obtaining a concentration of 40 µg/mL of the active ingredient.

Preparation of the placebo samples:

The polymeric TTS without IND was evaluated similarly to the ones containing active pharmaceutical ingredient.

Analytical performances evaluation:

The analytical performance of the proposed method was verified in terms of specificity, linearity, detection limit, quantification limit, accuracy, and precision. To calculate the statistical parameters Microsoft Office Excel 2010 (Microsoft Corporation, USA) was used.

Acceptability criteria for HPLC method validation to assay IND from TTS polymeric matrices:

- *Specificity:* the lack of interferences at the retention time corresponding to IND from the standard solution taking into consideration the results regarding the placebo sample.

- *Linearity:* obtaining a linear correlation by representing the active pharmaceutical ingredient signals area as a function of the concentration of IND and a value of the correlation coefficient larger than 0.999.
- *Accuracy:* by the stipulations found in the in-force Ph. Eur. 10 and the 2004 Romanian Pharmacopoeia Supplement [19,20], the acceptability limit ranges between 75-125 %.
- Precision: The calculated RSD% for the signals area and retention times belonging to the standard solutions must be less than 2%.

ACKNOWLEDGMENTS

This work was supported by the *George Emil Palade University of Medicine, Pharmacy, Science and Technology of Targu Mures*, Research Grant no. 10127/15/17.12.2020.

REFERENCES

1. W.Y. Jeong; M. Kwon; H.E. Choi; *Biomater. Res.*, **2021**, *25*, 24.
2. M. Qindeel; M.H. Ullah; et al; *J. Control Release*, **2020**, *327*, 595-615.
3. P. Antonoaea; M. Bîrsan; N. Todoran; E. Rédai; R.A. Vlad; D.L. Muntean; A. Rusu; A. Ciurba; *Farmacia*, **2020**, *68(6)*, 1029-1035.
4. A. Ciurba; P. Antonoaea; N. Todoran; E. Rédai; R.A. Vlad; A. Tătaru; D.L. Muntean; M. Bîrsan; *Process*, **2021**, *9*, 136.
5. P. Quan; B. Jiao; R. Shang; et al; *J. Ethnopharmacol.*, **2021**, *265*, 113294.
6. P. Ossowicz-Rupniewska; R. Rakoczy; et al; *Int. J. Mol. Sci.* **2021**, *22*(*12)*, 6252.
7. S. Lucas; *Headache*, **2016**, *56(2)*, 436-446.
8. S.A. Lopes; I.G. Veiga *Int. J. Polym. Mater. Polym. Bio*. **2019**, *68(16),* 956-964.
9. E.S. El-Leithy; H.K. Ibrahim; R.M. Sorour; *Drug Deliv*. **2015**, *22(8)*, 1010-1017.
10. M. Valentovic; Indomethacin, in *xPharm: The Comprehensive Pharmacology Reference*; S.J. Enna, David B. Bylund Eds.; Elsevier; ISBN 9780080552323; **2007**, pp. 1-5.
11. M. Nalesniak; K. Iwaniak; R. Kasperek; E. Poleszak; *Curr. Issues Pharm. Med. Sci.* **2013**, *26(1)*, 88-93.
12. A. Das; A. B. Ahmed; *Asian J. Pharm. Clin. Res.* **2017**, *10*(11), 320-325.
13. L.V. Allen; *US Pharm.* **2016**, *41(1),* 50-51**.**
14. P. Sanjay, P. Neelam; *I.J.P.E.R*. **2017**, *51(3)*, 388-392.
15. ICH Validation of Analytical Procedures: Text and Methodology Q2 (R1), International Conference on Harmonization IFPMA, Geneva. 2005.
16. A. Dandic, K. Rajkovaca; *Rev. Anal. Chem.* **2022**, *41*, 34-62.
17. A.K. Nehad, *I.J.D.D.T.*, **2020**, *10(1)*, 46-51.
18. L.M. Abdel-Aziz, *E.J.O.S.A.T.* **2021**, *1(2)*, 32-40.
19. European Pharmacopoeia, 10th edition, 2021.
20. Romanian Pharmacopoeia, 10th edition, Supl. 2004, Ed. Medicală, Bucureşti.

STUDIA UBB CHEMIA, LXVII, 3, 2022 (p. 109-116)
(RECOMMENDED CITATION)
DOI:10.24193/subbchem.2022.3.08

EFFECT OF GAMMA RADIATION ON SOME DOSIMETRIC INTEREST COMPOUNDS: AN EPR STUDY

VLAD BÎRLEA[a], DINA MARIANA PETRIŞOR[b*], GRIGORE DAMIAN[a]

ABSTRACT. The present research was undertaken in order to investigate if some compounds used as natural sweeteners (steviol and sucrose) can be used as EPR dosimeters. The samples were exposed to low doses of gamma ionizing radiation used in the practices of radiodiagnostic medicine and interventional radiology. The EPR spectra of the gamma irradiated compounds reveal large signals, with multiple lines, which are characteristic for the free radicals in the solid state. From the analysis of the dependence of EPR signal of the absorbed dose, it was observed that by γ-irradiation the amount of generated radicals shows a linear dependence, which mean that there exist a possibility to use these two compounds as EPR dosimeters.

Keywords: *EPR dosimeters, γ radiation, free radicals, steviol, sucrose*

INTRODUCTION

Electron paramagnetic resonance (EPR) is a spectroscopic technique widely used in biology, chemistry, medicine, geology, materials sciences, antropology, physics in order to study systems with one or more unpaired electrons [1-5]. EPR spectroscopy has matureted into a powerful, versatile, nondestructive and nonintrusive analytical method. It was used as an investigative tool for the study of free radicals formed in the materials, since the radicals typically produce an unpaired spin on the molecule from which an electron is removed [6,7].

Also, the EPR spectroscopy has the ability to measure radiation-induced paramagnetic species, which persist in certain tissues (e.g., teeth,

[a] *Babes-Bolyai University, Faculty of Physics, 1 Mihail Kogalniceanu str., RO-400084, Cluj-Napoca, Romania*
[b] *Babes-Bolyai University, Interdisciplinary Research Institute on Bio-Nano-Sciences,42 Treboniu Laurean str., RO-400271, Cluj-Napoca, Romania*
***** *Corresponding author e-mail: dina.petrisor@ubbcluj.ro*

fingernails, toenails, bone, and hair). This fact has led that this technique to become an important method for screening significantly radiation-exposed individuals, by using dosimeters [8-10]. EPR dosimetry is based on the quantitative detection of stable paramagnetic species induced by radiation as a direct result of interactions with molecules, measuring the doses of energy absorbed by a matter, necessary to make the transitions, between energy levels of electrons.

In order for a material to be used as a dosimeter, it must meet certain well-defined parameters, for example: EPR signal with few lines, narrow and without signal in case of non-irradiation; stable radicals produced by ionizing radiation under normal conditions; low dose rate at low doses; high chemical radiative efficiency; adequate microwave power saturation properties allowing high power values for increased sensitivity; robustness of the dosimeter in terms of mechanical stress. The valorization and optimization of these parameters are the main goals of EPR dosimetry technologies, the studies being focused on the highest possible efficiency of the devices and techniques used [11].

Natural and artificial sweeteners as sucrose, steviol, xylitol, eritriol, aspartame etc., have been studied over time for their possible use as EPR dosimeters [12-14]. These compounds meet most of the well-defined parameters, which make them eligible to be used as EPR dosimeters. One of the advantages of solid EPR dosimetry is the easy determination of absorbed dose and non-destructive character of readings permitting to store the dosimeter as a document for further estimation [15].

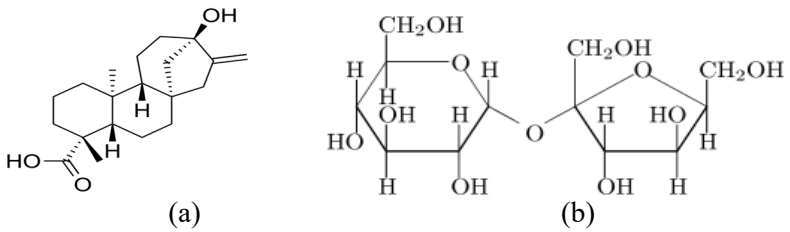

Figure 1. Molecular structure of: (a) steviol and (b) sucrose.

Steviol is a chemical compound found in plants in the form of glycosidic steviol. It is responsible for the sweet taste of the leaves of *Stevia Rebaudiana*, a plant originating in Central and South America. The general chemical formula of this compound is $C_{20}H_{30}O_3$, its molecular structure being represented in (Figure 1a). Stevioside and Rebaudioside A, the primary components, are glycosidically attached to the hydroxyl functions of steviol in the structure of stevia. This compound is used as a sugar substitute, especially in diabetics and people on carbohydrate-controlled diets because it does not induce a glycemic response to ingestion.

Sucrose (Figure 1b), with the general molecular formula C12H22O11, is common sugar. It is a disaccharide, a molecule composed of two monosaccharides: glucose and fructose connected via a glycosidic bond. This type of linking of two monosaccharides is called glycosidic linkage. This is an important process for the storage and compression of energy. In this way, via sucrose, the plants can transport much easier large amounts of energy [16]. Sucrose has a monoclinic crystal structure and is quite soluble in water. Sucrose is produced naturally in plants, from which table sugar is refined.

The present research was undertaken in order to investigate if this two natural sweeteners, steviol and sucrose, can be used as EPR dosimeters. The samples were exposed to low doses of γ-ionizing radiation used in the practices of radiodiagnostic medicine and interventional radiology. The EPR spectra of the γ-irradiated compounds reveal large signals, with multiple lines, which are characteristic for the free radicals in the solid state [17]. From the analysis of the dependence of EPR signal of the absorbed dose, it was observed that by γ - irradiation the amount of generated radicals shows a linear dependence, which mean that there exist a possibility to use these two compunds as EPR dosimeters.

RESULTS AND DISCUSSION

Unirradiated and γ-irradiated samples of steviol and sucrose were studied by EPR spectroscopy. The EPR spectra of the irradiated samples are represented in (Figure 2). The unirradiated samples give no detectable EPR signal. The fact that non-irradiated samples show no EPR signal is a first condition accomplished by steviol and sucrose to be used as EPR dosimeters [11].

After irradiation both samples showed EPR signals, even at low absorbed doses, indicating a sensitivity to gamma irradiation of these compounds. The shape of the radiation-induced EPR spectra is similar to those described in the literature and has been attributed to the overlapping spectra of some radical species present in the samples. [14, 15, 19]. Large signals, characteristic for free radicals in the solid state, are present in the EPR spectra of low doses γ-irradiated samples. As it can be observed from (Figure 2), these EPR spectra consist of a few lines which are characteristic for the presence of free radicals in carbohydrate compounds [17, 18].

Also, the EPR spectra of the studied samples, recorded at X-band frequency (~ 9 GHz) at room temperature, due to broadened overlapping hyperfine lines of the different species, are unresolved and its cannot provide information about the radicals giving rise to its features [19].

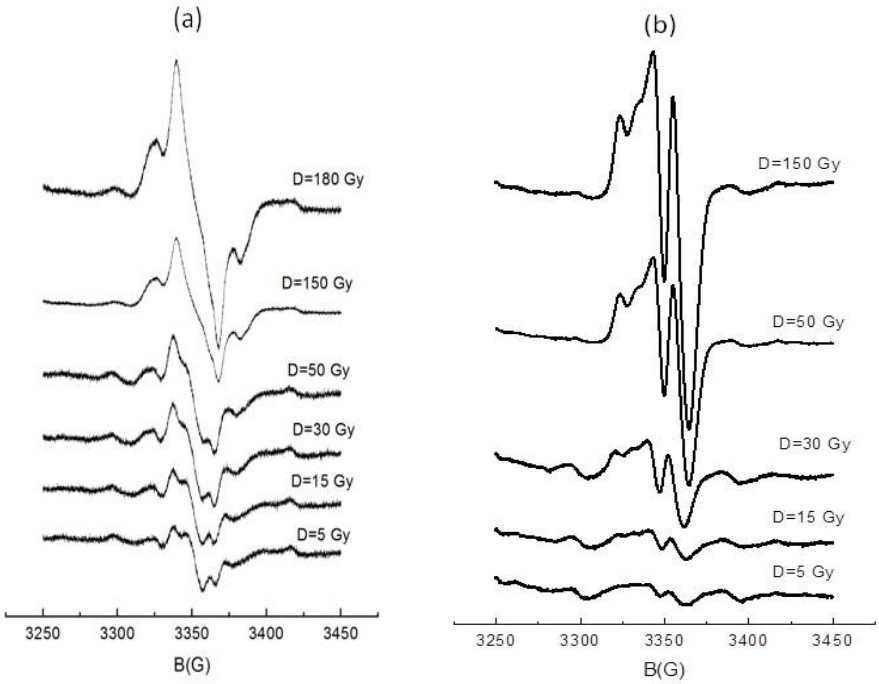

Figure 2. EPR spectra of γ-irradiated: (a) steviol and (b) sucrose, at different absorbed doses.

In (Figure 3) is represented the dependence of EPR signal intensities on the absorbed dose for steviol and sucrose. In order to generate the dose-response curve for steviol and sucrose, samples irradiated to 5, 15, 20, 30, 50, 70, 100 and 150 Gy absorbed doses were used.

A linear increase of EPR signal intensity is observed in both cases. The relative errors for all measurements were about 6%. The condition of linearity between dose and response is an essential one in biodosimetry, and the obtained results indicate a real possibility of using the studied chemical compounds in the determination of radiation doses.

Another important dosimetric property of a dosimeter is the stability over time of the radicals produced by ionizing radiation. It is an essential condition, because the measurement and estimation of the doses absorbed by the exposed persons is not done immediately [20]. There are studies in the literature that show that the intensity of EPR signals in stevia and sucrose samples decreases slightly over time [14, 21].

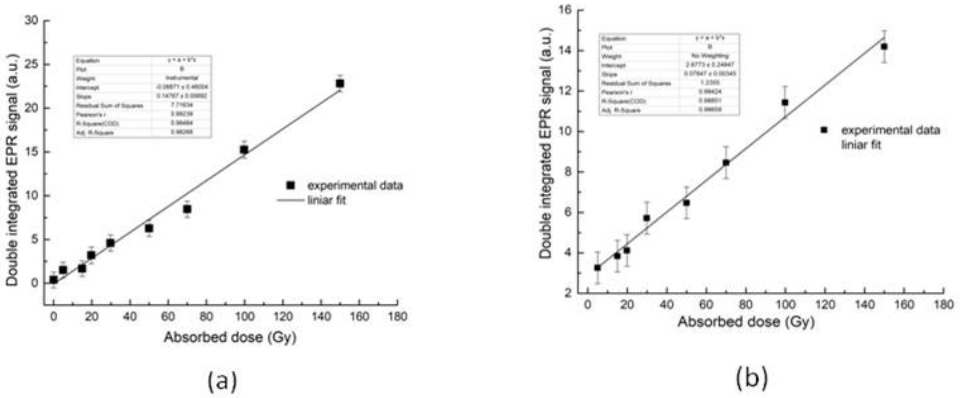

Figure 3. Dose response relationship for (a) steviol and (b) sucrose as a function of the irradiated dose (errors bars are provided with 6% error limits).

In the present study, the effect of free radical recombination was studied by measuring the samples at room temperature at different moments of time after irradiation, concluding that this effect is insignificant [22,23]. This means that these substances are eligible for identification of the irradiation process even after a period of time from the irradiation. Therefore, the stability condition of the radicals produced by the ionizing radiation in the studied samples is achieved.

One of the important experimental parameters in evaluating the intensity of EPR signals is the microwave power. The intensity of an EPR signal increases with the square root of the microwave power in the absence of saturation effects. The effect of microwave saturation leads to a decrease in the amplitude of the EPR line with an increase in microwave power due to the reversal of the distribution of unpaired electrons on energy levels [24]. In order to find optimal nominal power settings, it is necessary to determine the microwave power saturation curves for the spectra to ensure that nonsaturating conditions were being used in the representation of the dose response curve (Figure 4). From (Figure 4) it can be seen that the intensity of EPR spectra of irradiated samples depend on the applied microwave power [14, 25].

Based on the microwave saturation, it was found that, in the case of the steviol sample, the intensity of the EPR signal increases suddenly until 5 mW, between 5 mW and 9 mW a slow increase is observed, and over 9 mW a steady plateau is reached, but the EPR signal it is not completely saturated (Figure 4a). Furthermore, it is obvious that the intensity of the sucrose EPR signal increases linearly with the increase of microwave power from 0.25 mW to 9 mW (Figure 4b). Even above 9 mW, the intensity of the EPR signal continues to increase, and above 16 mW the increase of the intensity is significantly lower.

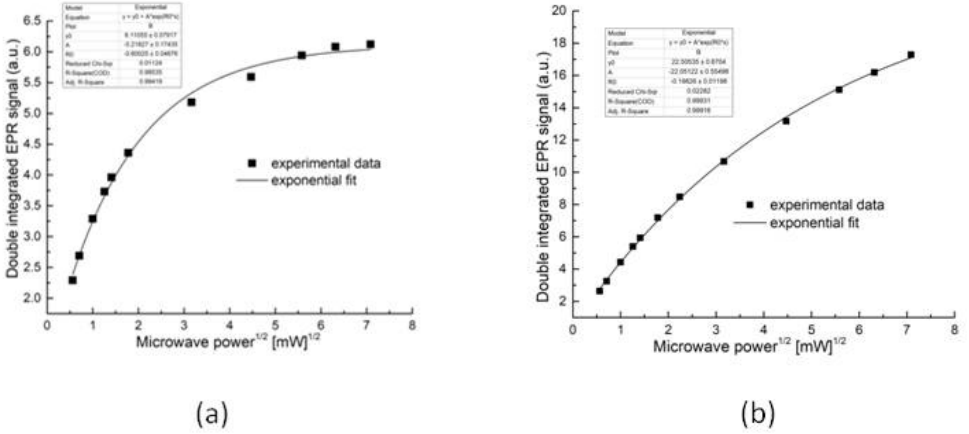

Figure 4. EPR power saturation curves for of irradiated steviol (a) and sucrose (b)

Continuous microwave saturation of EPR spectra indicated that faster spin-lattice relaxation-process existed in steviol sample than in sucrose sample (Figure 5).

It is obvious that the EPR line intensity reaches a maximum, much faster in the case of steviol than sucrose. That point in which the EPR line reaches a maximum is assigned as the "saturation point" based on the magnitude of the microwave power.

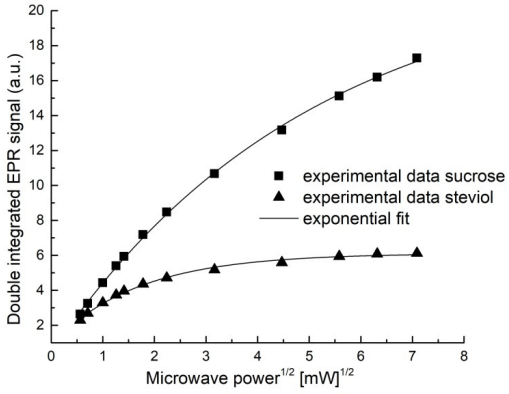

Figure 5. Comparation of EPR signal intensity irradiated samples.

CONCLUSIONS

EPR dosimetry is proving to be a method increasingly used in radiodiagnostics and interventional radiology, and as a result various compounds are studied to provide information "In vivo." The present research was undertaken in order to investigate if steviol and sucrose natural sweeteners, can be used as EPR dosimeter materials. The samples were exposed to low doses of γ-ionizing radiation used in the practices of radiodiagnostic medicine and interventional radiology.

A set of well-defined parameters specific to a material used as an EPR dosimeter was studied. From the results obtained, and following their analysis, it was found that the studied samples largely meet the requirements imposed on such a material. The non-irradiated samples show no EPR signal, and this is a first condition accomplished by steviol and sucrose to be used as EPR dosimeters. Also, the condition of linearity between dose and response is an essential one in biodosimetry, and the obtained results indicate a real possibility of using the studied chemical compounds in the determination of radiation doses. The stability condition of the radicals produced by the ionizing radiation in the studied samples it is achieved too.

Continuous microwave saturation of EPR spectra shows linearity between the intensity of the RES signal and the square root of the microwave power up to 5 mW for steviol, and up to 16 mW for sucrose, respectively (Figure 5).

EXPERIMENTAL SECTION

The samples with natural sweeteners, in polycrystalline form, were exposed to the action of low doses of gamma radiation generated by a ^{60}Co source (Gamma Chamber 600 from the Faculty of Physics) with a flow rate of D = 1.96 Gy/h, at different absorbed doses (from 5 Gy to 180 Gy). EPR measurements were performed using a Bruker EMX type EPR spectrometer operating in the X band (~ 9 GHz) with a modulation frequency of 100 kHz at room temperature. The amount of free radicals generated at different absorbed doses was assessed using the integrated and normalized double EPR signal per milligram of sample [17, 18], which is correlated with the number of paramagnetic species present in the sample. The integral intensities of the EPR spectra were obtained by evaluating their double integrals using the OriginPro2015 software.

REFERENCES

1. J.P. Klare**;** *Biomed. Spectroscopy Imaging,* **2012**, *1*, 101–124.
2. L.J. Berliner; *Biomed. Spectroscopy Imaging,* **2016**, *5*, 5–26.
3. A.M. Arangio; H. Tong; J. Socorro; U. Pöschl; M. Shiraiwa; *Atm. Chem. Phys.,* **2016**, *16*, 13105–13119.
4. Laurent Le Pape; *Modern Magn. Reson.,* **2016**, 1-25.
5. R. Grun; Electron Spin Resonance Dating. In *Chronometric Dating in Archaeology*, part of the series *AAMS*, vol. 2; R.E.Taylor, Martin J. Aitken Eds.; Springer, New York, U.S., **1997**, Chapter 8, pp. 217-260.
6. W. Sudprasert; P. Insuan; S. Khamkhrongmee; *J. Phys. Conference* Series*,* **2015**, *611(1)*, 012012.
7. N.D. Yordanov; R. Mladenova; *Spectr. Acta Part A*, **2004**, *60*, pp. 1395–1400.
8. A. Marciniak; B. Ciesielski; *App. Spectr. Rev.,* **2016**, *51(1)*, 73–92.
9. C.M. Desmet; P. Levêque; B. Gallez; *Rad. Prot. Dos.,* **2016**, *172 (1-3)*, pp. 96–102.
10. A. Kinoshita; O. Baffa; S. Mascarenhas; *PLOS ONE,* **2018**, *13(2): e0192444*, 1-11.
11. Tor Arne Vestad; On the development of a solid-state, low dose EPR dosimeter for radiotherapy. In *Series of dissertations,* Faculty of Mathematics and Natural Sciences; University of Oslo, Norway, **2005**, No. 441, pp. 1501-7710.
12. A. Kinoshita; F.A. Jose; O. Baffa; *Health Physics*, **2010**, *98(2)*, pp. 406 – 411.
13. A. Maghraby; E. Salama; *Rad. Prot. Dos.*, **2010**, *139 (4)*, 505–509.
14. Y. Karakirova; N.D. Yordanov; *Bulgarian Chem. Comm.*, **2014**, *46 (B)*,155-157.
15. N.D. Yordanov; Y. Karakirova; *Rad. Measurements*, **2007**, *42*, 347 – 351.
16. Biologydictionary.net Editors; Sucrose. In *Biology Dictionary;* BD Eds.; *https://biologydictionary.net/sucrose/ ,* **2018**.
17. D.M. Petrişor; G. Damian; S. Simon; *Rad. Phys. and Chem.,* **2008**, *77*, 463-466.
18. G. Damian; *Talanta*, **2003**, *60*, 923-927.
19. E.R. Georgieva et al.; *Free Rad. Res.*, **2006**, *40(6)*, 553–563.
20. F. Trompier et al.; *Rad. Measurements*, **2007**, *42*, 1025–1028.
21. K. Nakagawa; T. Nishio; *Rad. Res.,* **2000**, *153*, 835–839.
22. G. Vanhaelewyn; J. Sadlo; F. Callens; W. Mondelaers; D. De Frenne; P. Matthys; *Appl. Rad. Isotopes*, **2000**, *52*, 1221-1227.
23. Y. Karakirova; N.D. Yordanov; *Bulgarian Chem. Comm.,* **2015**, *47(1)*, 144-148.
24. J.A. Weil; J.R. Bolton; Relaxation times, linewidths and spin kinetic phenomena. In *Electron Paramagnetic Resonance,* Second Edition*,* John Wiley & Sons Inc. Eds.; Hoboken, New Jersey, U.S., **2007**, Chapter 10, pp. 301-356.
25. N.D. Yordanov; V. Gancheva; E. Georgieva; *Rad. Phys. and Chem.*, **2002**, *65*, 269–276.

STUDIA UBB CHEMIA, LXVII, 3, 2022 (p. 117-128)
(RECOMMENDED CITATION)
DOI:10.24193/subbchem.2022.3.09

MATHEMATICAL MODELLING OF THE ELECTROSPINNING PROCESS FOR PRODUCTION OF POLYVINYL ALCOHOL NANOFIBERS

HENRIETTA PETRUT[a], ATÁD VÉSZI[a], NORBERT MUNTEAN[a], OANA CADAR[b], RÉKA BARABÁS[a] *

ABSTRACT. The process parameters were studied during the fabrication of polyvinyl-alcohol (PVA) nanofibers via electrospinning. The factorial experiment design model described electrospinning as an efficient, versatile approach for fabricating nanofibers. The mathematical model was developed by considering the effect of voltage, concentration, the distance between the pin and the collector, and flow rate, respectively. The influence of these parameters on the diameter and morphology of obtained PVA fibers was investigated by transmission electron microscopy (TEM). It was found that the concentration had the most significant influence on the polymer fiber diameter.

Keywords: *electrospinning, process parameter, polyvinyl alcohol, response surface method, average fiber diameter*

INTRODUCTION

Electrospinning is a fast, efficient, and cheap way to produce polymer fibers in the micro, and nanometer range [1,2]. Briefly, electrospinning is based on the flow of the polymer solution through a needle under a field of electrostatic forces. During the process, most of the solution evaporates, and the polymer fiber accumulates on the sample collection surface, leading to a random two-dimensional fiber network [3]. Depending on the polymer type, the resulting structure may possess improved physical properties such as smaller pore size, higher porosity, higher surface-area-to-volume ratio and three-dimensional features [1-3]. The structural properties also depend on the

[a] *Babeş-Bolyai University, Faculty of Chemistry and Chemical Engineering, 11 Arany Janos str., RO-400028, Cluj-Napoca, Romania*
[b] *INCDO-INOE 2000, Research Institute for Analytical Instrumentation, 67 Donath Street, RO-400293, Cluj-Napoca, Romania*
* *Corresponding author: reka.barabas@ubbcluj.ro*

experimental conditions: concentration, applied voltage, needle to collector distance, flow rate, etc. [4-6]. Different polymers require individual process parameters optimization. In this regard, the response surface methodology (RSM) method was applied for chitosan-collagen nanofibers, using a sequence of designed experiments to obtain an optimal response [7]. The key parameters for the electrospinning process of PVA are the concentration of polyvinyl alcohol (PVA) solution, voltage applied, distance between the needle and collector, and flow rate [8-11].

PVA is a water-soluble, hydrophilic, non-toxic, and biocompatible polymer with good chemical and mechanical properties and widely used in creating hydroxyapatite matrixes, removing heavy metals' ions, drug carriers, tissue engineering, various intelligent materials, wound dressings, bone regeneration [12]. Elkasaby et al. optimized the production of PVA nanofibers using ANOVA and the Taguchi orthogonal array L27OA method. The PVA solution was prepared at a higher temperature of 70 ^{o}C and short mixing time [13]. The effects of five factors, namely applied voltage, concentration, collecting distance, flow rate and rotational speed, were also investigated [13]. For the investigation and optimization of the process, the design of experiment (DOE) is a suitable tool due to the excellent description of the investigated process and low number of experiments [14].

Usually, the experimental design has been done by studying one variable (factor) at a time. This approach is based on the incorrect assumption that the factors do not affect one another. The one variable at a time (OVAT) approach has certain disadvantages: many experiments are needed; the information is only available in the points studied; the interactions between factors cannot be observed, leading to the incorrect interpretation of the results; the researcher may find an acceptable response, but the chance of finding the global optimum is slight [15]. To eliminate these problems, the multivariate statistical approach named design of experiment (DOE) was introduced. This method is the most appropriate to determine the factor’s individual and combined effects, as well as their optimal points. The DOE methods' minimum and maximum level for each factor must be defined. It is helpful to place these levels on a coded scale (usually between -1 and +1) better to understand the significance of the factors and their interactions. It is recommended to perform the experiments in a randomized order to minimize the effects of unwanted factors. The experimental range of an analytical problem usually contains minima, maxima, and saddle points; hence, quadratic terms must be introduced to get an appropriate description. To estimate these terms, each factor must be assigned at least three levels.

One of the most used approaches is central composite design (CCD) [14,16]. CCD is the extension of the whole or fractional factorial design. These consist of N experiments, divided into the following categories: (a) Factorial points – the coded value of each factor is -1 or +1. These can be used to estimate the main and two-factor interactions. This part is technically a two-level full or fractional factorial design with 2^{k-m} data points, where k is the number of factors, and m is the number of applied fractions; (b) Axial points – in this part, one factor's coordinate is +α or –α, and all the other factors get their center point. The number of experiments in this part is 2^k; (c) Center points – in this part, every factor is assigned its center value. These experiments are used to estimate the experimental error and determine the quadratic terms. This study used the CCD method to correlate the process factors and the average diameter of PVA nanofiber obtained by electrospinning.

RESULTS AND DISCUSSION

Determination of fiber diameter

For every sample 10 TEM images were taken, from which around 100 segments were analyzed. It was clearly observed that the fiber diameter of the final product depends on the parameters used in the synthesis procedure. The low average diameter was 0.0749 μm for run 9 (Figure 1a) and the largest average diameter was 0.3096 μm for run 5 (Figure 1b).

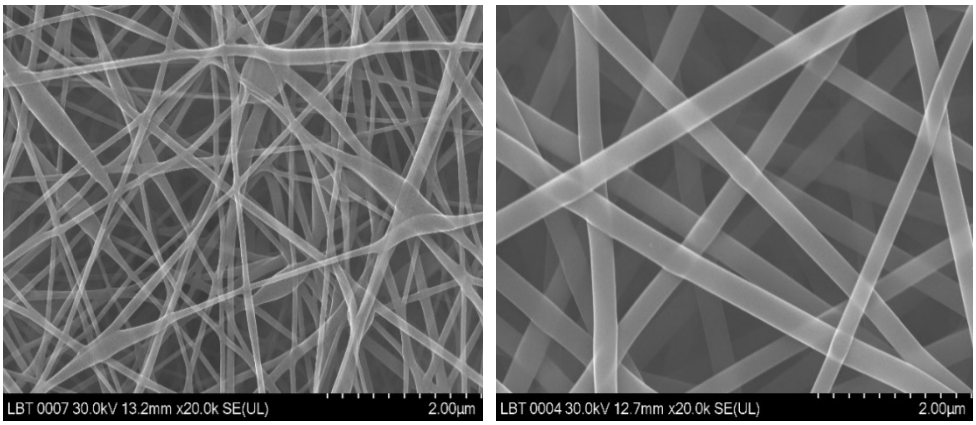

Figure 1. TEM image of the experimental runs (a) 9 and (b) 5

Estimation of coefficients in a mathematical polynomial function

After performing the experiments to obtain outputs according to the experimental design, the next step considered the vector of variables (c, U, I, q) and corresponding response (diameter). The typical response surface function for four inputs is in the form of the following equation:

$$\begin{aligned} \mathrm{Y(response)} = {} & \mathrm{b_0} + \mathrm{b_1x_1} + \mathrm{b_2x_2} + \mathrm{b_3x_3} + \mathrm{b_4x_4} + \mathrm{b_5x_1x_1} + \mathrm{b_6x_2x_2} + \mathrm{b_7x_3x_3} \\ & + \mathrm{b_8x_4x_4} + \mathrm{b_9x_1x_2} + \mathrm{b_{10}x_1x_3} + \mathrm{b_{11}x_1x_4} + \mathrm{b_{12}x_2x_3} + \mathrm{b_{13}x_2x_4} \\ & + \mathrm{b_{14}x_3x_4} \end{aligned}$$

where x_n is the corresponding factor and b_n is the coefficient, Y is the response, in our case the nanofiber diameter. Using multiple linear regression analysis on data obtained from experimental results, the following model was deduced:

$$\begin{aligned} d(\mu m) = {} & -0.166 + 0.0552 * c + 0.1179U - 0.2844 * I + 0.000954 * q - 0.00282 * c^2 \\ & - 0.00224 * U^2 + 0.01414 * I^2 - 0.000001 * q^2 - 0.000812 * c * U \\ & + 0.00417 * c * I + 0.000004 * c * q - 0.001917 * U * I + 0.000006 \\ & * U * q - 0.0000241 * I * q \end{aligned}$$

The correlation coefficient (R2) checked the efficiency of the correlated model. In the obtained model this coefficient value is 97.25%, which indicated that the model does not explain only 2.75% of the total variations. The value of adjusted R^2 is 94.68% is also high to advocate the significance of the model.

The goodness of fit was also characterized by ANOVA analysis (Table 1). The Fisher F-test with a very low probability value (P-value) demonstrates a high significance for the regression model.

The Pareto charts (Figure 2) reproduced from ANOVA results were used to visualize the main effects and their interactions. According to the results concentration (c), square of the distance (I^2), the interaction between concentration and distance (c*I), the square of flow rate(q^2) were found to be significant at 95% confidence level.

Factorial plots were obtained using the regression equation. One factor was varied, and all others remained constant at a specific value, usually their center point. Figure 3 shows the individual effect of the given factor on the response. Based on the obtained results, we can conclude that the flow rate is most affected by the other parameters.

Table 1. Analysis of variance ANOVA for central composite design

Source	DF	Adj SS	Adj MS	F-Value	P-Value
Model	14	0.133014	0.009501	37.89	0.000
Linear	4	0.120722	0.030180	120.37	0.000
c	1	0.118325	0.118325	471.94	0.000
U	1	0.000066	0.000066	0.26	0.615
I	1	0.002006	0.002006	8.00	0.013
q	1	0.000325	0.000325	1.30	0.273
Square	4	0.007394	0.001848	7.37	0.002
c*c	1	0.000336	0.000336	1.34	0.265
U*U	1	0.001051	0.001051	4.19	0.059
I*I	1	0.002622	0.002622	10.46	0.006
q*q	1	0.001573	0.001573	6.27	0.024
2-Way Interaction	6	0.004899	0.000816	3.26	0.030
c*U	1	0.000380	0.000380	1.52	0.237
c*I	1	0.002500	0.002500	9.97	0.007
c*q	1	0.000033	0.000033	0.13	0.722
U*I	1	0.001190	0.001190	4.75	0.046
U*q	1	0.000148	0.000148	0.59	0.455
I*q	1	0.000648	0.000648	2.58	0.129
Error	15	0.003761	0.000251		
Lack-of-Fit	10	0.002587	0.000259	1.10	0.487
Pure Error	5	0.001174	0.000235		
Total	29	0.136775			

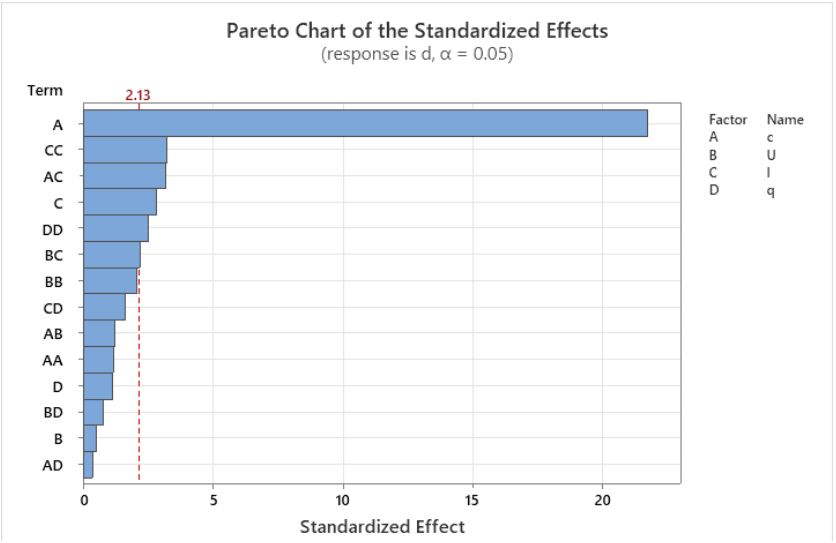

Figure 2. Pareto chart of the standardized factors

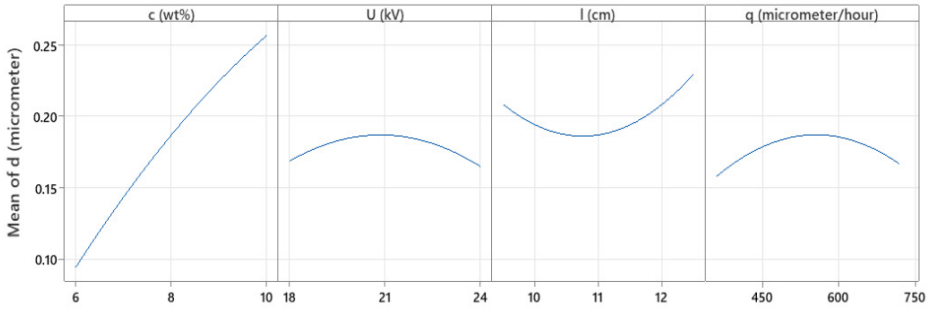

Figure 3. Factorial plot for the diameter vs. the parameters (c, U, l, q)

Response surface plots

The central composite design (CCD) results were used to generate response surfaces. The predicted values of the fiber diameters (d) calculated from the mathematical model were plotted against the factors as a response surface plot, a theoretical three-dimensional scheme to visually explain the relationship between the response and independent variables.

From the surface plots we can conclude that: (*i*) the concentration has the greatest effect on the fiber diameter and (*ii*) the concentration change in combination with the change of voltage, distance or flow rate causes the fiber diameter to behave non-linearly, which also indicates the interaction of

the concentration with the other parameters. According to Figure 4, the effect of any other parameters except concentration is significantly smaller. Also, their interactions are weaker.

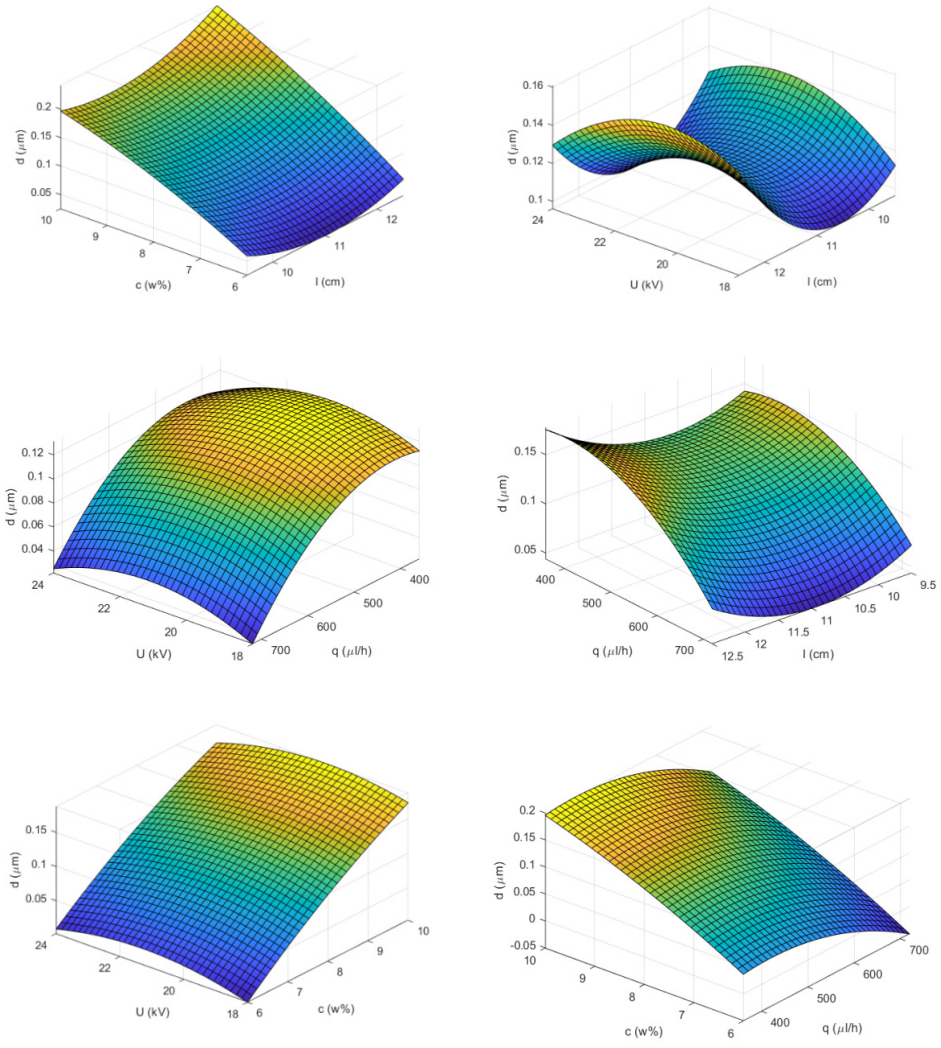

Figure 4. Surface plot of Diameter (d) vs. the factors: Plot of d vs. c, l; Plot of d vs. l, U; Plot of d vs. q, U; Plot of d vs. q, l; Plot of d vs. c, U; Plot of d vs. c, q

Response optimization

After checking the accuracy of the model, the optimal conditions are determined. Based on the obtained model, the level of each factor to get the optimal response signal was determined using Minitab software.

Table 2. Optimal levels of the factors

c (%wt)	U (kV)	L (cm)	q (μL/h)	Calculated fiber average diameters (μm)
6	18	10.7	360	0.046

CONCLUSIONS

Response surface method was used to optimize the production of PVA nanofibers by electrospinning. The resulting mathematical model can describe and predict the effect of the following factors: concentration, distance, voltage, and flow rate. Of the studied parameters, the concentration was found to have the most significant influence on the fiber diameter. The interaction between and individually of the other parameters is low and does not affect the diameter significantly. The appropriate diameter can be reached only by choosing the appropriate concentration.

EXPERIMENTAL SECTION

Materials, apparatus, and software

Hight purity PVA (>99.5%) with a molecular weight of ≈130 g/mol was purchased from Sigma-Aldrich. Distilled water was used as solvent in the preparation steps. Bionicia electrospinning system FLUIDNATEK 2017-F012 was used during the experiments. The fibers were investigated with Hitachi SU8230 (Tokyo, Japan) microscope, and the ImageJ software was used to interpret images. The regression analysis of experimental data was explored using the Minitab 19 and MATLAB 2018 software.

Design of experiment

Experimental design has three defining steps: performing statistically constructed experiments, estimating the mathematical model coefficients, and verifying the model. The goal is to write a mathematical equation that includes the effect of the studied parameters on fiber thickness and morphology.

The studied factors were PVA solution concentration (c), applied voltage (U), collector distance from the needle (l), and flow rate (q), where the levels of the studied parameters are shown in Table 3.

Table 3. The variables and their levels for the full factorial experimental design

Factor	Name	Units	Min	Max
c	Concentration	%wt	6.00	10.0
U	Voltage	kV	18.0	24.0
l	Distance	cm	9.50	12.50
q	Flow rate	μL/h	360	720

Elkasaby et al. tested the first three factors in a broader range, and the flow rate was set to a lower value (100-300 μL/h) compared to 360-720 μL/h used in this study. Accordingly, there are significant differences in the obtained fiber size, the obtained values of 0.0749 and 0.31, comparing to 0.51 and 1.87 obtained by Elkasaby et al. The authors also created two models, with the help of which they tried to predict the system's behavior. The correctness of the obtained model was verified using the average model accuracy (AMA) calculated from residuals, which in the case of the first model is 84.3%. In contrast, in the case of the second model is approximately 80%. In our case, this value is 94.0%. Despite the differences, similar conclusions were reached based on which solution concentration affects fiber size [17].

The coded and the real values of the factors are presented in Table 4.

Table 4. Explanation of the code system

Factor	Name	Units	-1	0	1
c	Concentration	%wt	6.00	8.00	10.0
U	Voltage	kV	18	21	24
l	Distance	cm	9.50	11	12.5
q	Flow rate	μL/h	360	540	720

The levels of the factors are selected based on the size of the experimental range, the error in the factor fixation and the choice of the variation interval. After determining the experimental design depending on the number of factors and the nature and magnitude of their influence, the mathematical model can be selected. The coefficients show the strength of each factor and interaction; their values express how much the response characteristic change when the given factor changes [18,19].

In order to determine the effect of the above-mentioned factors, the response surface method with a central composite design was applied. The data set was composed of 30 experiments for each of the responses collected, as it is shown in Table 5.

Table 5. Central composite design and the fiber average diameters for each experimental run

	Coded values of the factors				**Fiber average diameters (μm)**
Run	c(%wt)	U(kV)	l(cm)	q (μL/h)	d
1	1	-1	-1	-1	0.1945
2	1	-1	-1	1	0.2294
3	1	1	-1	-1	0.2082
4	1	1	-1	1	0.2445
5	1	-1	1	-1	0.3096
6	1	-1	1	1	0.2655
7	1	1	1	-1	0.2396
8	1	1	1	1	0.2480
9	-1	-1	1	-1	0.0749
10	-1	1	1	-1	0.0798
11	-1	-1	1	1	0.0848
12	-1	1	1	1	0.0787
13	-1	-1	-1	-1	0.0784
14	-1	1	-1	-1	0.0858
15	-1	-1	-1	1	0.0774
16	-1	1	-1	1	0.0905
17	1	0	0	0	0.2656
18	-1	0	0	0	0.0952
19	0	1	0	0	0.1741
20	0	-1	0	0	0.1692
21	0	0	1	0	0.2325
22	0	0	-1	0	0.2147
23	0	0	0	1	0.1814
24	0	0	0	-1	0.1529
25	0	0	0	0	0.1697
26	0	0	0	0	0.2077
27	0	0	0	0	0.1873
28	0	0	0	0	0.1871
29	0	0	0	0	0.1680
30	0	0	0	0	0.1714

The experiments were established according to Table 5.

Preparation of PVA solution and electrospinning process

The appropriate amount of PVA was dissolved in distilled water in an ultrasonic bath, stirred 6 h at 60 ℃, and then 24 h at ambient temperature. The resulting solution was introduced to the electrospinning device's syringe comprising a programable pump that ensures a specific flow rate. The collector was adjusted to the chosen distance and was covered with aluminum foil, where the PVA fibers were collected. The voltage and flow rate were adjusted via a microcontroller over a range of values suitable for most electrospinning. The electrospinning process was carried out at room temperature.

Characterization of prepared PVA fiber samples

The morphology of samples was investigated by transmission electron microscopy (TEM) and the resulting images were analyzed using the ImageJ software package (Version 1.51) with DiameterJ plugin.

ACKNOWLEDGMENTS

This work was supported by a grant of the Romanian National Authority for Scientific Research CNCS-UEFISCDI, project number PN-III-P2-2.1-PED-2019-3664. We gratefully acknowledge the technical support of Dr. L. Barbu-Tudoran regarding TEM images.

REFERENCES

1. A. Frenot. I.S. Chronakis, Curr. *Colloid. Interface. Sci.,* **2003**, *8*, 64-75
2. D. Li., W.Y. Xia, *Adv. Mater.* **2004**, *16*, 1151-1170
3. Joseph, Deitzel. James D, Kleinmeyer. Donovan, Harris. Nora C, Beck-Tan. *Polymer,* **2001**, *42*, 261-272
4. Z. Li., C. Wang. *One-Dimensional nanostructures. Springer Briefs in Materials*. Springer, Berlin, Heidelberg. **2013**. pp. 15-28
5. C.J. Thompson, G.G. Chase, A.L. Yarin, D.H. Reneker. *Polymer*, **2007**, *48*, 6913-6922
6. Y. Meyva-Zeybek, C. Kaynak, *J. Appl. Polym. Sci.*, **2020**, *138*, 3
7. N. Amiri, A. Moradi, S.A.A. Tabasi, J. Movaffagh, *Mater. Express*, **2018**, *5*, 4
8. A.K. Aljehani, M.A. Hussaini, M.A. Hussain, N.S. Alothmany, R.W. Aldhaheri, 2nd Middle East Conference on Biomedical Engineering, Doha, **2014**, 379-381

9. S.F. Dehghan, F. Golbabaei, B. Maddah, M. Latifi, H. Pezeshk, M. Hasanzadeh, *J. Air Waste. Manage.*, **2016**, *66*, 912-921
10. N.J. Kanu, E. Gupta, U.K. Vates, G. Singh, *Mater.Express*, **2020**, *7*, 3
11. R.-R. Yang, J.-H. He, L. Xu, J.-Y. Yu, *Mater. Sci. Tech-Lond*., **2010**, 26, 1313-1316
12. S. Ullah, M. Hashmi, N. Hussain, A. Ullah, M.N. Sarwar, Y. Saito, S.H. Kim, I.S. Kim, *J. Water Process. Eng.*, **2020**, *33*, 101-111
13. M. Elkasaby, H.A. Hegab, A. Mohany, G.M. Rixvi, *Adv. Polym. Tech.*, 2018, *37*, 2114-2122
14. X. Ji, J. Guo, F. Guan, Y. Liu, Q. Yang, X. Zhang, Y. Xu, *Gels*, **2021**, *7*, 223
15. S.S. Nasrollahi, Y. Yamini, A. Mani-Varnosfaderani, *J. Food Compos. Anal.*, 2022, *106*, 104339
16. Q. Zhang, T.M. Young, D.P. Harper, T. Liles, S. Wang, *Carbohyd. Polym.* **2021***, 2*, 100120
17. M. Elkasaby, H.A. Hegab, A. Mohany, G.M. Rizvi, *Adv. Polym. Tech*., **2017**, 37, 1-9
18. George E.P. Box, J. Stuart Hunter, William G. Hunter, Statistics for Experimenters: Design, Innovation, and Discovery, 2nd Edition, Wiley, **2005**
19. M.A. Badawi, L.K. El-Khordagui, *Eur. J. Pharm. Sci.* **2014**, *58*, 44-54